THE UNIVERSITY *of* EDINBURGH

THE UNIVERSITY *of* EDINBURGH
Edinburgh Medical School

Biomedical Sciences

Investigating white matter alterations and secondary neurodegeneration with MRI imaging and pathology in a mouse model of ischaemic stroke

Examination Number: S2797161

Course Name: Neuroscience (MSc by Research)
2025

Word Count: 23,917

DECLARATION

I declare that this thesis has been composed by myself and that the work presented is entirely my own, except where explicitly stated otherwise.

I confirm that this thesis has not been submitted for any other degree or professional qualification.

I certify that the work complies with the University of Edinburgh's regulations on research integrity and academic conduct.

Name: Sevgi Yaren Dogru

Matriculation Number: S2797161

Degree: MSc by Research in Neuroscience

University: University of Edinburgh

Signed: Sevgi Yaren Dogru

Date: 27/12/2025

Table of Contents

Abstract

Advances in acute ischaemic stroke treatment have increased survival rates, yet many individuals experience long-term complications such as post-stroke cognitive impairment and dementia. While the primary infarct is well characterised, the mechanisms driving chronic degenerative changes in remote but anatomically connected brain regions remain unclear, despite their importance for brain function and recovery after stroke. Emerging clinical imaging evidence suggests that white matter degeneration, secondary neurodegeneration and inflammation in areas like the corpus callosum and thalamus after a middle cerebral artery stroke may contribute to cognitive decline.

The aim of the current study was to examine remote grey and white matter alterations in anatomically connected brain regions following experimental cortical ischaemic stroke, with a particular focus on changes in cerebral perfusion, glial responses, and structural integrity. This study is based on the hypothesis that stroke involves disturbances of the neurogliovascular unit in remote, anatomically connected brain regions, and that these disturbances are associated with degenerative changes affecting both grey and white matter.

We used *in vivo* MRI imaging and immunohistochemistry to investigate remote brain changes pre-surgery and one month after cortical ischemic stroke induced by distal middle cerebral artery occlusion in male C57BL/6J mice (stroke: n=5, sham: n=4). Cerebral blood flow (CBF) was measured using arterial spin labelling (ASL) MRI in the white and grey matter regions. Diffusion tensor imaging (DTI) assessed white matter integrity via fractional anisotropy (FA) and mean diffusivity (MD). Immunohistochemistry evaluated astrocyte (GFAP) and microglia (Iba1) reactivity, axonal damage (APP), myelin integrity (MAG), and secondary neurodegeneration (NeuN).

Stroke mice exhibited sustained hypoperfusion in the corpus callosum/external capsule and conversely, hyperperfusion in the thalamus. DTI indicated elevated FA and unchanged MD in the corpus callosum/external capsule, suggesting microstructural disruption in white matter. Immunohistochemistry revealed axonal damage, gliosis, and axon-myelin alterations in the connected grey and white matter regions, as well as secondary neurodegeneration in the thalamus. Our findings indicate that cortical stroke triggers chronic, region-specific alterations in anatomically connected brain areas, with distinct patterns of hypoperfusion, hyperperfusion, inflammation, and structural degeneration. This work provides a foundation for future studies using spatial transcriptomic approaches to define the molecular correlates of these remote neuroimaging and pathophysiological changes.

Lay Abstract

Stroke is one of the leading causes of death and disability worldwide. It happens when there is a blockage in the blood supply to a part of the brain. This blockage prevents essential nutrients and oxygen from reaching brain cells called neurons which can cause them to die, resulting in a localised area of brain cell death.

Neurons send messages through axons, which are long, cable-like structures which transmit signals between different parts of the brain. The axons are wrapped in a tissue called myelin, which enables rapid, efficient communication of these signals. Neurons are surrounded and supported by glial cells that serve as the brain's defence system. Glial cells provide nutrients to neurons, detect damage, repair tissue, remove dead cells and protect the brain from infection. Together, axons, myelin, and glial cells form the white matter of the brain and connect distant regions. Healthy functioning white matter is essential for normal memory and thinking and is dependent on signalling between these different cellular components.

Advances in the treatment of stroke have increased survival rates; however, many individuals experience long-term complications such as difficulties with thinking, memory, and they have a higher risk of developing dementia. While the initial area of brain damage after a stroke is well characterised, researchers now know that the damage spreads to other brain regions over time via white-matter damage, leading to problems with thinking and memory.

The purpose of this study was to investigate the impact of a stroke on distant yet connected brain areas, including two parts of the brain called the corpus callosum and the thalamus. The corpus callosum is the main white matter structure in the brain that connects the left and right sides of the brain, allowing them to communicate. The thalamus acts as a sensory centre, passing information between different brain regions, and has a role in regulating memory, movement, and sensation.

Using a mouse model of stroke, we used brain scans with MRI imaging and tissue analysis to examine changes in the blood flow, white matter, and cell health one month after stroke in these distant brain regions. We found that stroke led to reduced blood flow and disrupted corpus callosum structure, but increased blood flow in the thalamus. Tissue analysis under the microscope revealed inflammation, axonal damage, and disrupted myelin. There was also neuronal loss in the thalamus, indicating secondary neurodegeneration, where brain cells die in regions that are far but connected to the original stroke site.

In conclusion, these results indicate that stroke can trigger widespread and long-lasting changes across the brain regions, extending far beyond the primary injury site. It is essential to understand these remote effects as they lead to problems with thinking, memory and even dementia. This research can serve as a guide to understanding the mechanisms and identifying new therapeutic targets to protect brain health and improve recovery after stroke.

1. Introduction

1.1 Stroke leads to cognitive impairment

Stroke is one of the leading causes of death and disability worldwide (Martin et al. 2024) and is broadly categorised by two main types: ischemic and haemorrhagic stroke. Ischemic stroke, being the most common type, accounts for approximately 60-80% of all cases (Hilkens et al. 2024). It occurs when blood flow to the brain is blocked by a blood clot formed within a blood vessel (Feigin et al. 2021). In contrast, haemorrhagic stroke arises from the rupture of a blood vessel within the brain, leading to bleeding and subsequent damage to brain tissues (Chen et al. 2014). Stroke survivors often experience chronic and debilitating consequences such as physical disability, emotional disturbances, and, notably, cognitive impairment and dementia (Rost et al. 2022). Post-stroke cognitive impairment (PSCI) is recognised as a major contributor to long-term morbidity, and a significant proportion of stroke survivors go on to develop vascular cognitive impairment (VCI), which encompasses a spectrum from mild deficits to full-blown vascular dementia (Iadecola et al. 2019). The prevalence and impact of PSCI and VCI underscore the urgent need for research into mechanisms driving these outcomes, since more people survive stroke and the population of survivors at risk of cognitive decline expands (King et al. 2020). Despite this growing clinical burden, there are currently no effective treatments for cognitive impairment after stroke; thus, there is an urgent unmet need to develop new therapies. Moreover, in the long-term recovery, in particular, memory, attention, and executive function remain understudied, as identified by stroke survivors, caregivers, and healthcare professionals as one of the top unanswered research questions (Pollock et al. 2014). Moreover, cerebrovascular pathology including stroke infarcts also contributes to dementia, including both Alzheimer's Disease and vascular dementia, particularly through disruption of the neurovascular unit and white matter damage (Dichgans and Leys 2017). These ongoing challenges greatly reduce the quality of life. Therefore, it is crucial to explore and address the chronic factors that lead to cognitive decline after stroke, as this is essential for enhancing long-term outcomes for stroke survivors.

1.2 Cellular composition of white matter and altered white matter integrity post-stroke

Even though stroke research has traditionally emphasised cortical grey matter injury, emerging evidence shows the critical role of white matter (WM) in cognitive function and long-term effects of stroke both locally and remotely (Filley and Fields 2016). White matter makes up over half of the brain's volume and is crucial for facilitating the transfer of information between cortical and subcortical regions through organised tracts of myelinated axons (Alber et al. 2019). Unlike grey matter, which contains neuronal cell bodies, white matter comprises primarily myelinated axons, oligodendrocytes, oligodendrocyte precursor cells (OPCs), astrocytes, and microglia, and vascular-associated cells collectively forming the neurogliovascular unit vital for maintaining cerebral homeostasis and function (Figure 1) (Horsburgh et al. 2018). Pre-clinical experimental stroke studies show widespread Wallerian

degeneration (WaD) after stroke, which is an anterograde degeneration of axon and myelin damage due to an injury (Zuo et al. 2019). Significantly, WaD evolves more slowly than the initial infarct, developing progressively over days to weeks, and is observed in remote, non-ischaemic regions such as the striatum and corpus callosum. This delayed but widespread degeneration highlights the vulnerability of the white matter after an injury such as stroke. Thus, healthy white matter integrity is essential for normal cognitive function. If there is any damage to any parts of this unit, it can disrupt the neuronal connectivity, ultimately leading to cognitive deficits.

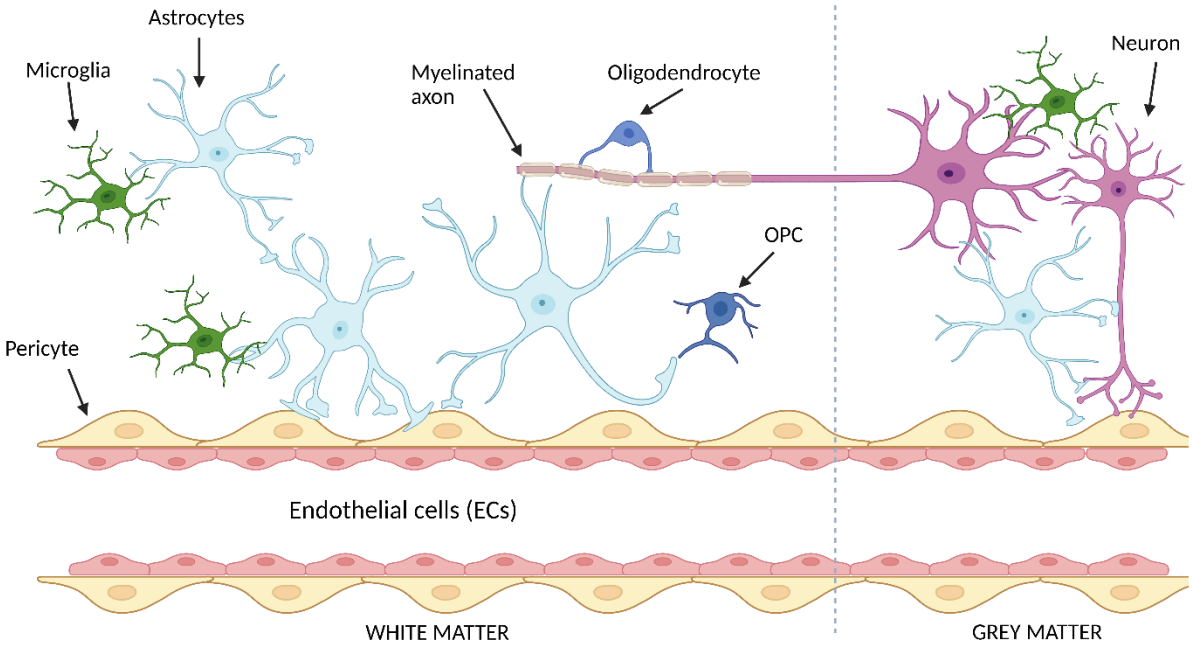

Figure 1. Cellular components of the glial-vascular unit in the white and grey matter. Neurons span both the white and grey matter; myelinated axons are in the white matter, while neuronal cell bodies and synapses are in the grey matter. Astrocytes are located in the centre between neurons and endothelial cells (ECs) and extend their processes between the two. They help contribute to maintaining homeostasis and blood-brain barrier (BBB) integrity. They regulate ion and water balance, provide metabolic support and help maintain myelin stability. Microglia account for 5-15% of all cells in the human brain and monitor the brain for injury and inflammation. Oligodendrocytes play an essential role in myelinating neurons' axons, which helps transmit information faster. Oligodendrocyte precursor cells (OPCs) interact closely with pericytes along the vasculature and maintain vascular stability and regulate oligodendrocyte differentiation. Pericytes are embedded within the vascular basement membrane that regulate BBB permeability and cerebral blood flow. Together, these cells form a dynamic glial-vascular unit that is essential for white matter structure and function.

1.3 Clinical neuroimaging and network-level brain changes post-stroke

Clinical studies using advanced imaging techniques, such as magnetic resonance imaging (MRI) and positron emission tomography (PET), show widespread white matter changes after stroke (Poirier et al. 2025; Egorova-Brumley et al. 2023). MRI is a practical, non-invasive method that shows detailed brain structure and pathology, particularly diffusion tensor imaging (DTI) and arterial spin labelling (ASL) (Cao et al. 2025). Through MRI, both grey and white matter changes after stroke can be characterised. DTI measures the directionality of

water along white matter tracts, providing information about axonal fibres and yielding indices such as fractional anisotropy (FA) and mean diffusivity (MD); where FA measures the water direction and gives information about the overall fibre integrity and MD measures the average water diffusion in all directions and gives information about the severity of tissue damage (Kern et al. 2022). ASL, on the other hand, provides non-invasive measures of cerebral blood flow (CBF) (Shan et al. 2025). Following cortical ischaemic stroke, FA and MD were found to show changes at the injury site and in remote but connected white matter regions, suggesting axonal disruption, gliosis, and demyelination/remyelination (Dacosta-Aguayo et al. 2014; Kern et al. 2022). Such microstructural alterations can be linked to vascular cognitive impairment and vascular dementia, suggesting that WaD seen after an injury can serve as an indicator of cognitive decline (Dacosta-Aguayo et al. 2014). Furthermore, on T2-weighted structural MRI, white matter hyperintensities (WMHs) can be visualised and are associated with an increased likelihood of cognitive impairment and dementia, as they are also observed in older populations (Alber et al. 2019). Importantly, while WMHs become more prevalent with ageing, they can also reflect underlying small vessel disease and pathological changes in the white matter after an injury (Wardlaw et al. 2015).

In addition, studies have shown that contralesional white matter tracts may undergo reorganisation and degeneration, a process thought to be driven by WaD, in which distant progressive axonal degeneration occurs, with the possibility of a compensatory response after stroke (Dacosta-Aguayo et al. 2014). Key clinical imaging biomarkers such as FA, MD, and WMH burden can capture these remote white matter alterations. These are summarised in Table 1. These imaging biomarkers can serve as predictors of long-term cognitive outcomes which are which are linked to attention, memory, and executive functioning (Tuladhar et al. 2015; Dacosta-Aguayo et al. 2014). This suggests that stroke is a network-wide pathology and not merely a focal event. In addition to clinical studies, pre-clinical findings from rodent models also provide insight into these imaging signatures (Singh et al. 2022). Ischaemic stroke in humans occurs mainly through the occlusion of the middle cerebral artery (MCA); therefore, MCA occlusion is the most common model employed in pre-clinical studies (McCabe et al. 2018). DTI changes observed in a post-stroke dMCAO model in rodents mirror findings in humans, including alterations in FA and MD values and WM disruption (Jung et al. 2017; Liang et al. 2020; Pitkonen et al. 2012). As a result, linking these clinical imaging findings with preclinical models enhances the relevance of white matter stroke research. It highlights the importance of imaging biomarkers for diagnosis and possible treatment strategies.

Study	Sample/Design	Remote White Matter Findings	Cognitive Association	Limitations
(Dacosta-Aguayo et al. 2014)	Ischaemic stroke patients n=25 3 months post-stroke DTI: FA, MD	Contralesional normal appearing white matter (NAWM) showed reduced FA, increased MD, and looked normal on T2 MRI	Low contra FA predicted worse cognitive performance (memory, attention, executive function)	Small cohort, cross-sectional cognitive follow-up, limited tract specificity
(Egorova et al. 2020)	Ischaemic stroke Longitudinal cohort n=100 Chronic stroke survivors (3-month to 1 year DTI, whole brain	Widespread WM degeneration beyond the lesion	WM degeneration correlated with global functional outcome (mRS): reduced WM was linked to attention deficits indirectly	Limited detailed cognition, heterogeneous lesions across participants
(Pinter et al. 2020)	Ischaemic stroke patients n=30 Longitudinal DTI, TBSS	Progressive FA decline in remote tracts indicates ongoing secondary neurodegeneration	Early remote WM changes predicted later impairments in processing speed and motor/executive functions	Lesion heterogeneity, small sample, limited cognitive battery
(X. Cao et al. 2021)	Ischaemic stroke patients with basal ganglia lesions (1 to 12 months) n=36 DTI	Degeneration in remote WM; corpus callosum, thalamic projections	Remote WM degeneration correlated with motor deficits	Cognition is not comprehensively tested; motor focus limits direct cognitive interpretations
(Schaapsmeerders et al. 2016)	First ischaemic stroke DTI 11-year follow-up	Persistent FA reductions in remote NAWM	Remote WM integrity predicted long-term deficits in executive function, processing speed and global cognition	Very long post-stroke survival: survival bias, Ageing effects may confound WM degeneration
(Egorova-Brumley et al. 2023)	Ischaemic stroke Longitudinal (1 year and 3 years)	Ongoing progressive degeneration in remote WM tracts	Progressive remote WM loss predicted worsening	Observational, cognitive batter limited

	DTI and volumetry		executive, attention and memory functions	
(Sagnier et al. 2020)	Acute ischaemic stroke n>100 DTI, focus on NAWM	Early FA reductions in NAWM predicted poorer outcomes, remote NWAM despite normal T2	Lower early NAWM integrity predicted worse executive and attentional outcomes	NAWM measured globally, a moderate cognitive assessment
(Fruhwirth et al. 2024)	Acute ischaemic stroke n=60 Multimodal MRI	Lower baseline FA and disrupted DMN connectivity indicate more disconnection	WM integrity and DMN connectivity predicted executive, memory and processing speed deficits	No deep cognitive profiling, small sample

Table 1. Summary of recent clinical papers that show evidence for remote white matter degeneration after stroke and its relationship to cognitive decline. NAWM=normal appearing white matter (looks normal macrostructurally in T2 but can contain microstructural damage)

1.4 Cellular and glial pathophysiology of white matter injury after ischaemic stroke

Following ischemic injury to white matter, several pathological processes are observed at microscopic level, such as axonal degeneration, demyelination, glial cell activation, and oligodendrocyte precursor cell (OPC) proliferation (Sozmen et al. 2019; Yang et al. 2025; Wang et al. 2016; Shira and Thomas 2015). These processes are not confined in the peri-infarct core but can extend into remote regions, and may contribute to secondary neurodegeneration and cognitive decline (Zuo et al. 2019; Wang et al. 2016).

Microglia are the resident immune cells of the central nervous system and play essential roles in homeostasis, immune surveillance, and injury response (Rawji et al. 2023; Xu et al. 2020). After the initial injury event, such as a stroke, they respond to this and become activated by undergoing morphological and transcriptional changes, known as reactive microglia (Xu et al. 2020). In general, glial cells are very heterogeneous and can have multiple roles and phenotypes in different contexts. Microglia, being one of them, can have both protective and detrimental effects depending on the stage and context of injury. In the early phase of the injury, they usually aid in debris clearance and secrete neurotrophic factors that promote repair. However, prolonged activation of microglia can lead to sustained production of pro-inflammatory cytokines and reactive oxygen species (ROS), leading to further white matter injury and potentially impairing recovery (Suenaga et al. 2015; Guo et al. 2025). On the other hand, transcriptomic analysis has revealed a population of microglia only present in disease contexts referred to as disease-associated microglia (DAM) (Keren-Shaul et al. 2017). While DAMs were originally characterised in Alzheimer's disease, emerging evidence suggests similar injury-induced microglial phenotypes after ischaemic stroke, initially promoting

neuroprotection but shifting into a pro-inflammatory state due to prolonged activation (Li et al. 2023; Zhang et al. 2023). These stroke-induced microglial states may contribute to early processes as well as chronic inflammation and secondary white-matter degeneration.

Astrocytes are another key glial cell that are involved in the response to ischaemic injury. In the absence of an injury, they regulate neurotransmitter balance, maintain the blood-brain barrier, and provide metabolic support to neurons (Rawji et al. 2023). When there is injury, astrogliosis occurs, and astrocytes become reactive, characterised by cellular hypertrophy and increased levels of inflammatory proteins (Xu et al. 2020). Just as microglia do, they help limit tissue damage and restore homeostasis, but persistent astrogliosis can form glial scars that inhibit axonal regeneration and functional recovery (Shen et al. 2021; Zhang et al. 2018; Escartin et al. 2021).

Axonal damage and demyelination are other key features of white matter pathology in stroke. Ischaemic stroke causes axonal pathology and disrupts cytoskeletal stability, leading to axonal swelling, fragmentation and eventually Wallerian degeneration in regions connected to the infarcted cortex (Zuo et al. 2019; Wang et al. 2016). Although axonal injury and myelin loss frequently co-occur, the precise temporal sequence of these events remains unclear. Nevertheless, myelin disruption further impairs signal conduction and network dysfunction following stroke. Oligodendrocytes are particularly vulnerable to ischemia because their primary role is to produce and maintain the myelin sheath (Wang et al. 2016). Following ischemic stroke, the brain responds by inducing a widespread inflammatory cascade of events characterised by activation of astrocytes and microglia that extends well beyond the infarcted region. Shi and colleagues (2021) describe this as “global brain inflammation”, referring to prolonged brain-wide immune activation that is not confined to the peri-infarct zone but also affects the connected regions throughout the brain (Shi et al. 2021). These changes in the brain could affect oligodendrocyte dynamics. Recent transcriptomic studies have revealed the emergence of disease-associated oligodendrocytes (DAOs), characterised by unique gene expression profiles linked to inflammation and cellular stress (Pandey et al. 2022; Kenigsbuch et al. 2022). While DAOs have been described in Alzheimer’s disease and multiple sclerosis, to our knowledge, they have not yet been reported in the context of ischaemic stroke.

Together, these cellular changes following chronic injury highlight the complex interplay among glial activation, axonal injury, and myelin loss. However, it is not entirely understood the extent of these alterations to these cells is in the white and grey matter, and the role of these glial cells is in the progression of secondary injuries.

1.5 Secondary neurodegeneration following stroke

As mentioned above, ischaemic stroke is the most common type of stroke and leads to inflammation, gliosis and cell death surrounding the cortical infarct within minutes to hours. This acute phase of the injury is referred to as the primary injury. It is characterised by necrosis

and apoptosis within the ischaemic core, resulting from oxidative stress, excitotoxicity, ATP dysregulation, glial cell activation, lymphocyte infiltration, calcium dysregulation, and blood-brain barrier breakdown (Stuckey et al. 2021; Kim et al. 2021). The primary injury can disrupt brain function in anatomically and functionally connected but distant brain regions and impede recovery (Seitz et al. 1999).

This so-called delayed and progressive process is not directly affected by the reduction in cerebral blood flow associated with the primary injury, is called secondary neurodegeneration and is associated with a gradual loss of neurons in brain regions anatomically connected with the infarct (Figure 2). Secondary neurodegeneration differs from acute injury in both timing and location and can persist from weeks to months to years (Shi et al. 2019). These secondary injuries are connected to the primary stroke infarct through axonal and synaptic pathways and are hypothesised to be driven by persistent neuroinflammation, glial cell activation, axonal degeneration and demyelination (Stuckey et al. 2021; Kim et al. 2021). As a result, secondary neurodegeneration can contribute to cognitive and functional decline in chronic stroke.

The thalamus acts as a key relay centre for sensory and motor input and is important for memory and cognitive processing (Brunelli et al. 2023; Fama and Sullivan 2015). Clinical imaging studies have shown thalamic atrophy, hypometabolism acutely and neuronal loss following cortical stroke, indicating secondary neurodegeneration here (Yamauchi et al. 2022; Nakane et al. 2002; Kuchcinski et al. 2017; Fernández-Andújar et al. 2014). Rodent models of chronic cortical stroke have also shown glial cell activation, axonal degeneration and neuronal loss in the ipsilateral thalamus (Schroeter et al. 2006; Dihné et al. 2002; Langen et al. 2007; X. Cao et al. 2021).

Evidence from both clinical and preclinical studies shows that reductions in secondary injuries are correlated with improved behavioural recovery, suggesting these remote regions as potential therapeutic targets (Villa et al. 2007; Han et al. 2015; Cao et al. 2017). Since these secondary degenerations develop over time, they provide an extended therapeutic window for intervention. However, the cellular and molecular mechanisms underlying this delayed degeneration remain poorly understood, particularly in white matter tracts and subcortical structures. It is important to address these mechanisms, as they are crucial for preserving neural connectivity and promoting cognitive recovery in the chronic phase of stroke.

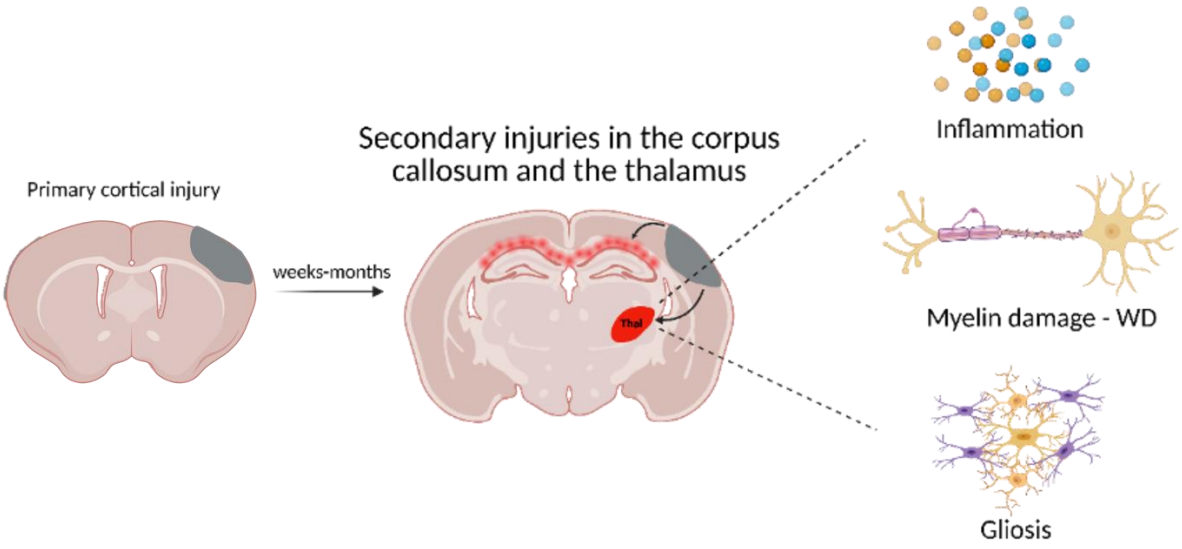

Figure 2: Secondary neurodegeneration in the anatomically connected brain regions after cortical ischaemic stroke results in inflammation, myelin damage and gliosis in the thalamus and white matter tracts.

1.6 Gap in Knowledge

Stroke survivors often develop cognitive impairment and are at increased risk of developing dementia, with chronic structural and pathological brain changes contributing to this long-term vulnerability. Advanced MRI imaging studies in patients have demonstrated alterations in cerebral perfusion and widespread reductions in white matter integrity in the infarcted region as well as the regions anatomically connected to the infarct. Secondary injuries that develop in the remote anatomically connected regions have been identified as a potential driver of this post-stroke cognitive impairment. Although clinical neuroimaging studies using MRI have shown evidence of this, most preclinical studies have focused on acute and subacute time points after injury, leaving a gap in understanding the chronic mechanisms linking the structural and functional changes seen in MRI to glial cell responses and axon-myelin disruption in remote white matter regions. It is important to bridge this translational gap since the cellular and molecular mechanisms underlying white matter damage and secondary neurodegeneration in anatomically connected brain regions in rodent models remain poorly understood. Specifically, it is unclear how the chronic structural alterations observed in MRI relate to secondary injury pathways, glial cell responses and axon-myelin disruption in remote brain regions following stroke. It is important to understand the chronic mechanism to identify therapeutic targets for cognitive recovery post-stroke.

To address this research gap, we investigated the development of secondary injuries, glial cell alterations, axonal damage, and demyelination patterns in the white matter tracts and the thalamus four weeks post-stroke using the distal middle cerebral artery occlusion (dMCAO) mouse model of cortical ischaemic stroke. Structural and functional changes were assessed longitudinally using MRI, followed by immunohistological analyses to examine glial cell response, axonal integrity, and myelination patterns in the white and grey matter tracts.

2. Hypothesis and Aims

It was hypothesised that cortical ischaemic stroke induces remote dysfunctions of the neurogliovascular unit in anatomically connected brain regions, characterised by disrupted cerebral blood flow and alterations in both white and grey matter, including glial cell reactivity and secondary neurodegeneration.

Aim 1: To use MRI to non-invasively assess the impact of cortical ischaemic stroke on brain perfusion and structural integrity in brain regions anatomically connected to the cortex:

a) Characterise regional cerebral blood flow (CBF) using arterial spin labelling (ASL) MRI at baseline (pre-surgery) and at 1-month post-ischaemic stroke.
b) Assess white matter microstructural integrity using diffusion tensor imaging (DTI) at 1-month post-stroke

Aim 2: To investigate cellular and molecular changes underlying neuroimaging alterations in white matter tracts and connected regions following cortical ischaemia, using immunohistochemical analyses conducted in the same animals:

a) Evaluate glial responses by quantifying GFAP (reactive astrocytes) and Iba1 (microglial activation) in white and grey matter regions at 1-month post-stroke.
b) Characterise axonal damage and axon-myelin integrity in white and grey matter regions at 1-month post-stroke using APP (amyloid precursor protein) and MAG (myelin-associated glycoprotein)**.**
c) Assess neuronal survival and secondary neurodegeneration using NeuN immunostaining in the thalamic nuclei and the striatum.

3. Materials and Methods

3.1 Animals

All experiments had permission from, and adhered to the regulations of the UK Home Office Animal (Scientific Procedures) Act 1989, with ethical veterinary approval from the Biomedical Research Resources at the University of Edinburgh, and followed the ARRIVE guidelines, and establishment licence; experimenters were blinded to surgery for the entirety of testing and data analysis (Percie du Sert et al. 2020). Male C57BL/6J mice of 5 - 8 months were used for animal experiments. The animals were housed in groups of 2 to 5 under controlled conditions in a 12-hour light/dark cycle, with room temperature at 23°C. They were provided ad libitum access to water and food. A total of 9 mice (sham n=4, stroke n=5) were included in this study, and all of them successfully recovered from experimental conditions. Experimental design and details of animals used in this study are outlined below (Figure 3.1).

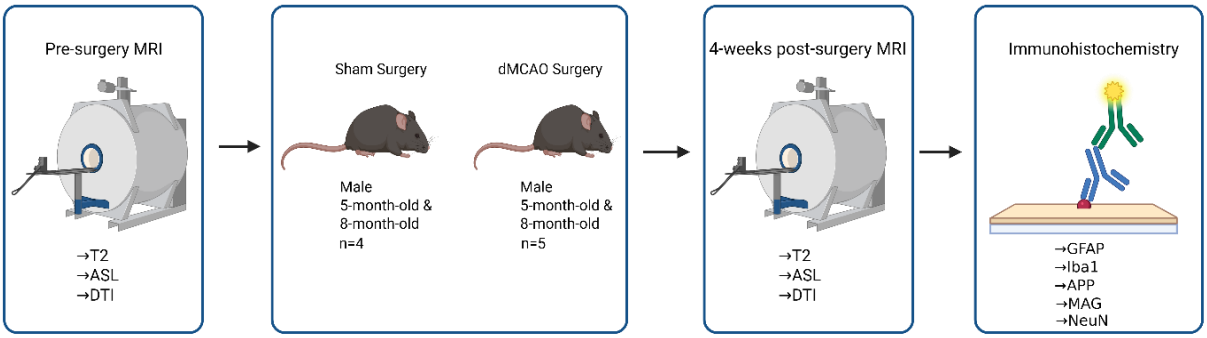

Figure 3.1. Experimental design. First, all mice underwent MRI scanning followed by surgeries. Four weeks post-surgery, mice underwent MRI scanning again, followed by perfusion the next day. All of the mice were used for pathological analysis to assess post-stroke cognitive impairment and dementia (sham n=4, stroke n=5). The experimental cohorts have been designed to use the minimal number of animals that can answer the aims of the study using statistical power analysis (InVivoStat software) with statistical significance set at $p<0.05$, with a power of 80%.

3.1.1 Distal middle cerebral artery occlusion surgery

Surgeries were performed by Dr Jill Fowler, and surgery allocation was randomised. Animals underwent permanent left distal middle cerebral artery occlusion (dMCAO) using electrocoagulation (Figure 3.2). This was performed using a modified protocol of the well-established Tamura method (Tamura et al. 1981). The permanent distal middle cerebral artery occlusion (dMCAO) model is a useful experimental design for ischaemic stroke because it targets the MCA, the vessel most commonly occluded in human stroke, thereby producing reproducible cortical infarcts within MCA territory (McCabe et al. 2018). Compared to other models, dMCAO typically shows less variability in lesion size, lower mortality, and limited oedema, yet still induces measurable cognitive deficits; importantly, severe sensorimotor and global neurological impairments are less prominent, reducing confounds in cognitive assessments (L. Zeng et al. 2023).

Mice were first anaesthetised in an induction box with 5% isoflurane, which was lowered to 1.75-2.5% on a facemask for the duration of the surgery. Aseptic technique was followed throughout, and body temperature was monitored and maintained at 37 °C ± 0.5 °C using a heat mat. To expose the middle cerebral artery (MCA) bifurcation, the temporalis muscle was dissected, and a burr hole was drilled through the saline-cooled skull. In stroke groups only, the distal MCA was electrocoagulated (bipolar cautery) to induce local occlusion, resulting in ischaemia distal to the coagulation site and a cortical infarct. The wound was sutured, and a topical analgesic was applied. Buprenorphine (Vetergesic) 0.1 mg/kg in 0.5 mL of saline was administered subcutaneously. Post-operatively, mice were kept in a 30 °C incubator for 2 hours and then transferred to a heated cabinet (27 °C) overnight, with a second dose of buprenorphine administered the following morning. Sham animals underwent identical procedures except that the MCA was not coagulated.

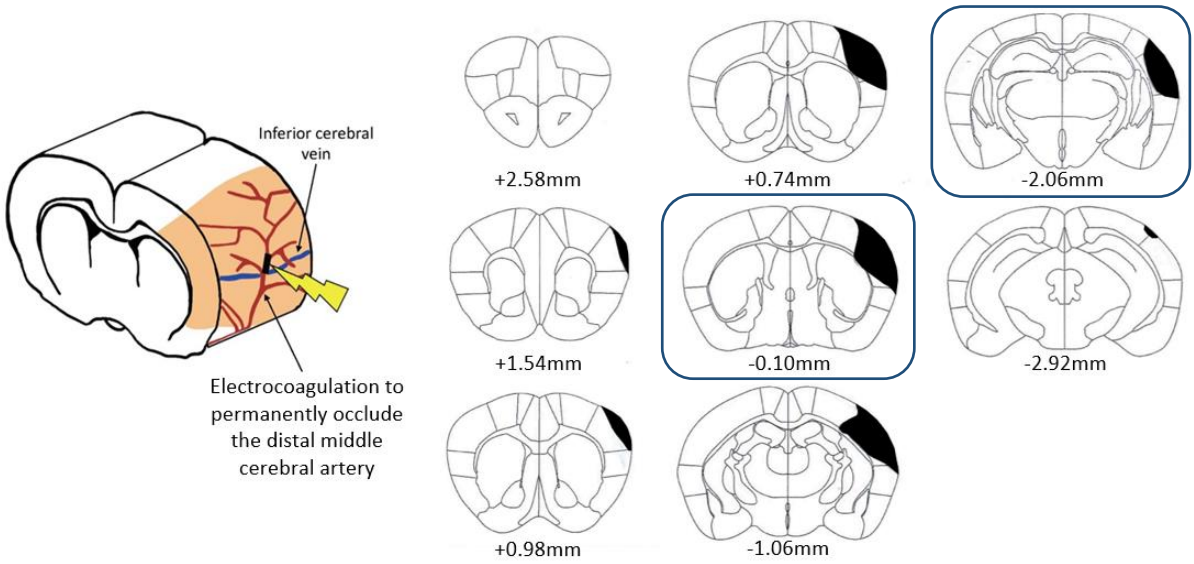

Figure 3.2 Distal middle cerebral artery occlusion surgery (dMCAO). Mouse model of ischaemic stroke by permanent occlusion of the distal middle cerebral artery and resulting cortical infarcts at bregma level +1.54mm to -2.92mm (black area). One striatal Bregma level -0.10, which corresponds with the initial injury site and one hippocampal Bregma level -2.06, further away from the primary lesion (circled in blue), were chosen for analysis.

3.2 Tissue processing

Recipes for the reagents and buffers used are defined in Appendix A, including phosphate buffer (PB), phosphate-buffer saline (PBS), tris buffer (TB), and paraformaldehyde (PFA). Four weeks post-surgery, mice were anaesthetised in isoflurane and transcardially perfused with 0.9% phosphate-buffered saline. Brains were dissected and fixed in 4% paraformaldehyde in PBS for 24 hours. After fixation, the forebrain was cut into two at (approx. Bregma -1.06) then rinsed under running water for 30 minutes, then dehydrated in 70% ethanol twice for 30 minutes each, followed by 90% ethanol twice for 30 minutes each, and finally 100% ethanol twice for 30 minutes each. Samples were cleared in xylene twice for 30 minutes each, infiltrated with paraffin wax in an oven at 60°C through three changes for 30 minutes each,

and held in molten wax overnight. The following morning, brains were paraffin-embedded in moulds, and the blocks were stored at 4 °C until sectioning. Sections were cut at 6 µm on a Leica RM 2235 microtome by Yaren Dogru and stored at room temperature.

3.3 Magnetic resonance imaging (MRI)

Mice underwent MRI scans 24 hours before surgery and 1 month post-surgery. Structural (T2-weighted), blood flow (arterial spin labelling), and white matter (diffusion tensor imaging, including fractional anisotropy and mean diffusivity) scans were taken at each time point for each mouse. During scanning, Yaren Dogru monitored the mice and recorded their temperature and breathing rates. All MRI scans were performed by Dr Jill Fowler and Mr Ross Lennon.

In vivo MRI was performed on a 9.4T horizontal-bore Biospec AVANCE neo preclinical imaging system equipped with a 116 mm bore gradient insert (Bruker BioSpin GmbH, Germany; maximum gradient strength 660 mT/m). Mice were anaesthetised with 1.5–2% isoflurane (Zoetis Ltd., London UK) in oxygen/air (50/50, 1 L/min) and secured in a cradle Bruker BioSpin GmbH, Germany). For each mouse, the respiration rate and rectal temperature were monitored (Model 1030 monitoring and gating system, Small Animal Instruments Inc. Stony Brook, NY, USA), with body temperature maintained at 37°C by a heat fan. An 86 mm volume RF coil (Bruker BioSpin GmbH, Germany) was used for transmission with signal reception by a four-channel phased-array mouse brain coil (Bruker BioSpin GmbH, Germany).

Localiser images were acquired in three planes to confirm correct positioning, and the magnetic field was optimised using an automated 3D field-mapping routine (mapshim).

For anatomical imaging, 34 axial slices covering the entire brain were acquired using a T2-weighted Rapid Acquisition with Relaxation Enhancement (RARE) sequence with the following parameters: field of view 18 x 18 mm, slice thickness 0.5mm, matrix size 260 × 260, TR 3600 ms, TE 44 ms, RARE factor 8, and number of signal averages 2. Each T2 scan per mouse lasted approximately 3 minutes and 43 seconds.

The perfusion imaging MRI protocol used a FAIR (Flow-sensitive Alternative Inversion Recovery) EPI sequence. Two 1mm slices (with a 1mm gap) were positioned at the frontal and midbrain levels based on anatomical scans to ensure consistent brain-level placement across mice. The field of view was 18 x 18 mm, with an acquisition matrix of 96 x 96. Cerebral blood flow maps were generated in Paravision 360 v3.3. Scan time per mouse was 9 minutes 27 seconds.

The diffusion tensor MRI protocol consisted of sets of T2-weighted and diffusion-weighted (b = 670s/mm^2) Echo Planar Imaging (EPI) volumes acquired with diffusion gradients applied in 30 non-collinear directions, producing a total of 35 volumes. A total of 23 axial slices were acquired with a field view of 18 × 18 mm, acquisition matrix 108 × 108 and slice thickness

0.74mm. The TR and TE times for each EPI volume were 2000 ms and 16.93 ms, respectively, and the scan time per mouse was 4 minutes 10 seconds. DTI parameter maps were generated in Paravision 360 v3.3.

To quantify the MRI data, ImageJ software was used. All T2-weighted scans were opened in ImageJ, and regions of interest (ROIs) were selected and saved, as shown in Figure 3.4. The same ROIs were subsequently applied to the ASL and DTI scans to extract corresponding quantitative values. Due to differences in image resolution, direct ROI transfer between T2 and ASL did not result in perfect alignment and required manual adjustment to ensure that equivalent anatomical regions were sampled across all images.

3.4 Histology and Immunohistochemistry

3.4.1 Immunofluorescence

For all primary antibodies (see Table 3.1), 2 brain sections were immunostained at two coronal levels (Bregma -0.10 and Bregma -2.06). For each antibody, a series of optimisation experiments was conducted using different incubation conditions and antibody concentrations to determine the optimal condition for each parameter. All immunohistochemistry experiments included a negative control, which was from the same cohort of mice. This section did not receive incubation with the primary antibody, and minimal immunostaining was detected in this control.

	Primary Antibody					*Secondary Antibody*		
Target	**Host**	**Supplier**	**Dilution**	**Heat Retrieval**	**Serum**	**Target**	**Supplier**	**Dilution**
GFAP	Rat	Invitrogen 13-0300	1:400	110°C	Goat	Goat anti-Rat Alexa fluor 555	Invitrogen A21434	1:500
IBA1	Rabbit	Abcam ab178847	1:2,000	90°C	Goat	Goat anti-Rabbit Alexa fluor 488	Invitrogen A11008	1:500
MAG	Mouse	Abcam ab89780	1:2,000	90°C	Goat	Goat anti-Mouse Alexa fluor 546	Invitrogen A11003	1:500
NeuN	Rat	Abcam ab279297	1:2,500	110°C	Goat	Goat anti-Rat Alexa fluor 488	Invitrogen A11006	1:500

Table 3.1. Details of the primary and secondary antibodies used for immunofluorescence. All dilutions were optimised before experimentation.

To remove paraffin medium, sections were put in a 60°C oven for 30 minutes. After ensuring the wax had completely melted, sections were placed in xylene (2 × 15 minutes), then hydrated in 100% ethanol (2 × 5 minutes), 90% ethanol for 2 minutes, and 70% ethanol for another 2 minutes. To improve antigenicity, sections underwent citrate heat retrieval in a 10mM citrate buffer (pH 6.0) at either 90°C or 110°C under pressure for 10 minutes (BioCare, Decloaking Chamber) (Table 3.1). After heat retrieval, sections were equilibrated in PBS (2 × 5 minutes) before being placed in a humidified chamber in a block for 1 hour at room temperature. A hydrophobic pen (Vector, Immedge pen) was used to outline the slide, ensuring that all of the solutions (100 µl) would remain on the sections. After this hour, the block was drained, and sections were incubated in primary antibody (100 µl/slide) in blocking solution at 4°C overnight in a humidified chamber. The negative control sections remained in the block only.

The following day, the slides were removed from the cold room, left to sit at room temperature for 10 minutes, and then washed twice in PBS for 10 minutes each. Slides were then incubated in humidity chambers with the appropriate secondary antibody in PBS (1:500, Vector) for two hours at room temperature. Sections were washed in PBS (twice, 10 minutes each) and TB (once, 10 minutes), then mounted in Vectashield with DAPI.

3.4.2 Immunohistochemistry

To remove paraffin medium, sections were put in a 60°C oven for 30 minutes. After ensuring the wax had melted completely, sections were placed in xylene (2 × 15 minutes) and endogenous peroxidase was quenched using 3% H_2O_2 in methanol for 30 minutes. The sections were then washed in running water for 15 minutes. Antigen retrieval was performed to enhance antigenicity using 10 mM citrate buffer (pH 6.0) at 110°C under pressure for 10 minutes (BioCare, Decloaking Chamber). After cooling, sections were equilibrated in PBS (twice, 5 minutes each) before being placed in a humidified chamber in a block for 1 hour at room temperature. A hydrophobic pen (Vector, Immedge pen) was used to outline the slide, ensuring that all block (100 µl) would remain on the sections. After this hour, the block was drained, and sections were incubated in the appropriate primary antibody (100 µl/slide) in blocking solution at 4°C overnight in a humidified chamber (Table 3.2). The negative control sections remained in the block only.

The following day, the slides were removed from the cold room, left to sit at room temperature for 10 minutes, and then washed twice in PBS for 10 minutes each. They were then incubated in the appropriate secondary antibody diluted in PBS for 1 hour at room temperature (Table 3.2). Sections underwent a signal amplification step with the ABC elite kit for 1hour, followed by PBS washes. Visualisation of peroxidase activity was carried out using 3,3’ diaminobenzidine tetrahydrochloride (DAB) substrate kit. DAB was placed on each section for 3 minutes. Sections were placed in running water, dehydrated through a series of ethanol dilutions (70% for 2 mins, 90% for 2 mins, 100% for 2x5 mins), placed in xylene for 10

minutes and mounted with DPX. Yaren Dogru performed all immunofluorescence and APP DAB immunohistochemistry.

Primary Antibody					*Biotinylated Secondary Antibody*		
Target	**Host**	**Supplier**	**Dilution**	**Serum**	**Target**	**Supplier**	**Dilution**
APP	Mouse	Millipore MAB348	1:5,000	Horse	Horse anti-Mouse	Vector BA-2000	1:100

Table 3.2. Details of the primary and secondary antibodies used for immunohistochemistry. The dilution used was optimised before experimenting.

3.5 Image Acquisition and Quantification

GFAP and Iba1 immunostained sections were used to understand reactive astrocyte and microglial/macrophage cell responses. As shown in Figure 3.4, 2 coronal levels were examined (Bregma -0.10 and Bregma -2.06). Small regions of the corpus callosum were analysed because the CC is known to undergo secondary white matter degeneration after cortical stroke, and periventricular callosal fibres may be particularly susceptible to microenvironmental disturbances (Z. Li et al. 2021; Huang et al. 2024). Images from GFAP and Iba1-stained sections were captured with a ZEISS AxioScan.Z1 slide scanner with a 20x objective magnification. Images were then processed into an 8-bit TIFF format and converted to greyscale using ZEN 2.1 SP1 (LSM800 edition). Quantification for GFAP and Iba1 was achieved by calculating the percentage area expression using ImageJ (Fiji, Version 2.14.0) software. For GFAP, auto-threshold was applied using 'Moments'. For Iba1, due to variability in the background intensity, each image was manually optimised in a blinded manner to ensure consistency.

APP immunostaining was quantified under a brightfield microscope. Two regions of interest (ROIs; each 0.05 mm^2) were defined per anatomical region in both hemispheres with two technical replicates. APP immunostaining was evaluated by manually counting the number of axonal bulbs and taking the average from two ROIs across two sections for statistical analysis.

MAG immunostaining was used to evaluate disruption of the axon-myelin integrity. Myelin damage was determined as the presence of disorganised white matter fibres and myelin debris, graded from 0 (no disorganisation) to 3 (extensive disruption of axon-myelin integrity) (Figure 3.3). Myelin damage was graded in all the regions of interest (Figure 3.4) and averaged in two technical replicates of each of the two coronal levels to get an overall myelin damage score.

To further investigate neuronal damage and loss in the thalamus and striatum, NeuN immunostaining was used. Corresponding images of the ROIs were obtained using the brightfield/fluorescent microscope and analysed in ImageJ. In the striatum, we quantified neuronal loss as total cell count. In the thalamus, we were interested in 3 thalamic nuclei: the

reticular thalamic nucleus (RTN), the ventral posteromedial (VPM), and the ventral posterolateral (VPL) nuclei. Since the RTN is smaller in size compared to the VPM and VPL, neuronal loss was quantified as neuronal density (neurons per mm^2) rather than total cell counts. This ensured consistent and comparable assessment of secondary neurodegeneration across different anatomical sizes.

Regions of interest are outlined in Figure 3.4. As shown in the figure, rectangular ROIs of the same size were used at all anatomical levels for the analysis of the cortex and the internal capsule. For the analysis of the striatum and thalamus, spheres of the same size were used for all anatomical levels. For corpus callosum analysis, ROIs were manually delineated to separately assess the midline, peri-lesion, and external capsule white matter regions. For all the regions, values from two adjacent sections were obtained, and their values were averaged for all counts and density analysis. All analyses were performed using ImageJ software.

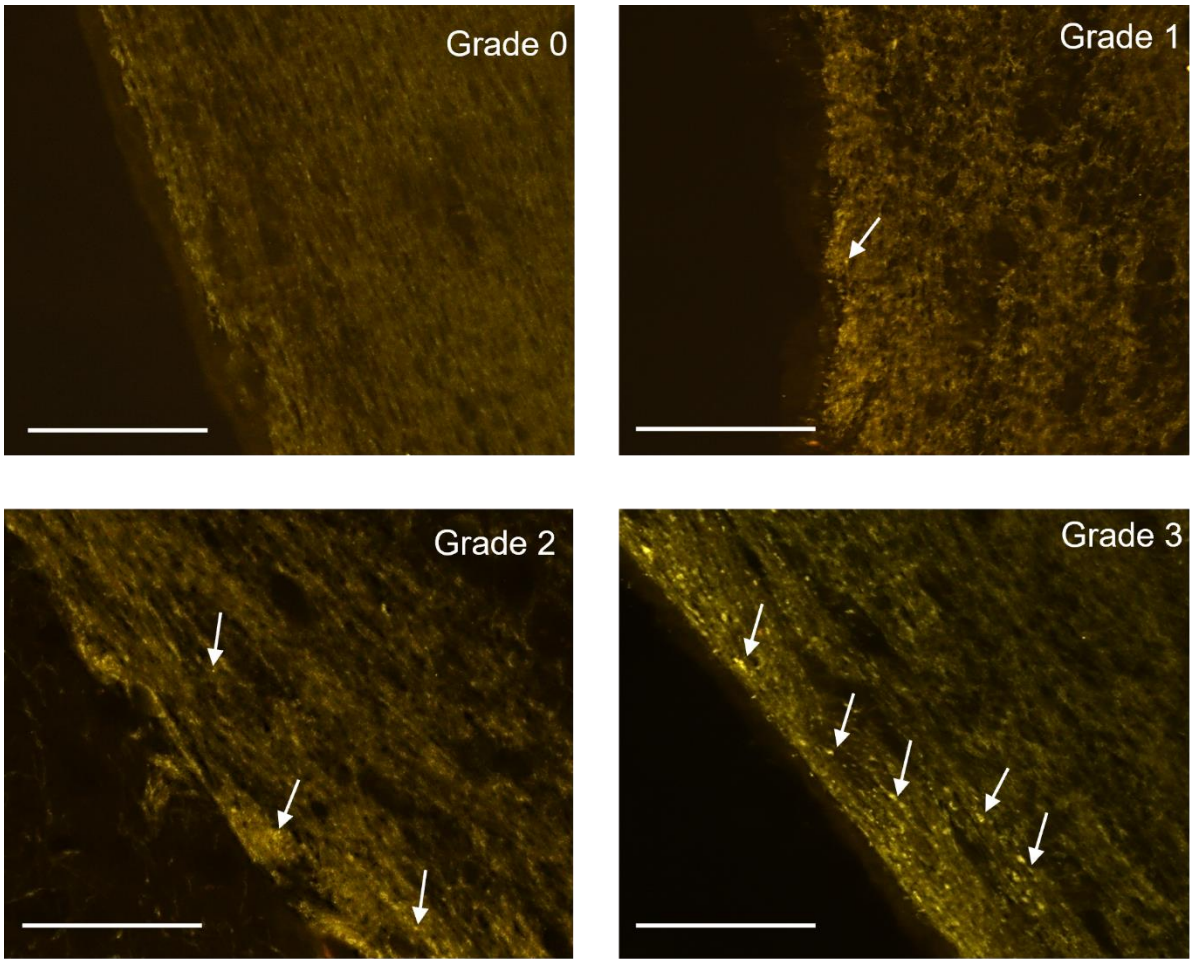

Figure 3.3 Grading scale used to score myelin integrity in the ROIs. Damage was graded as follows: Grade 0 – normal myelin integrity, Grade 1 – minimal myelin debris, slight disorganisation of fibres and vacuolation, Grade 2 – modest myelin debris, disorganisation of fibres and vacuolation, Grade 3 – severe myelin debris, extensive disorganisation of fibres and vacuolation. Images are magnified at 40X, and arrows show the myelin debris. Scale bar 50µm.

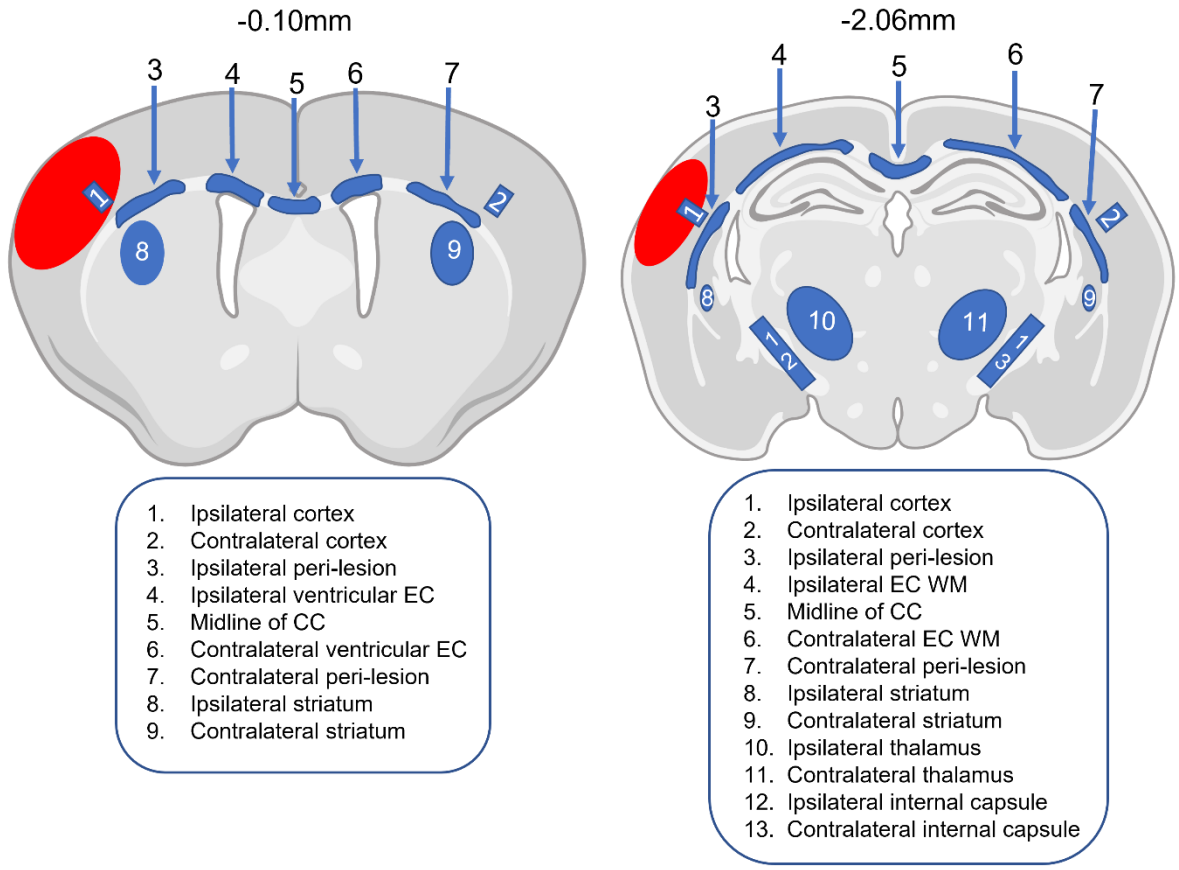

Figure 3.4. Bregma Stereotaxic Levels and the regions of interest of the mouse brain used for analysis. Labelled regions were manually delineated in the contralateral and ipsilateral hemispheres at bregma -0.10 and -2.06. Cell count analysis in all indicated regions was performed using two regions of interest boxes (each 0.05 mm²) placed in both the contralateral and ipsilateral hemispheres. The red circle represents the infarcted cortex, where the area it affects is slightly smaller, further away from the primary site. In bregma -0.10, areas 3 to 7 are parts of the corpus callosum, where 3 and 7 are part of the external capsule along the white matter tracts and 4 and 6 are right above the ventricles. In bregma -2.06, regions 3 to 7 are the entire corpus callosum where 4 and 6 represent the external capsule along the white matter tracts and 3 and 7 are perilesional white matter tracts right above the ventricles. For density analysis, the entire region was assessed, and the mean of two adjacent sections per region was used for statistical analysis.

3.6 Statistical Analysis

Graphpad Prism 10.0 software was used to create the graphs and analyse both immunohistochemistry and MRI data. Statistical tests used are outlined in Table 3.3. Due to missing values within some datasets, a mixed-effects model was chosen instead of a repeated-measures ANOVA, as the latter cannot incorporate missing data points. The mixed-effects model accounts for within-subject variability while retaining all available data. These results are valid under the assumption that missing values occurred at random (i.e., not systematically related to the measured outcome). Data are presented as mean ± SEM for all analyses and graphs. Significance was assumed when $p<0.05$ for all tests performed. During image acquisition, the experimenter was blinded to the surgery groups. Animal codes were broken for the final stage of statistical analysis.

Statistical Test	Measure
3-way ANOVA	Used to investigate the effect of time (pre- vs. post-surgery), surgery (sham vs. stroke) and hemisphere (contralateral vs. ipsilateral) on cerebral blood flow, fractional anisotropy and mean diffusivity in peri-lesion, ventricular external capsule, striatum, thalamus, cortex and internal capsule. Homogeneity of variances was confirmed (Levenes test >0.05). Normal distribution was assessed by visual inspection of QQ plots and a histogram of residuals. Due to the small sample size per group, formal normality tests could not be performed. Bonferroni adjustment is used for all post-hoc analyses to compare the differences within surgery, hemisphere and time.
2-way mixed-effects ANOVA	Used to investigate the effect of time (pre- vs. post-surgery) and surgery on cerebral blood flow, fractional anisotropy, and mean diffusivity in the midline of the corpus callosum Used to investigate the effect of surgery and hemisphere (ipsilateral vs. contralateral) on astrocyte reactivity, microglia activation, axonal damage and neuron loss. Bonferroni adjustment is used for all post-hoc analyses.
Kruskal-Wallis	Used to investigate differences in myelin damage (assessed with MAG immunofluorescence) between different hemispheres of stroke and sham surgeries. Dunn's adjustment was used for post-hoc analysis. Non-parametric test was chosen due to violations of the assumptions of equal variance and normality.
Mann-Whitney U test	Used to investigate myelin damage in sham vs. stroke mice in the corpus callosum Non-parametric test was chosen to compare two independent groups.

Table 3.3. Statistical tests used for data analysis. Statistical significance was set at 5% ($\alpha = 0.05$).

4. Results

4.1 Post-stroke weight loss

To ensure that all animals recovered well from surgery, we monitored their body weight both before and after the surgeries (Appendix B). Body weight decreased transiently in both sham and stroke groups after surgery, with a significant main effect of time ($F_{(9,70)}$=2.809; P=0.0071). However, there was no effect of surgery or surgery and time interaction (P>0.05), indicating that stroke induction did not produce additional weight loss compared to sham. These data suggest that our MCAO model is well tolerated.

4.2 Magnetic resonance imaging revealed structural, cerebral blood flow and functional changes following ischaemic stroke

We first used MRI to assess structural changes, cerebral perfusion, and white matter microstructural integrity prior to stroke, and 4-weeks post-surgery. T2 allowed for observation of structural changes between control and MCAO mice, ASL enabled us to observe cerebral blood flow throughout the brain, and DTI enabled us to characterise white-matter microstructural changes using FA and MD.

4.2.1 T2- weighted MRI reveals structural alteration following ischaemic stroke

We first examined T2-weighted MRI scans to assess structural integrity in sham control mice. As shown in Figure 4.1, T2-weighted images obtained before and after sham surgery revealed normal cortical and subcortical anatomy, with no visible hyperintensities or structural abnormalities. There was no infarct in the cortex, and ventricles remain clearly defined, confirming that the surgical procedure itself did not result in tissue damage or alteration in brain morphology.

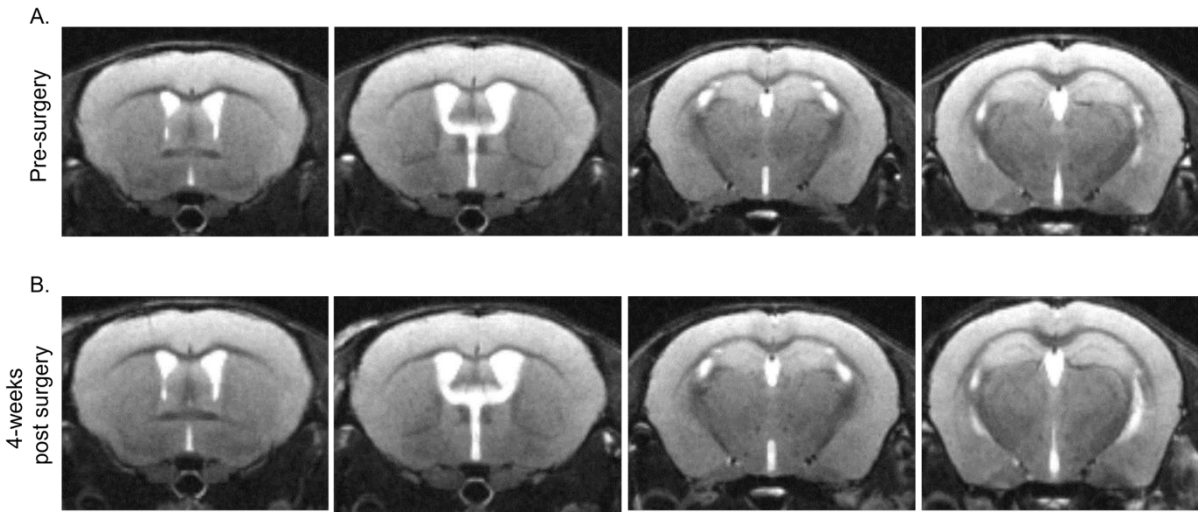

Figure 4.1. No lesion observed in the T2 MRI of sham controls. Multiple anatomical levels of a sham mouse are shown before (A) and after (B) sham surgery. No visible abnormalities are seen. No differences and hyperintensities are observed in the cortex and ventricles.

In contrast to sham controls, T2-weighted MRI scans from dMCAO mice revealed clear structural abnormalities within the ipsilateral hemisphere at 4 weeks post-surgery, as depicted in Figure 4.2. The cortex showed an apparent infarct, and the ventricles looked enlarged, consistent with tissue loss following ischaemic stroke. Additionally, a hypointense area was observed in the ipsilateral thalamus. These observations indicate primary cortical atrophy, accompanied by secondary changes in distant but anatomically connected areas following ischemic stroke.

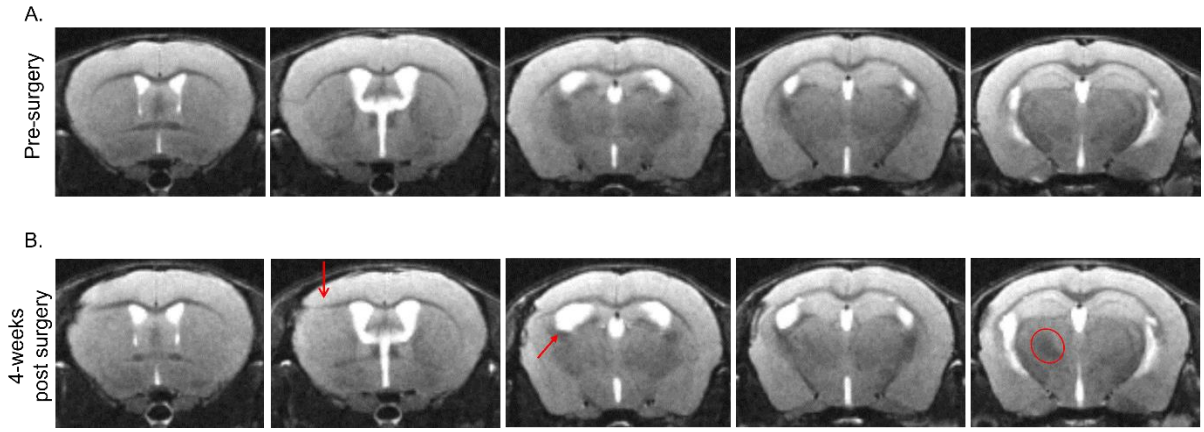

Figure 4.2. T2-weighted MRI reveals a cortical lesion following dMCAO stroke. Multiple anatomical levels of a dMCAO mouse are shown pre (A) and post (B) surgery. As shown by the arrows, at 4 weeks post-dMCAO surgery, there is a clear cortical infarct (open arrowhead) and ventricular enlargement (closed arrowhead). A hypointense area is also visible within the ipsilateral thalamus (circled).

4.2.2 Arterial spin labelling revealed cerebral blood flow changes following chronic ischaemic stroke

4.2.2.1 Hypoperfusion is observed in white matter regions following ischaemic stroke

Next, we examined CBF, firstly analysing the white matter of the external capsule and the corpus callosum. To capture spatial variation in white matter integrity due to potential region-specific vulnerability and non-uniform patterns of secondary degeneration, we were specifically interested in the midline of the CC, perilesional WM, and the external capsule, which correspond to the WM region above the ventricle at the rostral level (ventricular WM) and the lateral CC (external capsule WM) at the caudal level. In a healthy mouse pre-surgery, we usually observe higher CBF around the cortex, appearing red, consistent with the higher energy demands of grey matter (Iadecola 2004; Shen et al. 2005), and lower CBF in white matter structures, appearing blue. In sham animals, we also observed this, with the white matter structures showing no difference before and after surgery and mostly appearing blue (Figure 4.3A). In contrast, in the chronic response to ischaemic stroke, we observed a very dark blue region along the white matter closest to the stroke lesion, indicating reduced blood flow (hypoperfusion).

To quantify these changes, we analysed CBF using three-way ANOVA to determine the effects of stroke, time (pre- vs. post-surgery) and hemisphere (contralateral vs. ipsilateral). At a

rostral level of the brain, corresponding with caudate-putamen (bregma -0.10), we first examined the peri-lesion site. Our analysis showed there was an effect of time ($F_{(1,14)}$=25.16; P=0.0002), an interaction between time and hemisphere ($F_{(1,14)}$=13.53; P=0.0025), an interaction between hemisphere and stroke ($F_{(1,14)}$=4.872; P=0.044), and an interaction between hemisphere, stroke and time ($F_{(1,14)}$=19.38; P=0.0006). Bonferroni corrected post-hoc analysis showed a reduction in blood flow in the ipsilateral hemisphere following stroke, both compared to the contralateral hemisphere (P=0.0009) and to pre-surgery values within the same region (P<0.0001) (Fig. 4.3Bi). However, three-way ANOVA in the external capsule above the ventricle did not show significant effects of time, stroke or surgery or of an interaction between hemisphere, stroke and time (P>0.05) (Fig. 4.3Biii). Similarly, in the midline of the corpus callosum, two-way mixed-effects of ANOVA revealed no significant effect of time ($F_{(1,14)}$=1.74; P=0.21), stroke ($F_{(1,14)}$=1.47; P=0.25) or of an interaction between time and stroke ($F_{(1,14)}$=0.19; P=0.67) (Fig. 4.3Bii).

We next investigated the same white matter tracts in a caudal region of the brain corresponding with the hippocampal level (bregma -2.06) (Fig. 4.3Aii). In the peri-lesion, three-way ANOVA revealed a significant interaction between hemisphere and surgery ($F_{(1,14)}$=7.50; P=0.016), and an interaction between hemisphere and time ($F_{(1,14)}$=10.12; P=0.0067), as well as an interaction between hemisphere, time and surgery ($F_{(1,14)}$=4.71; P=0.047). Bonferroni corrected post-hoc analysis showed a reduction in blood flow in the ipsilateral hemisphere of the perilesion following stroke, both compared to the contralateral hemisphere (P=0.0096) and to pre-surgery values within the same region (P=0.041). In addition, post-stroke CBF in the ipsilateral perilesional white matter was significantly lower than in sham mice (P=0.016) (Fig. 4.3Ci). Similarly, along the external capsule, lateral to the midline of corpus callosum, three-way ANOVA revealed a significant interaction between hemisphere and time ($F_{(1,14)}$=10.95; P=0.0052) and an interaction between hemisphere, surgery and time ($F_{(1,14)}$=5.95; P=0.029). Post-hoc analysis showed a reduction in CBF in the ipsilateral stroke in ventricular EC compared to the contralateral groups (P=0.0081) (Fig. 4.3Ciii). In the midline of the corpus callosum, two-way mixed-effects ANOVA showed no significant effect of time ($F_{(1,4)}$=0.57; P=0.50), or surgery ($F_{(1,4)}$=0.89; P=0.40), or of an interaction between time and surgery ($F_{(1,2)}$=0.73; P=0.49) (Fig. 4.3Cii).

The internal capsule is another white matter region that is anatomically and functionally connected to the peri-infarct cortex, containing major thalamocortical fibres traversing the peri-infarct area; therefore, we examined CBF changes in the IC. Three-way ANOVA revealed significant effects of time ($F_{(1,14)}$=7.45; P=0.016), but not hemisphere or surgery, or of an interaction between any of them (P>0.05). Post hoc analysis revealed that there were no significant differences in CBF in the internal capsule caused by stroke or sham treatment (P>0.05) (Fig. 4.3Civ).

Together, ASL data revealed that white matter is vulnerable to blood flow changes after chronic stroke compared to sham. These findings showed that chronic ischaemic stroke leads to region-specific hypoperfusion within the ipsilateral white matter, particularly in the peri-

lesional white matter tracts. In contrast, distant white matter tracts such as the midline of the CC, contralateral external capsule and the internal capsule remain unaffected.

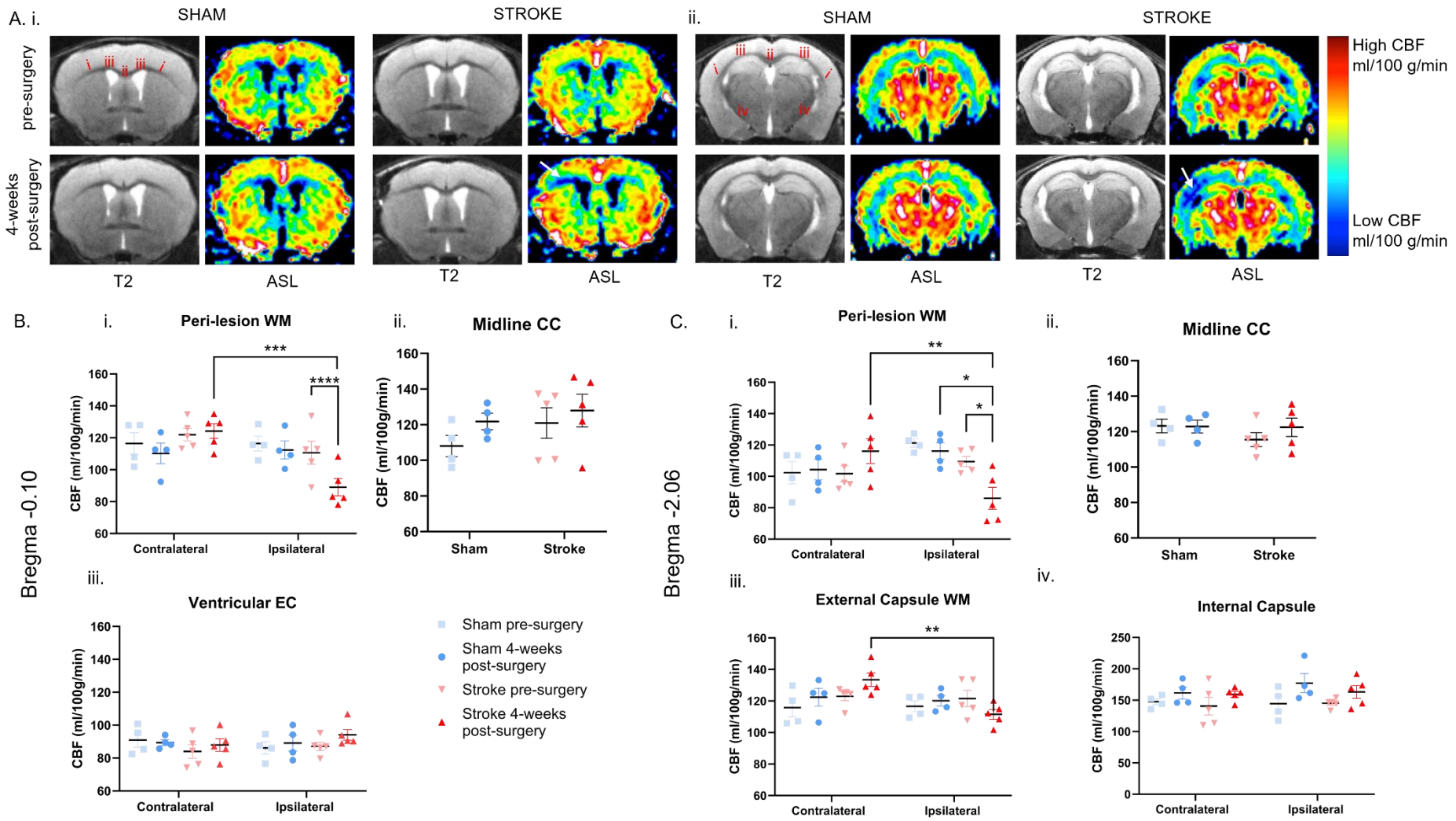
A. i.
SHAM
STROKE
ii.
SHAM
STROKE
pre-surgery
4-weeks post-surgery
T2
ASL
High CBF ml/100 g/min
Low CBF ml/100 g/min
B.
Bregma -0.10
i. Peri-lesion WM
ii. Midline CC
iii. Ventricular EC
CBF (ml/100g/min)
Contralateral
Ipsilateral
Sham
Stroke
Sham pre-surgery
Sham 4-weeks post-surgery
Stroke pre-surgery
Stroke 4-weeks post-surgery
C.
Bregma -2.06
i. Peri-lesion WM
ii. Midline CC
iii. External Capsule WM
iv. Internal Capsule

Figure 4.3. Representative ASL-derived CBF maps and corresponding quantitative analyses in control and stroke mice after 4-weeks post-surgery. (A) Representative T2 and corresponding ASL scans in sham and stroke mice in rostral (i) and caudal (ii) levels, respectively. White arrows show the hypoperfusion site in the white matter tract on both levels. Numbers on the T2 scans represent the areas of interest for analysis, each number corresponding to a graph in B. (B) Quantification of the CBF in the rostral level showed a reduction in ipsilateral peri-lesion WM compared to contralateral hemisphere (***P=0.0009) and pre-surgery (****P<0.0001) (i) with no changes in the midline of CC (ii; two-way mixed-effects ANOVA) and ventricular EC (iii) (P>0.05). (C) Quantification of the CBF in the caudal level showed a reduction in ipsilateral peri-lesion WM compared to the contralateral side (**P=0.0096), pre-surgery (*P=0.041), as well as sham (*P=0.016) (i), and reduction along the ipsilateral EC of stroke groups compared to contralateral groups (**P= 0.0081), with no changes in the midline of CC (ii; two-way mixed-effects ANOVA) and IC (iv). Data shown as mean ± SEM; individual animals overlaid (n=4 sham, 5 stroke). Three-way ANOVA with Bonferroni post hoc tests, except where indicated.

4.2.2.2 Cerebral blood flow fluctuates in grey matter regions

To further investigate cerebral blood flow changes within and beyond the lesion site, we analysed the cortex at both rostral and more caudal levels, along with the caudate-putamen and thalamus. The striatum and the thalamus are anatomically distant from the primary infarcted cortex but functionally connected grey matter regions.

We first examined the peri-infarct cortex, which lies very close to the primary lesion site and is likely to exhibit structural and functional alterations following stroke. In the cortex, at the rostral level, three-way ANOVA revealed significant effects of hemisphere ($F_{(1,14)}$=6.32; P=0.025), surgery ($F_{(1,14)}$=7.05; P=0.019), and an interaction between hemisphere and surgery ($F_{(1,14)}$=5.20; P=0.039), hemisphere and time ($F_{(1,14)}$=14.45; P=0.0019), surgery and time ($F_{(1,14)}$=17.97; P=0.0008), as well as an interaction between hemisphere, surgery and time ($F_{(1,14)}$=5.70; P=0.03). Bonferroni corrected post-hoc analysis showed a reduction in blood flow in the ipsilateral hemisphere following stroke, both compared to the contralateral hemisphere (P<0.0001) and to pre-surgery values within the same region (P=0.0009). In addition, post-stroke CBF in the ipsilateral cortex was significantly lower than in sham mice (P<0.0001) (Fig. 4.4Ai). Similarly, at the caudal level, three-way ANOVA revealed significant effects of surgery ($F_{(1,14)}$=5.37; P=0.036), time ($F_{(1,14)}$=7.46; P=0.016), and an interaction between hemisphere and surgery ($F_{(1,14)}$=5.87; P=0.029), hemisphere and time ($F_{(1,14)}$=10.45; P=0.0060), surgery and time ($F_{(1,14)}$=21.57; P=0.0004), as well as an interaction between hemisphere, surgery and time ($F_{(1,14)}$=9.47; P=0.0082). Post-hoc analysis showed a reduction in blood flow in the ipsilateral cortex following stroke, both compared to the contralateral hemisphere (P=0.0001) and to pre-surgery values within the same region (P<0.0001). In addition, post-stroke CBF in the ipsilateral cortex was significantly lower than in sham mice (P<0.0001) (Fig. 4.4Aii)

Next, we examined the caudate putamen because the striatum receives dense glutamatergic input from the somatosensory cortex. In the striatum at the rostral level, three-way ANOVA revealed significant effects of an interaction between hemisphere and time ($F_{(1,14)}$=6.05; P=0.028), with no interactions between hemisphere, time and surgery (P>0.05)(Fig. 4.4Bi). At the caudal level, three-way ANOVA did not reveal any significant effects of time, stroke, hemisphere or of an interaction between hemisphere, surgery and time (P>0.05) (Fig 4.4Bii).

Post hoc analysis showed no significant cerebral blood flow changes in the striatum at both coronal levels between the hemispheres and pre- and post-surgery(P>0.05) (Fig. 4.4B).

Lastly, we examined the thalamus because it receives dense reciprocal connections from the somatosensory cortex via thalamocortical projections. It also showed signal alterations on MRI (a hypointense region on T2) (Figure 4.2), prompting further investigation into their cellular correlates. Three-way ANOVA revealed significant effects of hemisphere ($F_{(1,14)}$=4.80; P=0.046), time ($F_{(1,14)}$=24.96; P=0.0002), and an interaction between hemisphere surgery and time ($F_{(1,14)}$=5.68; P=0.032). Bonferroni corrected post hoc analysis revealed increased cerebral blood flow in the ipsilateral thalamus in stroke animals compared to the contralateral hemisphere (P=0.024) and pre-surgery (P=0.0089) (Fig. 4.4C).

Together, these findings suggest region-specific alteration to CBF across grey matter regions following chronic ischaemic stroke. As expected, there is a persistent hypoperfusion in the lesioned cortex. A marked hypoperfusion in the cortex after stroke reflects metabolic impairment at the injury site. In contrast, no changes in the CBF were observed in the striatum, indicating preservation of cerebral blood flow in this region. Interestingly, hyperperfusion is observed in the thalamus, which may reflect compensatory or reactive changes in regions functionally connected to the injured cortex.

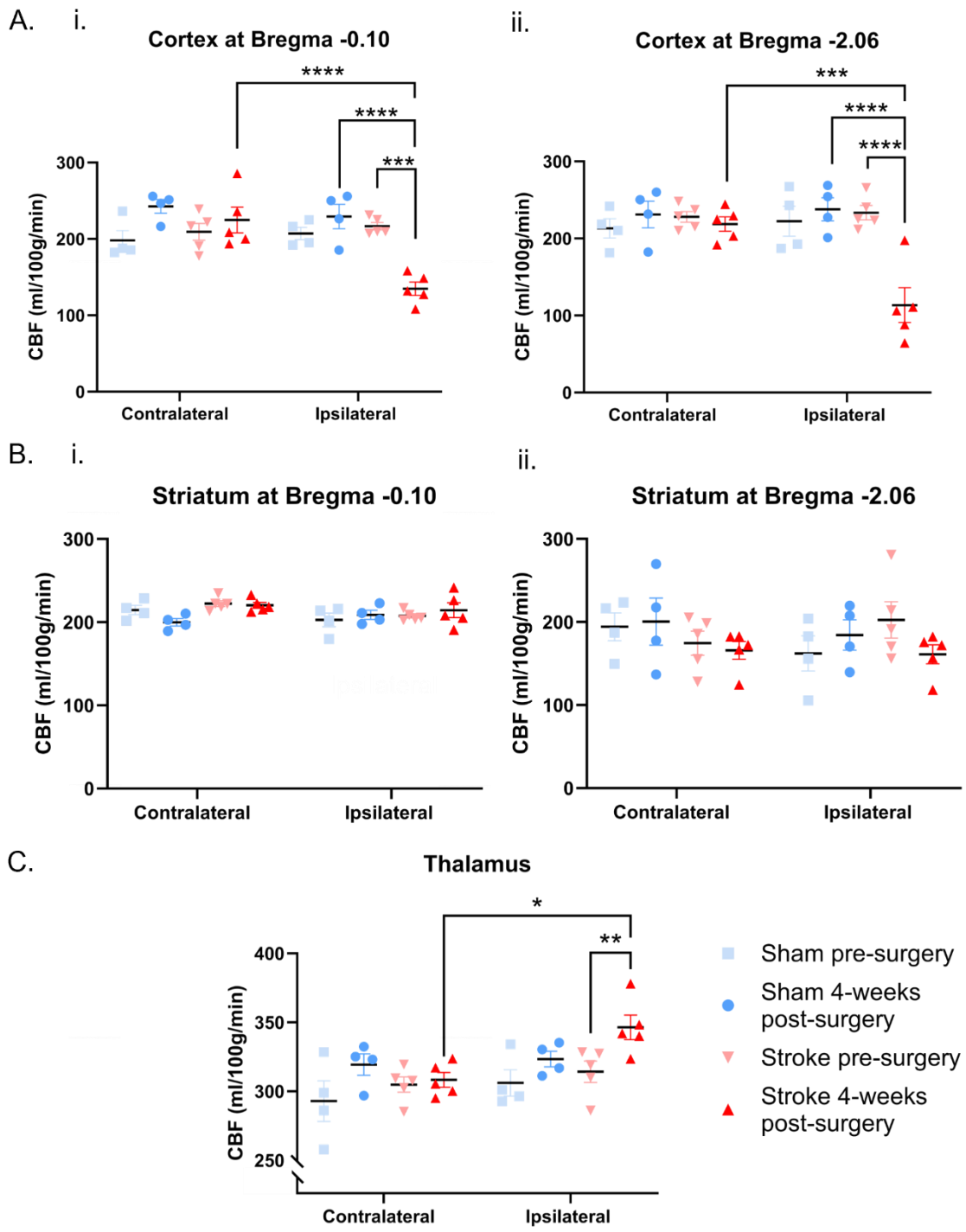

Figure 4.4. Quantitative analysis of CBF in grey matter regions following chronic ischaemic stroke. (A) Quantification of CBF in the ipsilateral cortex showed hypoperfusion at the rostral level compared to the contralateral side (****P<0.0001), pre-surgery (***P=0.0009) and sham group within the region (****P<0.0001) (i) and caudal level compared to the contralateral side (***P=0.0001), pre-surgery (****P<0.0001) and sham group within the region (****P<0.0001). (B) Quantification of CBF in the striatum at rostral (i) and caudal (ii) levels showed no changes in the blood flow (P>0.05). (C) Quantification of CBF in the ipsilateral thalamus revealed hyperperfusion in stroke compared to the contralateral side (*P=0.024) and pre-surgery (**P=0.0089). Data shown as mean ± SEM; individual animals overlaid (n=4 sham, 5 stroke). Three-way ANOVA with Bonferroni post hoc tests.

4.2.3 Diffusion tensor imaging reveals microstructural alterations in the brain following chronic ischaemic stroke

To further investigate white matter integrity, DTI was performed to assess microstructural changes through FA and MD metrics. FA measures the directionality of water diffusion and gives us information about the white matter fibre integrity (Le Bihan et al. 2001), whereas MD measures the average water diffusion and gives us information about the severity of tissue damage (Le Bihan et al. 2001). These measurable white matter changes are linked with cognitive decline in chronic stroke (Sagnier et al. 2020; Schaapsmeerders et al. 2016).

4.2.3.1 Chronic ischaemic stroke leads to an increase in FA in white matter tracts

Firstly, we examined FA in the white matter of the external capsule and the corpus callosum. In sham mice, FA scans appeared relatively stable, with no microstructural changes, whereas in stroke, the peri-lesion showed subtle microstructural changes, depicted in Figure 4.5A.

To quantify these changes, we analysed FA using three-way ANOVA to determine the effects of stroke, time, and hemisphere. At a rostral level of the brain, we first examined the peri-lesion site. Three-way ANOVA showed there was a significant effect of hemisphere ($F_{(1,14)}$=18.35; P=0.0008), an interaction between hemisphere and stroke ($F_{(1,14)}$=8.16; P=0.013), an interaction between time and stroke ($F_{(1,14)}$=9.83; P=0.0073), as well as an interaction between hemisphere, stroke and time ($F_{(1,14)}$=16.26; P=0.0012). Bonferroni corrected post-hoc analysis revealed a significant increase in FA in the ipsilateral perilesion following stroke, both compared to the contralateral hemisphere (P<0.0001) and to pre-surgery values within the same region (P=0.0024). In addition, post-stroke FA in the ipsilateral perilesion was significantly higher than in sham mice (P<0.0001) (Fig. 4.5Bi). Furthermore, in the external capsule above the ventricles, three-way ANOVA did not reveal significant effects of hemisphere, stroke and time, or of an interaction between the three (P>0.05) (Fig. 4.5Biii). Similarly, in the midline of the corpus callosum, two-way mixed-effects of ANOVA revealed no significant effect of time ($F_{(1,4)}$=0.43; P=0.55), stroke ($F_{(1,4)}$=2.84; P=0.18) or of an interaction between time and stroke ($F_{(1,2)}$=0.12; P=0.76) (Fig. 4.5Bii).

We next investigated the caudal region of the brain (Fig. 4.5Aii). In the peri-lesion, three-way ANOVA revealed significant effects of hemisphere ($F_{(1,14)}$=8.95; P=0.0097), stroke ($F_{(1,14)}$=6.43; P=0.024), and time ($F_{(1,14)}$=4.85; P=0.044), as well as an interaction between time and stroke ($F_{(1,14)}$=5.21; P=0.039). Bonferroni corrected post-hoc analysis showed increased FA in the ipsilateral perilesion following stroke, both compared to the contralateral hemisphere (P=0.0025) and to pre-surgery values within the same region (P=0.0058). In addition, post-stroke CBF in the ipsilateral perilesion was significantly lower than in sham mice (P=0.0085) (Fig. 4.5Ci). Similarly, along the external capsule, lateral to the midline of the corpus callosum, three-way ANOVA revealed significant effects of hemisphere ($F_{(1,14)}$=12.71; P=0.0031), and time ($F_{(1,14)}$=6.33; P=0.025), and an interaction between hemisphere, stroke and time ($F_{(1,14)}$=6.95; P=0.020). Post-hoc analysis showed a significant increase in FA in the ipsilateral

external capsule following stroke, both compared to the contralateral hemisphere (P=0.0004) and to pre-surgery values within the same region (P=0.013) (Fig. 4.5Ciii). In the midline of the corpus callosum, two-way mixed-effects ANOVA showed no significant effect of time ($F_{(1,4)}$=0.0081; P=0.93), or surgery ($F_{(1,4)}$=0.15; P=0.72), or of an interaction between time and surgery ($F_{(1,2)}$=7.04; P=0.12) (Fig. 4.5Cii).

In the internal capsule, a three-way ANOVA revealed no significant effects of stroke, time, hemisphere, or an interaction among the three (P>0.05) (Fig. 4.5Civ).

Together, these findings suggest localised increases in FA in the peri-lesional and adjacent external capsule white matter following stroke. In contrast, other major white matter tracts, such as the midline of the corpus callosum and the internal capsule, remain relatively unaffected.

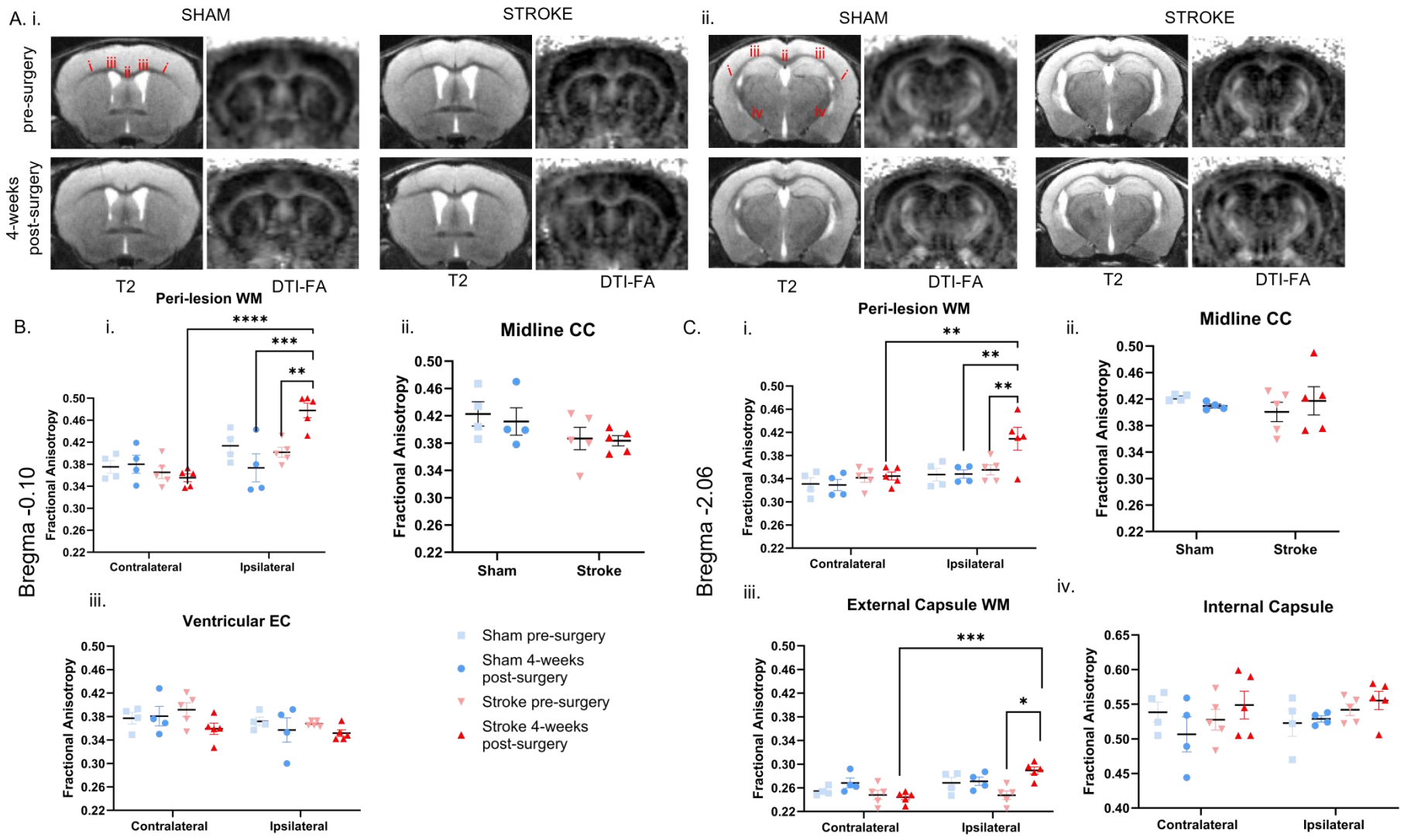
A. i.
SHAM
STROKE
ii.
SHAM
STROKE
pre-surgery
4-weeks post-surgery
i
ii
iii
iv
T2
DTI-FA
B.
Bregma -0.10
Peri-lesion WM
Midline CC
Ventricular EC
Fractional Anisotropy
Contralateral
Ipsilateral
Sham
Stroke
Sham pre-surgery
Sham 4-weeks post-surgery
Stroke pre-surgery
Stroke 4-weeks post-surgery
C.
Bregma -2.06
External Capsule WM
Internal Capsule

Figure 4.5. Representative DTI-FA maps and corresponding quantitative analyses in control and stroke mice after 4-weeks post-surgery. (A) Representative T2 and corresponding FA scans in sham and stroke mice in rostral (i) and caudal (ii) levels, respectively. Numbers on the T2 scans represent the areas of interest for analysis, each number corresponding to a graph in B. (B) Quantification of the FA in the rostral level showed an increase in ipsilateral peri-lesion WM compared to contralateral hemisphere (****P<0.0009), pre-surgery (**P=0.0024) and sham (***P=0.001) (i) with no changes in the midline of CC (ii; two-way mixed-effects ANOVA) and ventricular EC (iii) (P>0.05). (C) Quantification of the FA in the caudal level showed an increase in ipsilateral peri-lesion WM compared to contralateral hemisphere (**P=0.0025), pre-surgery (**P=0.0058) and sham (**P=0.0085) (i) and an increase along the ipsilateral EC of stroke groups compared to contralateral groups (***P= 0.0004) and pre-surgery (*P=0.013), with no changes in the midline of CC (ii; two-way mixed-effects ANOVA) and IC (iv). Data shown as mean ± SEM; individual animals overlaid (n=4 sham, 5 stroke). Three-way ANOVA with Bonferroni post hoc tests, except where indicated.

4.2.3.2 Chronic ischaemic stroke leads to a slight increase in FA in grey matter regions

To further investigate fibre integrity and compare it with the white matter, we examined the cortical lesion site at rostral and caudal levels, along with anatomically connected grey matter regions, such as the thalamus and the striatum. The thalamus exhibited a hypointense region on T2-weighted structural scans following stroke, indicating potential secondary degeneration or altered connectivity with the peri-lesional white matter. Therefore, we quantified FA and MD within these regions to assess whether diffusion changes extended to connected grey matter nuclei, providing insight into widespread microstructural alterations associated with chronic ischemic stroke.

In the cortex, at the rostral level, three-way ANOVA revealed significant effects of hemisphere ($F_{(1,14)}$=57.71; P<0.0001), stroke ($F_{(1,14)}$=28.30; P=0.0001), time ($F_{(1,14)}$=20.13; P=0.0005) and an interaction between hemisphere and stroke ($F_{(1,14)}$=17.96; P=0.0008), hemisphere and time ($F_{(1,14)}$=16.06; P=0.0013), stroke and time ($F_{(1,14)}$=17.24; P=0.0010), as well as an interaction between hemisphere, surgery and time ($F_{(1,14)}$=22.34; P=0.0003). Post-hoc analysis revealed a significant increase in FA in the ipsilateral cortex following stroke, both compared to the contralateral hemisphere (P<0.0001) and to pre-surgery values within the same region (P<0.0001). In addition, post-stroke FA in the ipsilateral cortex was significantly higher than in sham mice (P<0.0001) (Fig. 4.6Ai). At the caudal level, three-way ANOVA revealed significant effects of hemisphere ($F_{(1,14)}$=11.01; P=0.0051) and stroke ($F_{(1,14)}$=5.11; P=0.040) but not their interactions (P>0.05). Post-hoc analysis revealed a significant increase in FA in the ipsilateral cortex following stroke compared to the contralateral hemisphere (P=0.0028) (Fig. 4.6Aii).

In the striatum at the rostral level, three-way ANOVA revealed significant effects of hemisphere ($F_{(1,14)}$=6.27; P=0.025), stroke ($F_{(1,14)}$=6.59; P=0.022), time ($F_{(1,14)}$=9.90; P=0.0071), and an interaction between hemisphere and stroke ($F_{(1,14)}$=7.83; P=0.014), interaction between stroke and time ($F_{(1,14)}$=4.66; P=0.049), as well as an interaction between hemisphere, stroke and time ($F_{(1,14)}$=11.07; P=0.0050). Post-hoc analysis revealed a significant increase in FA in the ipsilateral striatum following stroke, both compared to the contralateral hemisphere (P<0.0001) and to pre-surgery values within the same region (P=0.0008). In

addition, post-stroke FA in the ipsilateral thalamus was significantly higher than in sham mice (P=0.0001) (Fig. 4.6Bi). At the caudal level, a three-way ANOVA showed a significant effect of stroke ($F_{(1,14)}$=6.73; P=0.021) but not hemisphere, time or an interaction between them (P>0.05) (Fig. 4.6Bii).

In the thalamus, three-way ANOVA revealed significant effects of an interaction between hemisphere and stroke ($F_{(1,14)}$=6.07; P=0.027) and an interaction between time and stroke ($F_{(1,14)}$=6.29; P=0.025). Bonferroni corrected post-hoc analysis revealed a significant increase in FA in the ipsilateral thalamus following stroke, both compared to the contralateral hemisphere (P=0.012) and to pre-surgery values within the same region (P=0.021). In addition, post-stroke FA in the ipsilateral thalamus was significantly higher than in sham mice (P=0.0019) (Fig. 4.6C).

Together, these findings demonstrate widespread post-stroke increases in FA across multiple grey matter regions, suggesting extensive microstructural remodelling in cortical and subcortical areas.

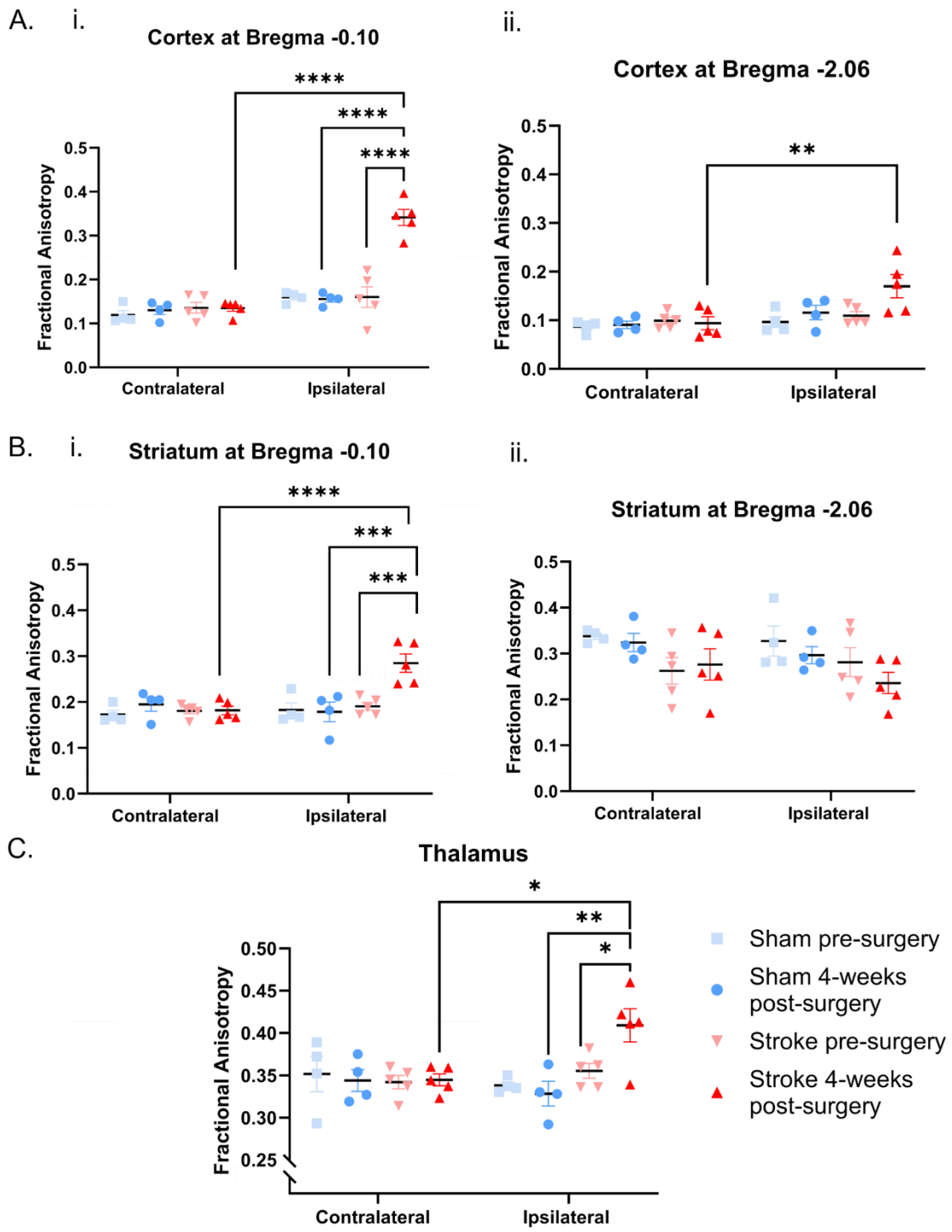

Figure 4.6. Quantitative analysis of FA in grey matter regions following chronic ischaemic stroke. (A) Quantification of FA in the cortex at rostral (i) and caudal (ii) levels revealed increased FA in the ipsilateral cortex at both levels compared to the contralateral hemisphere (****P<0.0001, **P=0.0028), pre-surgery (****P<0.0001) and sham (****P<0.0001). (B) Quantification of FA in the striatum at rostral (i) and caudal (ii) levels showed a significant increase in the ipsilateral striatum at the rostral level compared to the contralateral hemisphere (****P<0.0001), pre-surgery (***P=0.0008), and sham (***P=0.0001), while no changes were observed at the caudal level (P>0.05). (C) Quantification of FA in the thalamus revealed a significant increase in the ipsilateral hemisphere following stroke compared to the contralateral side (*P=0.012), pre-surgery (*P=0.021), and sham (**P=0.0019). Data shown as mean ± SEM; individual animals overlaid (n=4 sham, 5 stroke). Three-way ANOVA with Bonferroni post hoc tests.

4.2.3.3 MD is unchanged in white matter tracts following chronic ischaemic

To further investigate the severity of tissue damage, we next examined MD in the white matter of the external capsule and corpus callosum (Fig. 4.7A).

To quantify these changes, we analysed MD using three-way ANOVA to determine the effects of stroke, time, and hemisphere. At a rostral level of the brain, we first examined the peri-lesion site. Three-way ANOVA showed a significant effect of hemisphere ($F_{(1,14)}$=10.79; P=0.0054) and stroke ($F_{(1,14)}$=25.16; P=0.0002), with no significant interactions between them. Bonferroni corrected post-hoc analysis revealed no significant change in MD in perilesion following stroke (P>0.05) (Fig. 4.7Bi). Furthermore, in the external capsule above the ventricles, three-way ANOVA did not reveal significant effects of hemisphere, stroke and time, or of an interaction between the three (P>0.05) (Fig. 4.7Biii). Similarly, in the midline of the corpus callosum, two-way mixed-effects of ANOVA revealed no significant effect of time ($F_{(1,14)}$=0.81; P=0.38), stroke ($F_{(1,14)}$=1.08; P=0.32) or of an interaction between time and stroke ($F_{(1,14)}$=0.0041; P=0.95) (Fig. 4.7Bii).

We next investigated the caudal region of the brain (Fig. 4.7Aii). In the peri-lesion, a three-way ANOVA did not reveal significant effects of hemisphere, stroke, or time, or an interaction among the three (P>0.05) (Fig. 4.7Ci). Furthermore, along the external capsule, lateral to the midline of the corpus callosum, three-way ANOVA revealed a significant effect of time ($F_{(1,14)}$=6.76; P=0.021), with no effects of stroke, hemisphere, or the interaction between time and hemisphere (P>0.05). Post-hoc analysis showed no significant changes in MD in the external capsule following stroke (P>0.05) (Fig. 4.5Ciii). In the midline of the corpus callosum, two-way mixed-effects ANOVA showed no significant effect of time ($F_{(1,4)}$=0.42; P=0.55), or surgery ($F_{(1,4)}$=1.74; P=0.26), or of an interaction between time and surgery ($F_{(1,2)}$=1.03; P=0.42) (Fig. 4.7Cii).

In the internal capsule, a three-way ANOVA revealed no significant effects of stroke, time, hemisphere, or an interaction among the three (P>0.05) (Fig. 4.7Civ).

In summary, MD values in white matter regions did not show significant alterations following stroke, suggesting no measurable diffusion-related tissue damage within the external capsule, corpus callosum, or peri-lesion white matter.

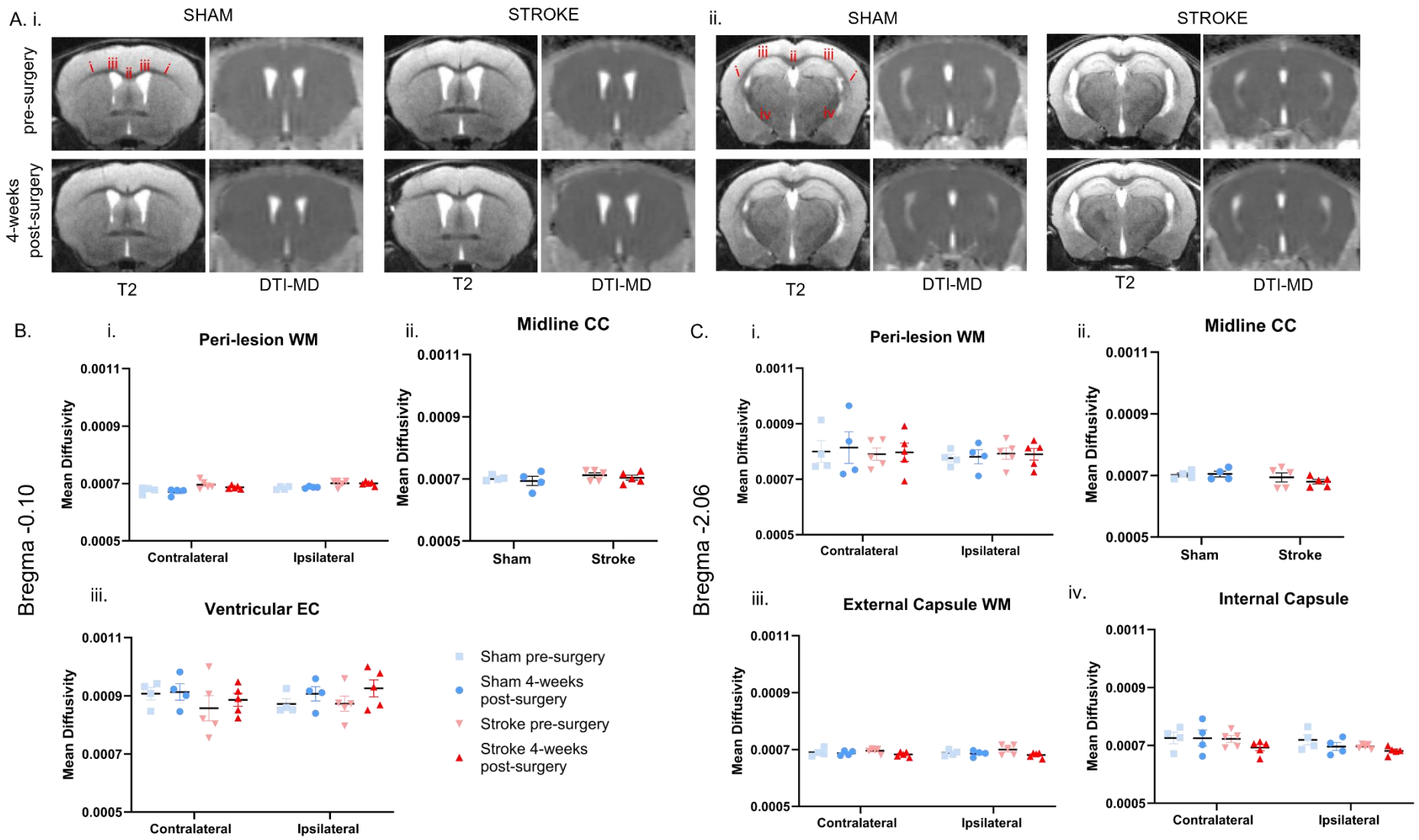
A. i.
SHAM
STROKE
ii.
SHAM
STROKE
pre-surgery
4-weeks post-surgery
i
ii
iii
iv
T2
DTI-MD
B.
Bregma -0.10
i.
Peri-lesion WM
ii.
Midline CC
iii.
Ventricular EC
Mean Diffusivity
0.0011
0.0009
0.0007
0.0005
Contralateral
Ipsilateral
Sham
Stroke
Sham pre-surgery
Sham 4-weeks post-surgery
Stroke pre-surgery
Stroke 4-weeks post-surgery
C.
Bregma -2.06
i.
Peri-lesion WM
ii.
Midline CC
iii.
External Capsule WM
iv.
Internal Capsule

Figure 4.7. Representative DTI-MD maps and corresponding quantitative analyses in control and stroke mice after 4-weeks post-surgery. (A) Representative T2 and corresponding MD scans in sham and stroke mice in rostral (i) and caudal (ii) levels, respectively. (B) Quantification of the MD in the rostral did not show any change in MD in perilesion (i), in the midline of CC (ii) and ventricular EC (iii) (P>0.05). (C) Quantification of the MD in the caudal level did not show a difference in perilesion WM (i), in the EC WM (ii), midline CC (iii) and IC (iv). Data shown as mean ± SEM; individual animals overlaid (n=4 sham, 5 stroke). Three-way effects ANOVA with Bonferroni post hoc tests.

4.2.3.4 MD increased in the thalamus but remained unchanged in other grey matter regions following chronic ischaemic stroke

To further investigate tissue damage and compare it with white matter, we examined the cortical lesion site at rostral and caudal levels, along with anatomically connected grey matter regions, such as the thalamus and the striatum.

In the cortex, at the rostral level, three-way ANOVA revealed significant effects of stroke ($F_{(1,14)}$=27.32; P=0.0001), and an interaction between hemisphere and stroke ($F_{(1,14)}$=7.29; P=0.017). Post-hoc analysis revealed no significant changes in MD in the cortex following stroke (P>0.05) (Fig. 4.8Ai). At the caudal level, three-way ANOVA revealed no significant effects of hemisphere, stroke or time nor an interaction between them (P>0.05) (Fig. 4.8Aii).

In the striatum at the rostral level, three-way ANOVA revealed no significant effects of hemisphere, stroke or time, nor an interaction between them (P>0.05) (Fig. 4.8Bi). Similarly, at the caudal level, a three-way ANOVA showed no significant effects of hemisphere, stroke, or time, nor an interaction among them (P>0.05) (Fig. 4.8Bii).

In the thalamus, three-way ANOVA revealed significant effects of hemisphere ($F_{(1,14)}$=7.23; P=0.018), stroke ($F_{(1,14)}$=8.94; P=0.0097) and an interaction between hemisphere, stroke and time ($F_{(1,14)}$=7.79; P=0.014). Bonferroni corrected post-hoc analysis revealed a significant decrease in MD in the ipsilateral thalamus following stroke, compared with the contralateral hemisphere in sham groups (P=0.0097) (Fig. 4.8C).

Together, diffusion analysis revealed significant decrease in MD in the ipsilateral thalamus following stroke, but no significant changes were detected in the striatum or cortex at either rostral or caudal levels. These suggest that microstructural alterations are most prominent in the thalamus among grey matter regions.

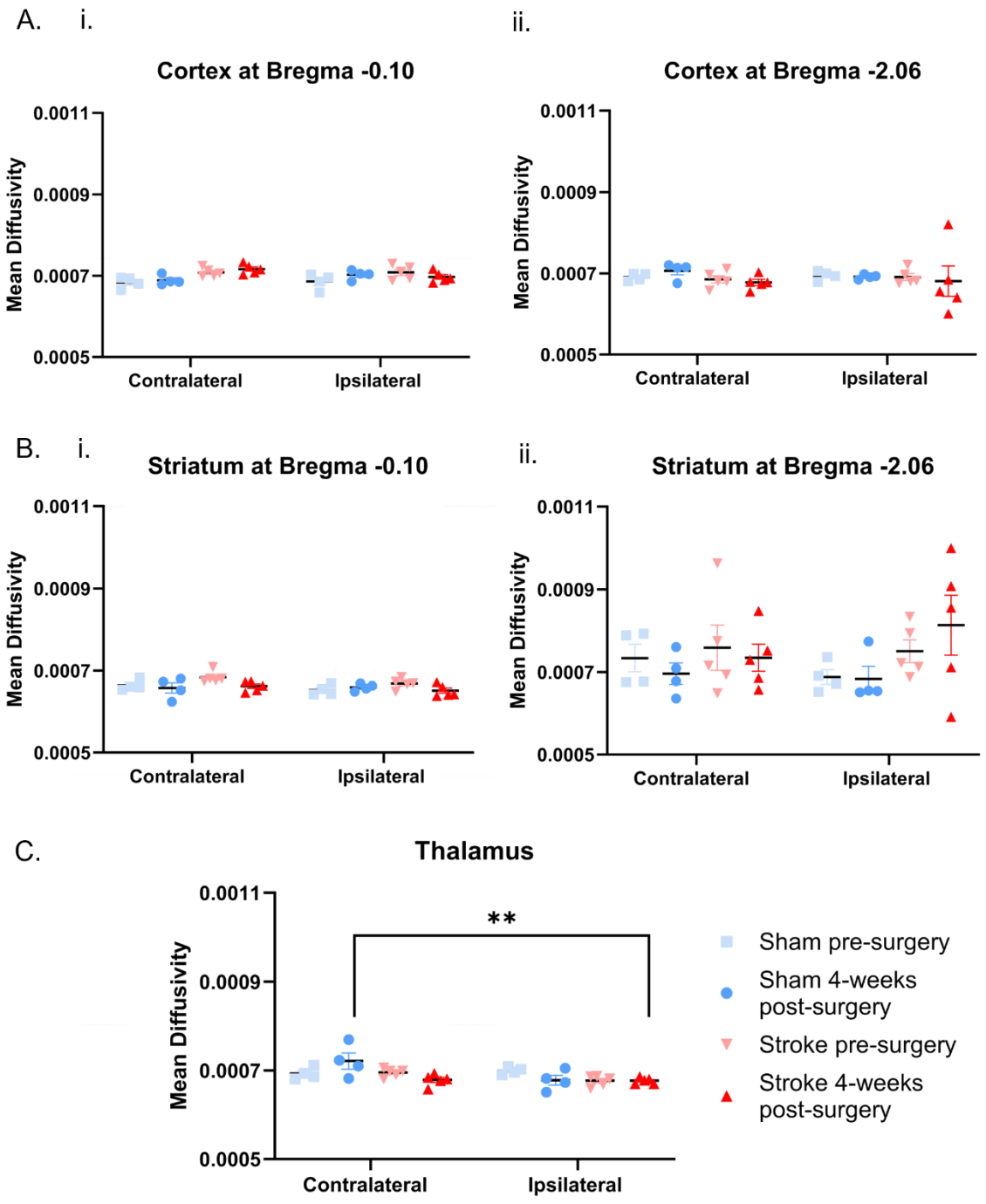

Figure 4.8. Quantitative analysis of MD in grey matter regions following chronic ischaemic stroke. (A) Quantification of MD in the cortex at the rostral (i) and caudal (ii) levels showed no changes (P>0.05). (B) Quantification of MD in the striatum at the rostral (i) and caudal (ii) levels showed no changes (P>0.05). (C) Quantification of MD in the thalamus revealed a significant decrease in MD in the ipsilateral stroke compared to the contralateral sham (**P=0.0097). Data shown as mean ± SEM; individual animals overlaid (n=4 sham, 5 stroke). Three-way ANOVA with Bonferroni post hoc tests.

Given the MRI evidence of white and grey matter alterations and hypoperfusion, this raised the question of whether these structural and functional alterations were accompanied by cellular and pathological changes, which we addressed through immunohistochemical analyses in the same animals at post-mortem.

4.3 Widespread increase in reactive astrocytes was observed following chronic ischaemic stroke

We first determined alterations to astrocytes in the chronic response to stroke. Astrocytes are star-shaped glial cells that play a number of roles in supporting the neuroglial-vascular unit, including regulation of cerebral blood flow, antioxidant support, and control of synaptic activity (Beard et al. 2022). To investigate spatial changes to reactive astrocytes in the chronic response to stroke, we analysed glial fibrillary acidic protein (GFAP) immunostaining at two rostro-caudal levels. GFAP immunostaining is a widely used marker of reactive astrocytes in the context of CNS injury and inflammation, which features upregulation of GFAP protein and hypertrophy of reactive astrocyte processes (Escartin et al. 2021). Previously, the Fowler lab reported increased levels of reactive astrocytes in the peri-lesion area in the acute response to stroke.

4.3.1 Astrocyte reactivity is increased closer to the lesion core along the white matter tracts

GFAP immunoreactivity extended along with the corpus callosum into the contralateral external capsule; however, the astrocyte density and process hypertrophy were reduced with increased distance from the lesion. The extent of GFAP reactivity is also shown in Figure 4.9 in both bregma levels. We first examined GFAP expression in white matter in the external capsule and corpus callosum. In sham animals, GFAP-labelled fibrous astrocytes were sparsely distributed along white matter tracts. These cells exhibited small, oval-shaped cell bodies with a few long, thin processes aligned with axonal bundles, without evidence of hypertrophy or overlapping networks. In chronic ischaemic stroke, we observed increased levels of reactive astrocytes. In the white matter closest to the stroke lesion (peri-lesion), astrocytes displayed dense reactive astrocytosis, characterised by markedly increased GFAP immunoreactivity, hypertrophic cell bodies, and thickened, highly branched processes that formed an overlapping network (Fig. 4.10).

To quantify these changes, we analysed % area of GFAP immunostaining and used two-way mixed-effects ANOVA to determine the effects of stroke and distance from the lesion. At the rostral level of the brain, there were significant main effects of stroke ($F_{(1,15)}$=110.8; P<0.001), and region ($F_{(4,20)}$=4.42; P=0.010), and a significant interaction between stroke and distance from the lesion site ($F_{(4,15)}$=10.60; P=0.0003). Bonferroni corrected post hoc analysis (Fig. 4.10B) revealed significantly greater GFAP immunoreactivity in stroke compared to sham in the ipsilateral perilesional white matter (P<0.0001), the ipsilateral ventricular external capsule (P=0.0016), and the midline of the corpus callosum (P=0.0064). No significant group

differences were observed in contralateral perilesional external capsule white matter tracts (P=0.47 and P=0.31, respectively).

We next investigated the same white matter tracts in the caudal brain region. Two-way mixed-effects ANOVA analysis (Fig. 4.10C) showed significant main effects of surgery ($F_{(1,15)}$=7.60; P=0.015); however, there were no effects of distance from the lesion site (P=0.099) and no interaction (P=0.13). Bonferroni corrected post hoc analysis at the hippocampal level (Fig. 4.10C) revealed a significant increase in %area GFAP+ immunostaining in ipsilateral perilesional white matter in stroke compared to sham (P=0.011). No significant group differences were detected in the ventricular EC, contralateral peri-lesion, or midline of the corpus callosum (P>0.05).

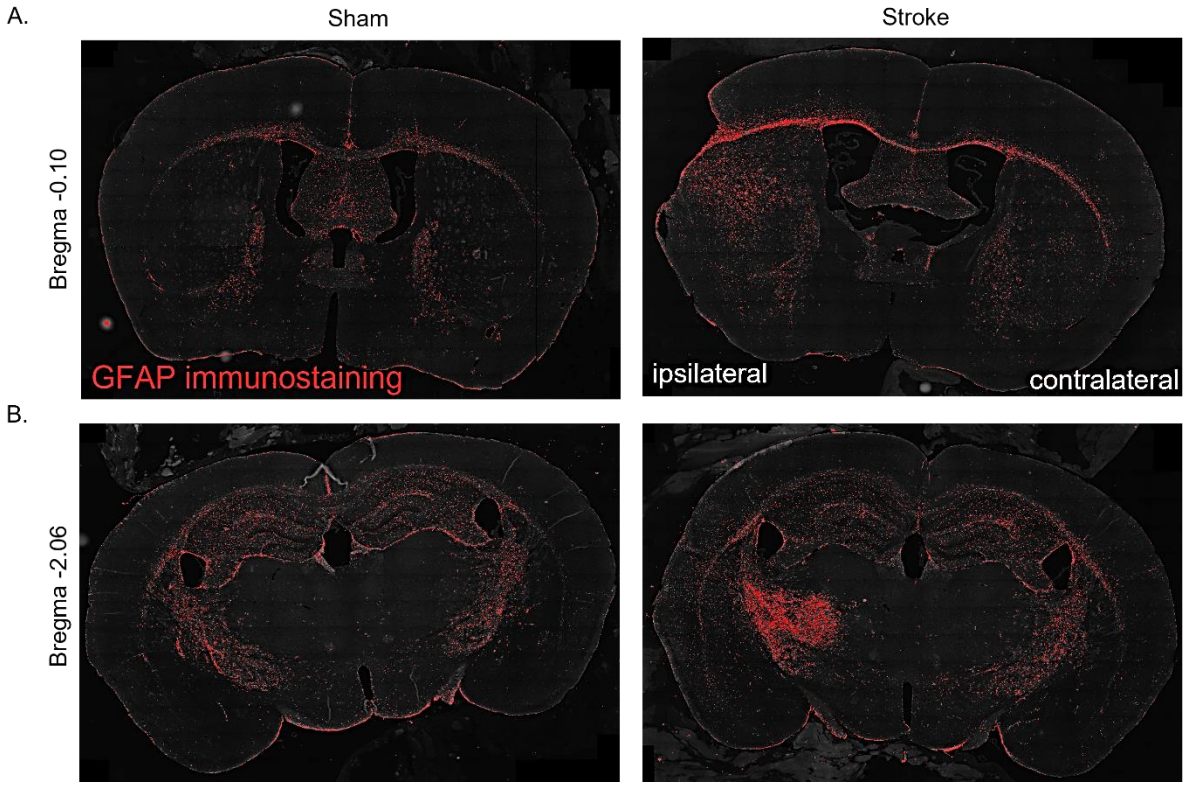

Figure 4.9. Axisoscan images of GFAP immunostaining at both bregma levels. (A) Shows bregma level -0.10, where in stroke, increased intensity of GFAP is seen in the corpus callosum as we go along the white matter closer to the lesion site. (B) Shows bregma level -2.06, where the intensity of GFAP is relatively high in the external capsule closest to the lesion site, as well as a very intense signal in the thalamus and the internal capsule compared to both the sham and the contralateral hemisphere.

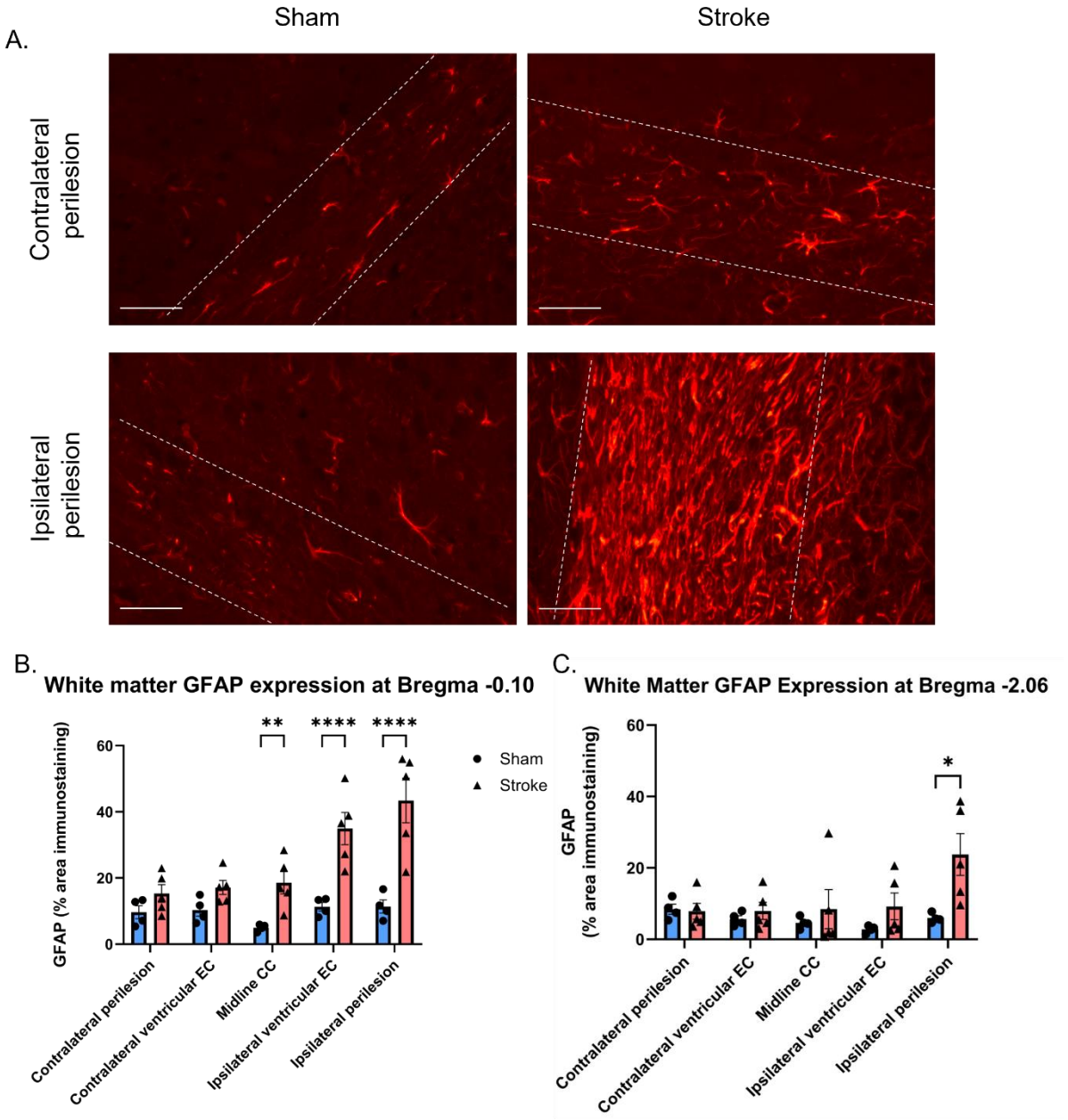

Figure 4.10. GFAP immunoreactivity in rostro-caudal sections of the white matter tracts increases closer to the lesion site post-stroke. (A) Representative images of GFAP immunoreactivity between sham and stroke in the peri-lesional white matter (scale bar = 50 µm) (bregma -0.10). Note the increase in intensity along the white matter. (B) Quantification at a rostral level (bregma –0.10) revealed significantly greater GFAP+ area in stroke compared to sham in ipsilateral peri-lesional WM (****P<0.0001), ipsilateral ventricular external capsule (****P=0.0016), and corpus callosum (**P=0.0064), with no differences in contralateral tracts. (C) Quantification at a caudal level (bregma –2.06). GFAP reactivity was significantly increased in ipsilateral peri-lesional WM only (*P=0.011). Data shown as mean ± SEM; individual animals overlaid (n=4 sham, 5 stroke). Two-way mixed-effects ANOVA with Bonferroni post hoc tests.

4.3.1.1 Astrocyte reactivity is increased in distant but anatomically connected WM brain region

To further assess astrocyte reactivity in white matter tracts beyond the primary cortical lesion site, we focused on the internal capsule because it is anatomically and functionally connected to the infarcted cortex.

Increased GFAP+ reactive astrocyte cell density was clearly present on the ipsilateral side but not in the contralateral side. In the ipsilateral internal capsule, astrocytes exhibit morphological changes of 'reactive' astrocytes, characterised by hypertrophy and thickened processes (Figure 4.11).

Two-way mixed effects ANOVA for the internal capsule showed that there was a significant main effect of surgery ($F_{(1,6)}$=8.32; P=0.028), hemisphere ($F_{(1,8)}$=11.21; P=0.010), and a significant interaction between the two ($F_{(1,6)}$=21.96; P=0.0034). Bonferroni corrected post-hoc tests (Fig. 4.11B) showed that there was higher GFAP+ density in the ipsilateral stroke compared to the sham (P=0.0035). However, the contralateral side did not differ between surgery groups (P>0.05).

Together, these findings indicate enhanced astrocytic activity in distant but anatomically connected white matter tracts, including the internal capsule, midline corpus callosum, and external capsule. This pattern is consistent with disruption of callosal, thalamocortical, and corticostriatal projections following cortical stroke.

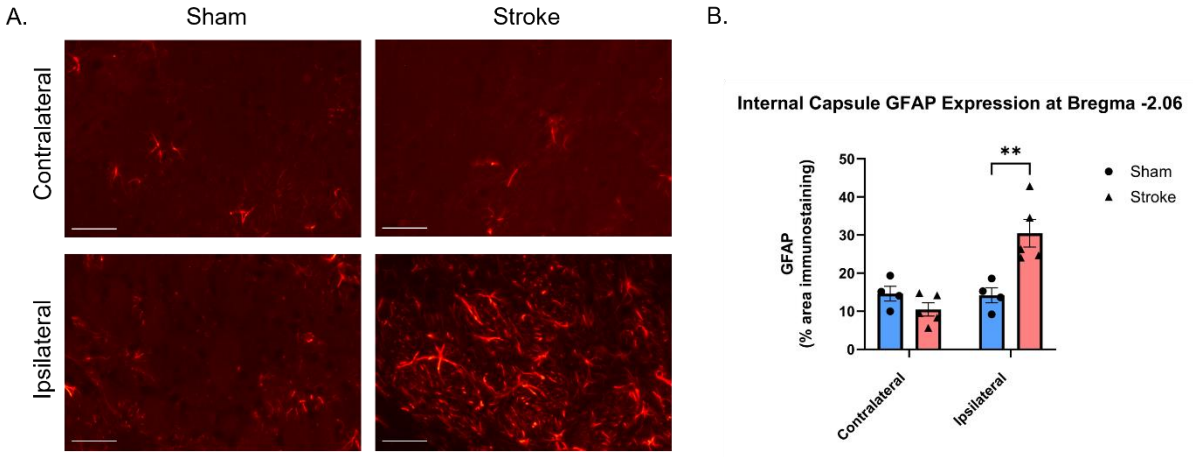

Figure 4.11. Astrocyte reactivity in the internal capsule at the caudal level (bregma –2.06). (A) Representative GFAP immunostaining shows minimal astrocytic labelling in contralateral regions of sham and stroke animals, but dense reactive astrocytosis in ipsilateral regions following stroke. (B) Quantification of % GFAP+ area confirmed a significant increase in stroke compared to sham in the ipsilateral internal capsule (**P=0.0035), with no differences between groups in contralateral regions. Data represent mean ± SEM; individual animals overlaid (n=4 sham, 5 stroke). Two-way mixed-effects ANOVA with Bonferroni post hoc tests. Scale bar = 50 µm.

4.3.2 Astrocyte reactivity is increased in grey matter areas following stroke

To further investigate astrocyte reactivity within and beyond the lesion site, we examined the cortex at both rostral and caudal levels, along with the thalamus and the striatum. Increased GFAP reactive astrocyte cell density was clearly present on the ipsilateral side in all regions, but not in the contralateral side (Fig. 4.12A,B,C).

In the cortex, at the rostral level, two-way mixed-effects ANOVA in the cortex showed significant main effects of stroke ($F_{(1,14)}$=6.56; P=0.023) and hemisphere ($F_{(1,14)}$=6.53; P=0.023), as well as an interaction between the two ($F_{(1,14)}$=6.24; P=0.026). Bonferroni corrected post hoc analysis confirmed that there was higher GFAP+ density in the ipsilateral cortex (P=0.0061) (Fig. 4.12D) following stroke compared to sham, whereas no group differences were observed in the contralateral side (P>0.05). At the caudal level, there were no significant effects of stroke or hemisphere or the interaction between the two (P>0.05) (Fig. 4.12E).

We next studied the striatum at the rostral level. Two-way mixed-effects showed that there was a significant main effect of surgery ($F_{(1,6)}$=19.66; P=0.0044) and hemisphere ($F_{(1,8)}$=18.59; P=0.0026) and an interaction between the two ($F_{(1,6)}$=20.20; P=0.0041). Bonferroni-corrected post hoc analysis confirmed that GFAP+ density was higher in the ipsilateral striatum (P=0.0015) following stroke compared to sham (Fig. 4.12F). In contrast, no group differences were observed on the contralateral side (P>0.05). Similarly, at the caudal level, there were significant effects of stroke ($F_{(1,6)}$=8.67; P=0.026) and hemisphere ($F_{(1,8)}$=6.98; P=0.022), with a significant interaction ($F_{(1,6)}$=13.93; P=0.0097). Bonferroni corrected post hoc analysis confirmed a significant increase in GFAP+ density in the ipsilateral striatum following stroke compared to sham (P=0.0065), whereas contralateral values did not differ between groups (Fig. 4.12G).

In the thalamus, two-way mixed-effects ANOVA showed that there was a significant main effect of surgery ($F_{(1,6)}$=9.17; P=0.023), hemisphere ($F_{(1,8)}$=9.67; P=0.014), and a significant interaction between the two ($F_{(1,6)}$=9.55; P=0.021). Bonferroni corrected post-hoc tests (Fig. 4.12H) showed there was an increased density of GFAP immunostaining compared to sham (P=0.0099). However, no changes are observed in the contralateral side between the surgery types (P>0.05). These findings indicate stroke-related astrocytosis is lateralised to the ipsilesional thalamus.

Together, these findings demonstrate that stroke-induced astrocytosis is present in the peri-infarct cortex and also extends into other grey matter regions with increased reactivity, such as the thalamus and the rostral and caudal levels of striatum, consistent with disruption of thalamocortical and corticostriatal pathways.

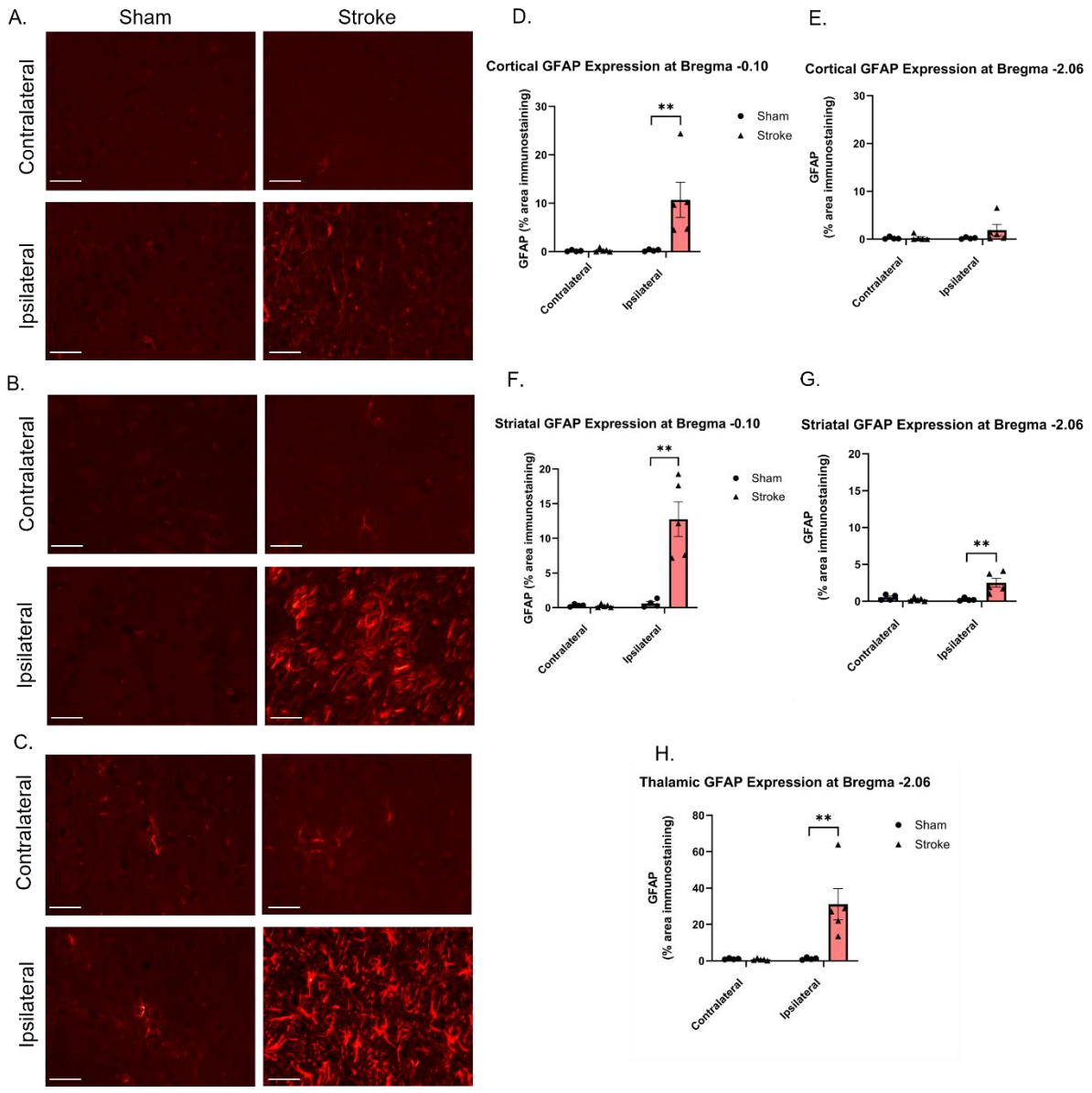

Figure 4.12. Stroke induces rostro-caudal differences in astrocyte reactivity in cortex, striatum, and thalamus. (A-C) Representative GFAP immunostaining in the cortex at the caudal level, striatum, and thalamus shows sparse astrocytes in sham animals and dense reactive astrocytosis in the ipsilateral hemisphere after stroke (scale bar = 50 µm). (D-E) Quantification revealed increased GFAP+ area in the ipsilateral cortex at the rostral (**P=0.0061), but no changes in the contralateral side. (F-G) Quantification revealed increased GFAP+ area in the ipsilateral striatum at the rostral (**P=0.0015) and caudal level (**P=0.0065). (H) Quantification of GFAP+ area confirmed significantly greater reactivity in stroke compared to sham in the ipsilateral thalamus (**P=0.0099), with no changes in the contralateral thalamus. Data represent mean ± SEM; individual animals overlaid (n=4 sham, 5 stroke). Two-way mixed-effects ANOVA with Bonferroni post hoc tests.

4.4 The microglial/macrophage response after chronic response to stroke

To determine whether other glial cell responses accompanied astrocytic activation and further investigate alterations in the neurogliovascular unit, we next assessed the response of microglia in chronic response to stroke. Microglial reactivity is believed to play a central role in the neuroinflammatory process of stroke (Lalancette-Hébert et al. 2007). To investigate spatial changes to microglial reactivity after stroke, we analysed ionised calcium-binding adaptor molecule 1 (Iba1) immunostaining at two rostro-caudal levels. Iba1 is a well-established marker of microglia/macrophages, allowing for the detection of changes in both cell density and morphology (Paolicelli et al., 2022). Previously, the Fowler lab reported increased levels of reactive microglia in the peri-lesion area in the acute response to stroke.

4.4.1 Microglia reactivity is increased closer to the lesion core along the white matter tracts

We first examined Iba1 expression in white matter in the external capsule and corpus callosum. In sham animals, Iba1-labelled microglia were relatively sparse and evenly distributed, with small, elongated cell bodies, suggesting a homeostatic state. In chronic ischaemic stroke, there were increased levels of reactive microglia. In the white matter peri-lesion site, microglia displayed hypertrophic cell bodies and thickened, retracted processes. They appeared amoeboid and densely clustered, consistent with a transition towards a phagocytic phenotype, characterised by markedly increased Iba1 immunoreactivity (Figure 4.13A). Iba1 immunoreactivity extended along with the corpus callosum to the contralateral white matter; however, microglia density and hypertrophy were reduced with further distance from the lesion.

To quantify these changes, we analysed the percentage area of Iba1 immunostaining and used a two-way mixed-effects ANOVA to determine the effects of stroke and distance from the lesion. At the rostral level, there were significant main effects of stroke ($F_{(1,35)}$=41.13; P<0.0001) and region ($F_{(4,35)}$=4.32; P<0.0060) and a significant interaction between stroke and distance from the lesion ($F_{(4,35)}$=4.57; P<0.0045). Bonferroni corrected post hoc analysis for striatal level (Fig. 4.13B) revealed significantly greater Iba1 immunoreactivity in stroke compared to sham in ipsilateral perilesional white matter (P<0.0001) and the midline of the corpus callosum (P=0.0008). No significant group differences were observed in ipsilateral ventricular EC, contralateral perilesional and external capsule white matter tracts (P>0.05).

We next investigated the same white matter tracts in a caudal region of the brain. Two-way mixed-effects ANOVA analysis showed significant main effects of stroke ($F_{(1,34)}$=9.72; P=0.0037), and region ($F_{(4,34)}$=5.56; P<0.0015) and a significant interaction between stroke and distance from the lesion ($F_{(4,34)}$=5.55; P<0.0015). Bonferroni corrected post hoc analysis for hippocampal level (Fig. 4.13C) revealed a significant increase in %area Iba1+ immunostaining in ipsilateral perilesional white matter in stroke compared to sham (P=0.011). No significant group differences were detected in the ventricular EC, contralateral peri-lesion or midline of the corpus callosum (P>0.05).

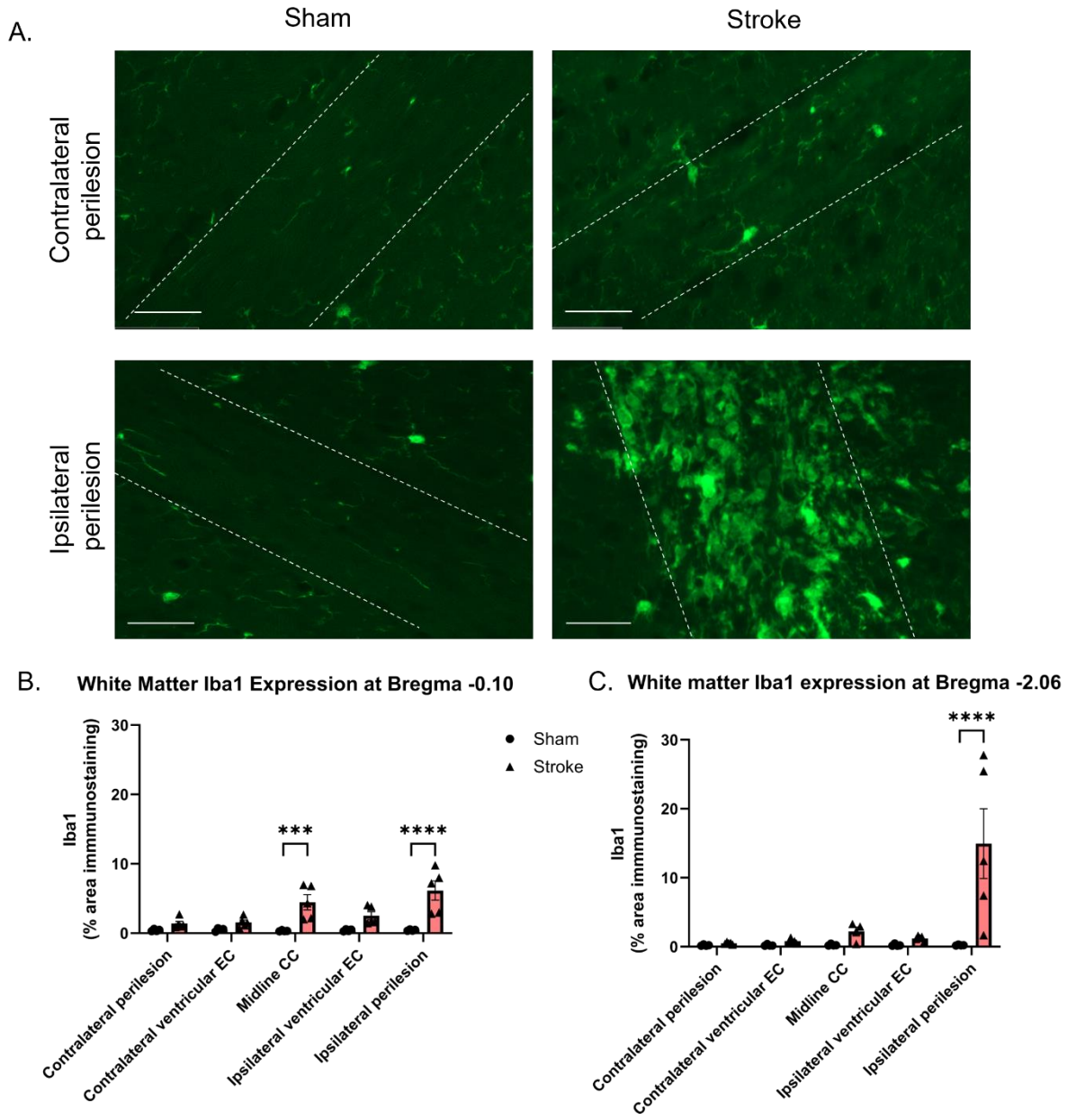

Figure 4.13. Microglial reactivity in white matter tracts following chronic ischaemic stroke. (A) Representative Iba1 immunofluorescence images are shown from the peri-lesion of sham and stroke animals at the rostral level. In sham animals, Iba1-labelled microglia were sparse and evenly distributed, with small, elongated cell bodies, consistent with a homeostatic state. In contrast, stroke animals displayed markedly increased Iba1 immunoreactivity in the peri-lesional white matter, with microglia exhibiting hypertrophic soma, thickened and retracted processes, and an amoeboid clustered morphology indicative of a reactive state. (B) Quantification of Iba1 % area at the rostral level revealed significantly greater immunoreactivity in stroke compared to sham animals at the ipsilateral peri-lesional white matter (****P<0.0001) and the midline of the corpus callosum (***P=0.0008). (C) Quantification of Iba1% area at the caudal level revealed greater immunoreactivity in stroke compared to sham in the ipsilateral peri-lesional white matter at the caudal level (****P=0.011). No significant differences were observed in contralateral regions (P>0.05). Data are presented as mean ± SEM (n=4 sham, 5 stroke). Two-way mixed-effects ANOVA with Bonferroni post hoc tests. Scale bars = 50 µm.

4.4.1.1 Microglia reactivity is increased in distant but anatomically connected WM brain region

To further assess immune cell response in white matter tracts beyond the primary cortical lesion site, we focused on the internal capsule since it is anatomically connected with the infarcted cortex. Increased Iba1+ reactivity was clearly present on the ipsilateral side but not in the contralateral side. In the ipsilateral internal capsule, microglia exhibited morphological changes of 'reactive' microglia, characterised by hypertrophic cell bodies, thickened and retracted processes, and increased clustering compared to sham animals (Figure 4.14A).

Two-way mixed effects ANOVA analysis of the internal capsule showed that there was a significant main effect of surgery ($F_{(1,6)}$=31.79; P=0.0013), hemisphere ($F_{(1,8)}$=17.17; P=0.0032) and a significant interaction between the two ($F_{(1,6)}$=15.87; P=0.0073). Bonferroni-corrected post-hoc tests (Fig. 4.14B) showed that there is a higher Iba1+ density in the ipsilateral stroke compared to the sham (P = 0.0010). However, the contralateral side did not differ between surgery groups (P>0.05).

Together, these findings demonstrate a chronic increase in microglial reactivity within white matter tracts anatomically connected to the lesion site, including the corpus callosum and internal capsule. The spatial gradient of Iba1 immunoreactivity, strongest in peri-lesional regions and reduced with increasing distance, suggests a sustained neuroinflammatory response propagating along affected projection pathways after cortical stroke.

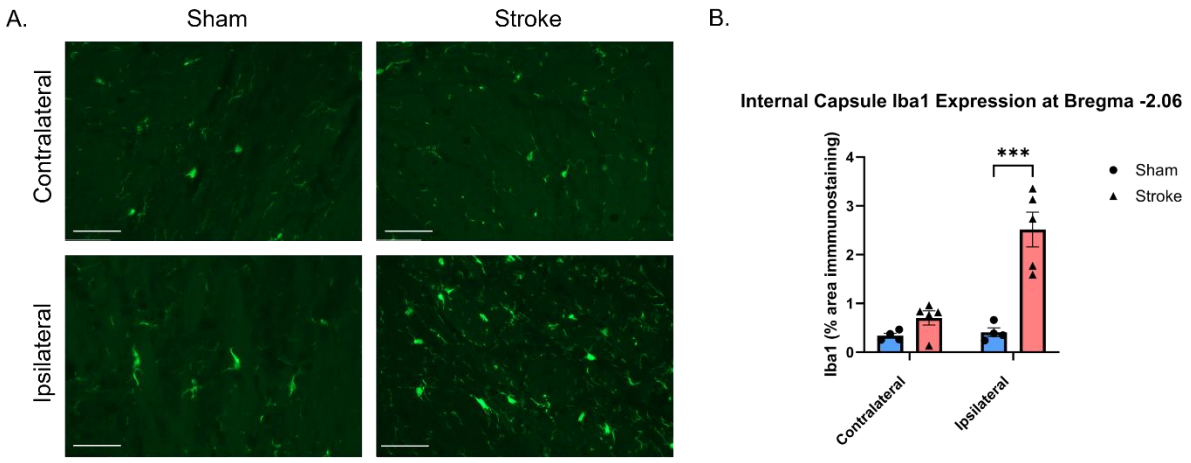

Figure 4.14. Microglial reactivity in the internal capsule following chronic ischaemic stroke. (A) Representative Iba1 immunofluorescence images from sham (left panels) and stroke (right panels) animals are shown. (B) Quantification of Iba1 % area demonstrated significantly higher immunoreactivity in the ipsilateral internal capsule of stroke animals compared to sham (***P=0.0010), with no group differences in the contralateral hemisphere (P>0.05). Data are presented as mean ± SEM (n=4 sham, 5 stroke). Two-way mixed-effects ANOVA with Bonferroni post hoc tests. Scale bars = 50 µm.

4.4.2 Microglia reactivity is increased in grey matter areas following stroke

To further investigate microglia reactivity within and beyond the lesion site, we examined the peri-infarcted cortex, thalamus and striatum. Increased Iba1+ reactive microglia cell density was clearly present on the ipsilateral side in all regions, but not in the contralateral side. In the ipsilateral thalamus, cortex, and striatum, microglia exhibit morphological changes of 'reactive' microglia, forming hypertrophic cell bodies (Fig. 4.15A,B,C).

In the cortex, at the rostral level, two-way mixed-effects ANOVA showed a significant main effect of stroke ($F_{(1,14)}$=57.68; P<0.0001), hemisphere ($F_{(1,14)}$=51.26; P<0.001) and an interaction between the two ($F_{(1,14)}$=51.77; P<0.0001). Bonferroni corrected post hoc analysis confirmed that there was higher Iba1+ density in the ipsilateral cortex (P<0.0001) (Fig. 4.15D) following stroke compared to sham. In contrast, no group differences were observed in the contralateral side (P>0.05). At the caudal level, no significant effects of stroke or hemisphere was observed (P>0.05) (Fig.4.15E).

In the striatum, at the rostral level, two-way mixed-effects ANOVA showed significant main effects of stroke ($F_{(1,6)}$=65.07; P=0.0002) and hemisphere ($F_{(1,8)}$=37.90; P=0.0003) as well as an interaction between the two ($F_{(1,6)}$=54.57; P=0.0003). Bonferroni corrected post hoc analysis confirmed that there was higher Iba1+ density in the ipsilateral striatum (P<0.0001) (Fig. 4.15F) following stroke compared to sham. In contrast, no group differences were observed in the contralateral side (P>0.05). At the caudal level, there was a significant effect of stroke (F(1,6)=37.71; P=0.0009), with no effects of hemisphere or interaction between the two (P>0.05). Bonferroni corrected post hoc analysis confirmed a significant increase in Iba1+ density in the ipsilateral striatum (Fig. 4.15G) following stroke compared to sham (P=0.0027), as well as the contralateral stroke group (P=0.044) (Fig. 4.15G).

In the thalamus, two-way mixed-effects ANOVA showed that there was a significant main effect of stroke ($F_{(1,14)}$=29.09; P<0.0001), hemisphere ($F_{(1,14)}$=26.43; P=0.0001) and a significant interaction between the two ($F_{(1,14)}$=25.40; P=0.0002). Bonferroni-corrected post-hoc tests (Fig. 4.15H) indicated that stroke surgery alone increases the density of Iba1+ cells in the ipsilateral thalamus, as surgery showed an increase in density compared to sham (P<0.0001). However, no changes are observed in the contralateral side between the surgery types (P>0.05). These findings indicate stroke-related microglial reactivity is lateralised to the ipsi-lesional white matter tracts.

Together, these findings demonstrate that, consistent with reactive astrocytes changes, stroke-induced microglial reactivity extends into distant grey matter regions, with robust activation in the ipsilateral cortex and striatum at rostral levels, persistent microglial changes in the striatum across both rostral and caudal levels, and pronounced reactivity in the thalamus at caudal levels, consistent with ongoing neuroinflammatory responses along thalamocortical and cortico-striatal pathways.

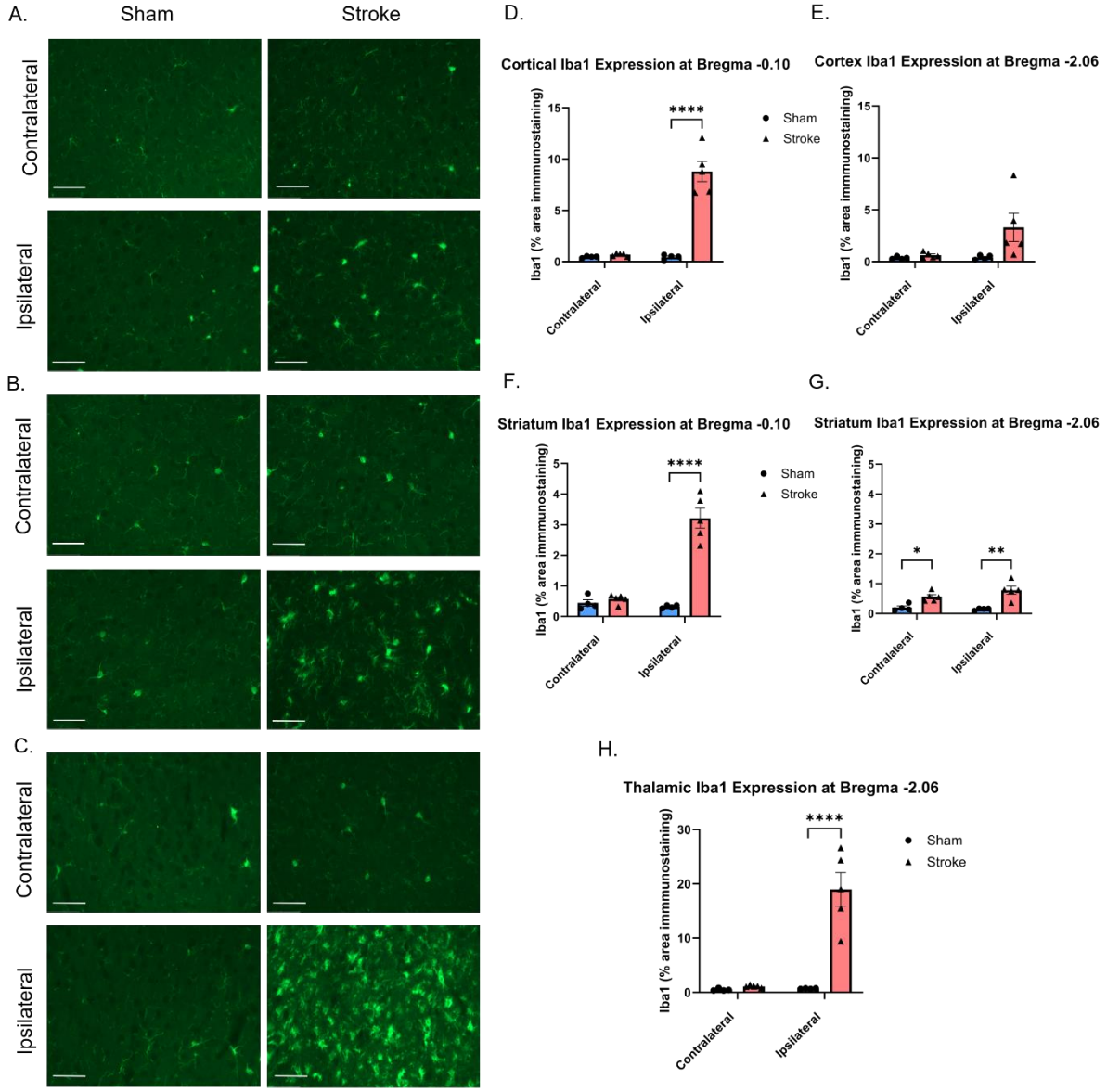

Figure 4.15. Microglial reactivity in grey matter regions following chronic ischaemic stroke. (A-C) Representative Iba1 immunofluorescence images are shown from the thalamus (caudal level), cortex (rostral level), and striatum (rostral levels) of sham and stroke animals. (D-E) Quantification of Iba1% area revealed greater microglial density in the ipsilateral cortex at the rostral level of stroke animals compared to sham (****P<0.0001). No significant effects were observed in the contralateral side. (F-G) Quantification of Iba1% area revealed greater microglial density in ipsilateral striatum at the rostral level and both ipsilateral and contralateral increase at the caudal level (****P<0.0001, **P=0.0027, *P=0.044). (H) Quantification of Iba1 % area revealed significantly greater microglial density in the ipsilateral thalamus at the caudal level in stroke animals compared to sham (P< 0.0001), with no changes in the contralateral thalamus (P>0.05). Data are presented as mean ± SEM (n=4 sham, 5 stroke). Two-way mixed-effects ANOVA with Bonferroni post hoc tests. Scale bars = 50 µm.

4.5 Axonal injury after chronic response to stroke

Having characterised astrocytic and microglial responses in white and grey matter regions, we next assessed whether these regions also showed evidence of axonal pathology. Axonal damage was examined by quantifying axonal bulbs of accumulated amyloid precursor protein (APP). APP is usually transported by retrograde transport along axons; however, following injury, axonal transport becomes impaired, resulting in focal accumulations of APP (Yam et al. 1997). This makes APP a sensitive marker of axonal injury in the post-stroke brain (Yam et al. 1997).

4.5.1 Axonal injury is increased in white matter tracts following stroke

Initially, we observed APP axonal bulbs in the external capsule and corpus callosum following a stroke. Since APP is widely expressed throughout the brain, these accumulations were distinguished from other cell types, such as cytoplasmic oligodendrocyte immunoreactivity, by their staining morphology. After ischaemic stroke, APP accumulated in swollen axonal profiles, appearing as irregular, beaded or wavy swellings along tract fibres. This was distinct from APP staining in oligodendrocytes, which appeared as discrete, spherical cytoplasmic labelling (Fig. 4.16).

At the rostral level, APP immunostaining revealed a marked increase in axonal bulbs within white matter regions of stroke animals compared to sham in the external capsule along with the midline of corpus callosum and the contralateral regions (Figure 4.16A). To quantify these changes, APP-positive bulbs were counted using a standardised grid. Two-way mixed-effects ANOVA demonstrated significant main effects of stroke ($F_{(1,15)}$=128.7; P<0.0001), and region ($F_{(4,20)}$=6.29; P=0.0019) as well as an interaction between the two ($F_{(4,15)}$=6.94; P=0.0023). Bonferroni-corrected post hoc analysis at the rostral level revealed significantly greater APP-positive axonal bulb counts in stroke compared to sham animals within the ipsilateral perilesional white matter (P<0.0001), ipsilateral ventricular white matter (P=0.0005), and the corpus callosum (P=0.0001) (Fig. 4.16B). In addition, a significant increase was observed in the contralateral ventricular white matter in stroke compared to sham (p=0.041), indicating axonal injury extended beyond the ipsilateral hemisphere of the brain. No significant differences were observed in the equivalent peri-lesion white matter of the contralateral hemisphere (P>0.05).

At the caudal level, APP-positive bulbs were similarly increased in stroke animals compared to sham animals in ventricular white matter along with midline of the corpus callosum. Two-way mixed-effects ANOVA demonstrated significant main effects of stroke ($F_{(1,34)}$=54.12; P<0.0001), and region ($F_{(4,34)}$=8.39; P<0.0001) and an interaction between the two ($F_{(4,34)}$=2.06; P=0.11). Bonferroni-corrected post hoc analysis revealed significantly greater APP bulbs in stroke compared to sham animals in the ipsilateral peri-lesion (P<0.0001), ipsilateral EC (P=0.0005), and the midline of the corpus callosum (P=0.022). No changes were observed on the contralateral side (P>0.05) (Fig. 4.16C).

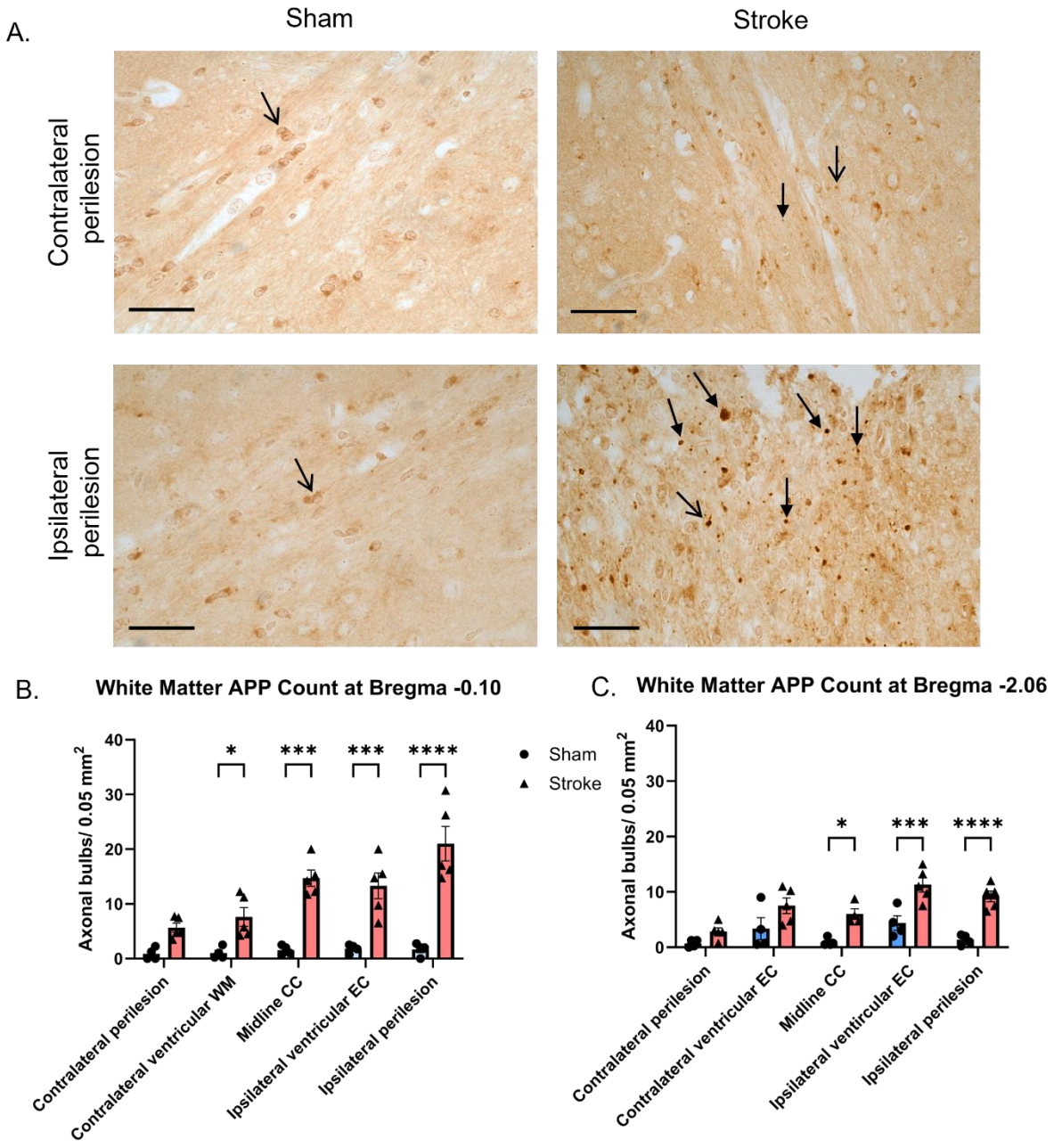

Figure 4.16. APP-positive axonal bulbs in white matter tracts following chronic ischaemic stroke. (A) Representative APP immunostaining in sham (left panels) and stroke (right panels) animals, showing axonal bulb accumulations in white matter regions. Closed arrows showing the axonal swellings and open arrows pointing to oligodendrocyte staining (B) Quantification of APP-positive bulbs at the rostral level revealed significantly higher counts in stroke compared to sham animals within the ipsilateral peri-lesional white matter (P****<0.0001), ipsilateral ventricular white matter (P***=0.0005), and corpus callosum (***P=0.0001). An increase was also observed in the contralateral ventricular white matter (*P=0.041), while no differences were detected in the contralateral peri-lesional region (P>0.05). (C) Quantification at the caudal level showed significantly higher APP-positive bulb counts in stroke compared to sham animals in the ipsilateral peri-lesional white matter (****P<0.0001), ipsilateral external capsule (***P=0.0005), and midline corpus callosum (*P=0.022), with no significant changes contralaterally (P > 0.05). Data represent mean ± SEM; individual animals overlaid (n=4 sham, 5 stroke). Two-way mixed-effects ANOVA with Bonferroni post hoc tests. Scale bar = 50 µm.

4.5.1.1 Stroke-induced axonal injury in the internal capsule, a deep white matter tract

To further investigate whether axonal injury extends into distant white matter pathways, we examined the internal capsule. APP-positive axonal bulbs were clearly increased in the ipsilateral internal capsule of stroke animals compared to shams, consistent with disrupted axonal transport (Figure 4.17).

Two-way mixed-effects ANOVA revealed significant main effects of surgery ($F_{(1,14)}$=97.43; P<0.0001), and hemisphere ($F_{(1,14)}$=93.57; P<0.0001) as well as an interaction between the two ($F_{(1,14)}$=83.69; P<0.0001). Bonferroni-corrected post-hoc tests (Fig. 4.17B) showed that APP-positive axonal bulbs were significantly more numerous in the ipsilateral stroke group compared to the sham group (P<0.0001). However, the contralateral side did not differ between surgery groups (P>0.05).

Together, these findings show that stroke-induced axonal injury spreads into distant white matter tracts, including the internal capsule, indicating secondary degeneration along projection pathways away from the cortical lesion.

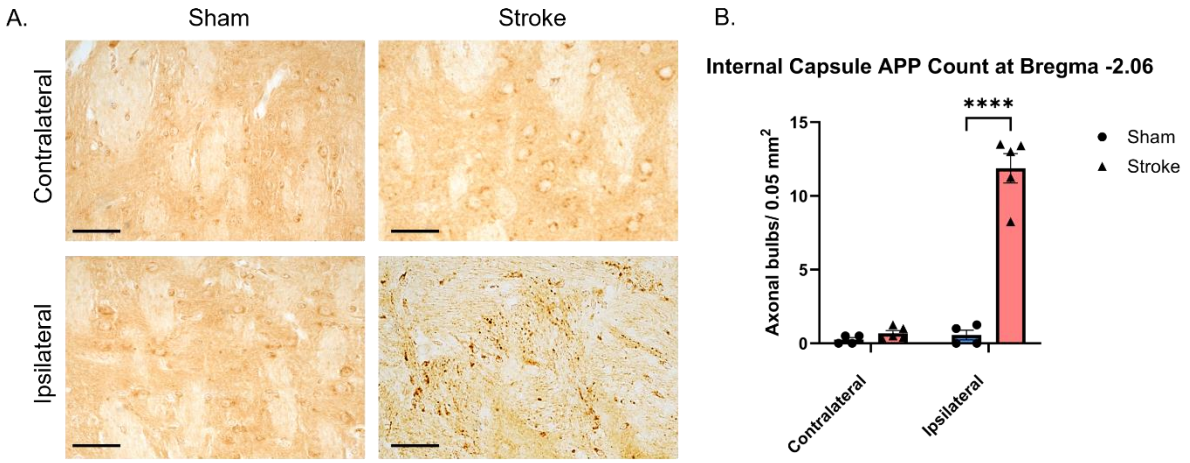

Figure 4.17. APP-positive axonal bulbs in the internal capsule following chronic ischaemic stroke. (A) Representative APP immunostaining in sham (left panels) and stroke (right panels) animals, showing increased APP-positive axonal bulbs in the ipsilateral internal capsule. (B) Quantification of APP-positive bulbs demonstrated significantly higher counts in stroke compared to sham animals in the ipsilateral internal capsule (****P<0.0001). At the same time, no group differences were observed in the contralateral hemisphere (P>0.05). Data represent mean ± SEM; individual animals overlaid (n=4 sham, 5 stroke). Two-way mixed-effects ANOVA with Bonferroni post hoc tests. Scale bar = 50 µm.

4.5.2 Axonal injury is increased in grey matter regions following stroke

To further investigate whether axonal injury extends into distant but anatomically connected grey matter regions, we examined the ventral posterior medial (VPM) and ventral posterior lateral (VPL) thalamic nuclei, and striatum at both rostral and caudal levels. We also examined the peri-infarct cortex grey matter area. APP-positive axonal bulbs were clearly present in the ipsilateral thalamic nuclei, cortex, and striatum of stroke animals, whereas contralateral regions showed little to no APP accumulation (Fig. 4.18A,B,C).

In the cortex, at the rostral level, two-way mixed-effects ANOVA showed a significant main effect of stroke ($F_{(1,14)}$=287.8; P<0.0001), hemisphere ($F_{(1,14)}$=269.8; P<0.0001), and an interaction between the two ($F_{(1,14)}$=260.7; P<0.0001). Bonferroni-corrected post hoc analysis confirmed greater APP-positive bulb in the ipsilateral cortex (P<0.0001) (Fig. 4.18D) following stroke compared to sham. In contrast, no group differences were observed on the contralateral side (P>0.05). At the caudal level, there were significant effects of stroke ($F_{(1,14)}$=362.5; P<0.0001), hemisphere ($F_{(1,14)}$=320.1; P<0.0001) and an interaction between the two ($F_{(1,14)}$=344.8; P<0.0001). Bonferroni-corrected post hoc analysis confirmed greater APP-positive bulb counts in the ipsilateral cortex (P<0.0001) (Fig. 4.18E) following stroke compared to sham.

We next examined the striatum at the rostral level. Two-way mixed-effects ANOVA showed significant main effects of stroke ($F_{(1,6)}$=18.25; P=0.0053) with no effects of hemisphere and interaction between the two (P>0.05). Bonferroni-corrected post hoc analysis confirmed greater APP-positive bulb counts in the ipsilateral striatum (P=0.018) (Fig. 4.18F) following stroke compared to sham. In contrast, no group differences were observed on the contralateral side (P>0.05). At the caudal level, striatum showed significant effects of stroke ($F_{(1,14)}$=29.12; P<0.0001), hemisphere ($F_{(1,14)}$=24.37; P=0.0002) and an interaction between the two ($F_{(1,14)}$=37.03; P<0.0001). Post-hoc analysis confirmed greater APP-positive bulb counts in the ipsilateral striatum (P<0.0001) (Fig. 4.18G) following stroke compared to sham.

Two-way mixed-effects ANOVA for the VPM revealed significant main effects of stroke ($F_{(1,6)}$=40.16; P=0.0007), and hemisphere ($F_{(1,8)}$=19.85; P=0.0021) and an interaction between the two ($F_{(1,6)}$=35.28; P=0.0010). Post hoc Bonferroni analysis (Fig. 4.18H) confirmed that APP-positive bulb counts were significantly higher in the ipsilateral VPM of stroke animals compared to shams (P=0.0003). At the same time, no differences were observed in the contralateral side (P>0.05).

Similarly, two-way mixed-effects ANOVA for the VPL showed significant main effects of stroke ($F_{(1,6)}$=124.6; P<0.0001) and hemisphere ($F_{(1,8)}$=94.51; P<0.0001), and an interaction between the two ($F_{(1,6)}$=106.1; P<0.0001). Bonferroni-corrected post hoc analysis revealed greater APP-positive bulb counts in the ipsilateral VPL of stroke animals compared to sham animals (p<0.0001), with no differences observed contralaterally (P>0.05) (Fig. 4.18I).

Together, these findings demonstrate that axonal injury, as indicated by APP bulbs after damage, is persistent in grey matter areas, including the thalamic nuclei, striatum, and cortex. We observed this damage being localised to the ipsilateral hemisphere of stroke animals. This is clear evidence of widespread axonal disruption propagating along connected neural pathways following stroke.

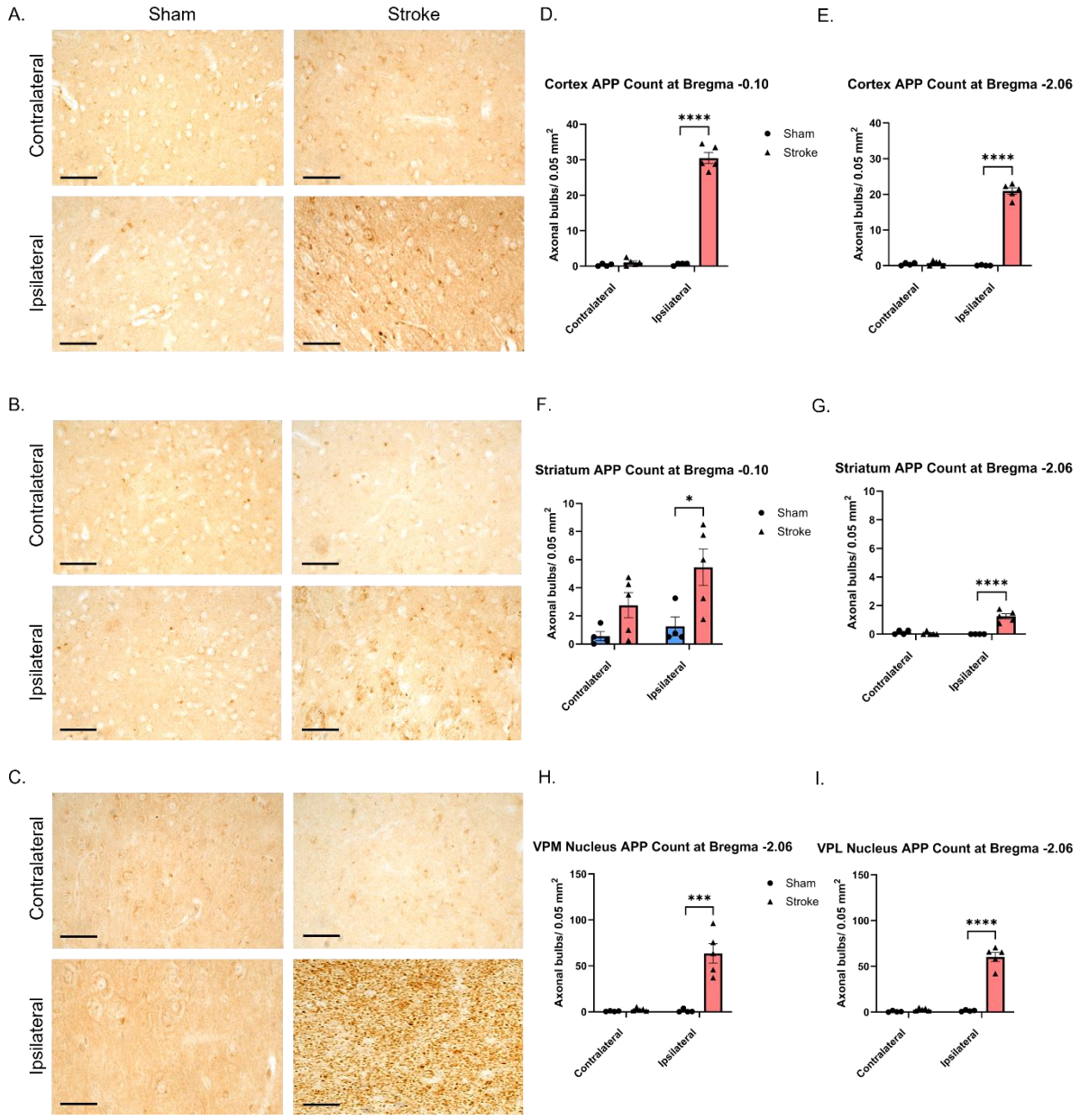

Figure 4.18. APP-positive axonal bulbs in grey matter regions following chronic ischaemic stroke. (A–C) Representative APP immunostaining in sham and stroke animals, showing APP-positive axonal bulb accumulations in the thalamic nuclei, striatum and cortex. (D-I) At the rostral level, bulb counts were significantly increased in the ipsilateral striatum (*P=0.018; F) and ipsilateral cortex (****P<0.0001; D) of stroke animals compared to sham, with no changes in contralateral regions (P>0.05). At the caudal level, APP-positive bulbs were significantly more numerous in the ipsilateral striatum (****P<0.0001; G) and ipsilateral cortex (****P<0.0001; E) of stroke animals relative to sham, with no contralateral differences (P > 0.05). Quantification of APP-positive bulb counts revealed significantly greater accumulations in the ipsilateral VPM (***P=0.0003; H) and ipsilateral VPL (****P<0.0001; I) of stroke animals compared to shams, with no differences contralaterally (P>0.05). Data represent mean ± SEM; individual animals overlaid (n=4 sham, 5 stroke). Two-way mixed-effects ANOVA with Bonferroni post hoc tests. Scale bar = 50 µm.

4.6 Myelin integrity after chronic response to stroke

Having evaluated glial and axonal responses, we next assessed whether white matter regions showed evidence of myelin pathology. Myelin integrity was examined by immunostaining for myelin-associated glycoprotein (MAG). MAG is expressed at the axon-glial interface, however, following injury, there is axon-glial disruption and myelin damage, making it a reliable marker of myelin alterations after stroke (Zuo et al. 2019; Wang et al. 2020). Myelin damage was graded on a scale from 0 (no axon-myelin disruption) to 3 (extensive axon-myelin disruption) in the ipsilateral and contralateral regions of the rostral and caudal levels. Two replicates of the same slide were averaged to get an overall myelin damage score.

4.6.1 Axon-myelin integrity is disrupted in white matter tracts following stroke

We first assessed myelin integrity using MAG immunostaining in the external capsule and corpus callosum in post-stroke. We observed clear evidence of myelin pathology in stroke animals, including increased myelin debris, vacuolation, and disorganisation of fibres, indicative of axon-glial disruption and loss of myelin integrity (Fig. 4.19).

At the rostral level, MAG immunostaining revealed clear evidence of myelin disruption within white matter regions of stroke animals compared to sham (Fig. 4.19A). To quantify these, statistical analysis using Kruskal-Wallis was performed in the perilesion and ventricular EC white matter tracts. This test revealed a significant effect of stroke on MAG damage scores in the perilesion white matter ($H(3, N=18) = 15.80$, $P<0.0001$) and the ventricular EC ($H(3, N=18)=14.69$, $P<0.0001$).Dunn's post hoc tests indicated that MAG damage scores were significantly higher both in the ipsilateral perilesion ($P=0.0098$) and EC ($P=0.049$) of stroke animals compared to sham ipsilateral groups, consistent with increased myelin pathology following stroke. No other group comparisons reached significance ($P>0.05$) (Fig. 4.19B,D).

In the corpus callosum, the Mann-Whitney U test similarly revealed significantly higher MAG damage scores in stroke animals (median = 2.50, n=5) compared to shams (median = 0.00, n = 4; $U = 0$, $P=0.016$) (Fig. 4.19C).

At the caudal level, Kruskal–Wallis tests revealed significant stroke effects on MAG damage scores in both the perilesion white matter ($H(3, N=18)=13.70$, $P<0.0001$) and the external capsule ($H(3, N=18)=11.33$, $P=0.0019$). Post-hoc Dunn's test indicated a difference between the sham contralateral and stroke ipsilateral groups (Fig. 4.19E,G).

Interestingly, in the caudal corpus callosum, Mann–Whitney U test did not reveal a significant difference in MAG damage scores between stroke (median = 0.50, n = 4) and sham animals (median = 0.00, n = 4; $U = 2$, $P=0.14$) (Fig. 4.19F).

These findings suggest that myelin disruption following stroke is region-specific, with white-matter tracts proximal to the lesion, particularly the external capsule and perilesion areas,

being the most susceptible to myelin integrity disruption, although changes are also evident in the contralateral hemisphere.

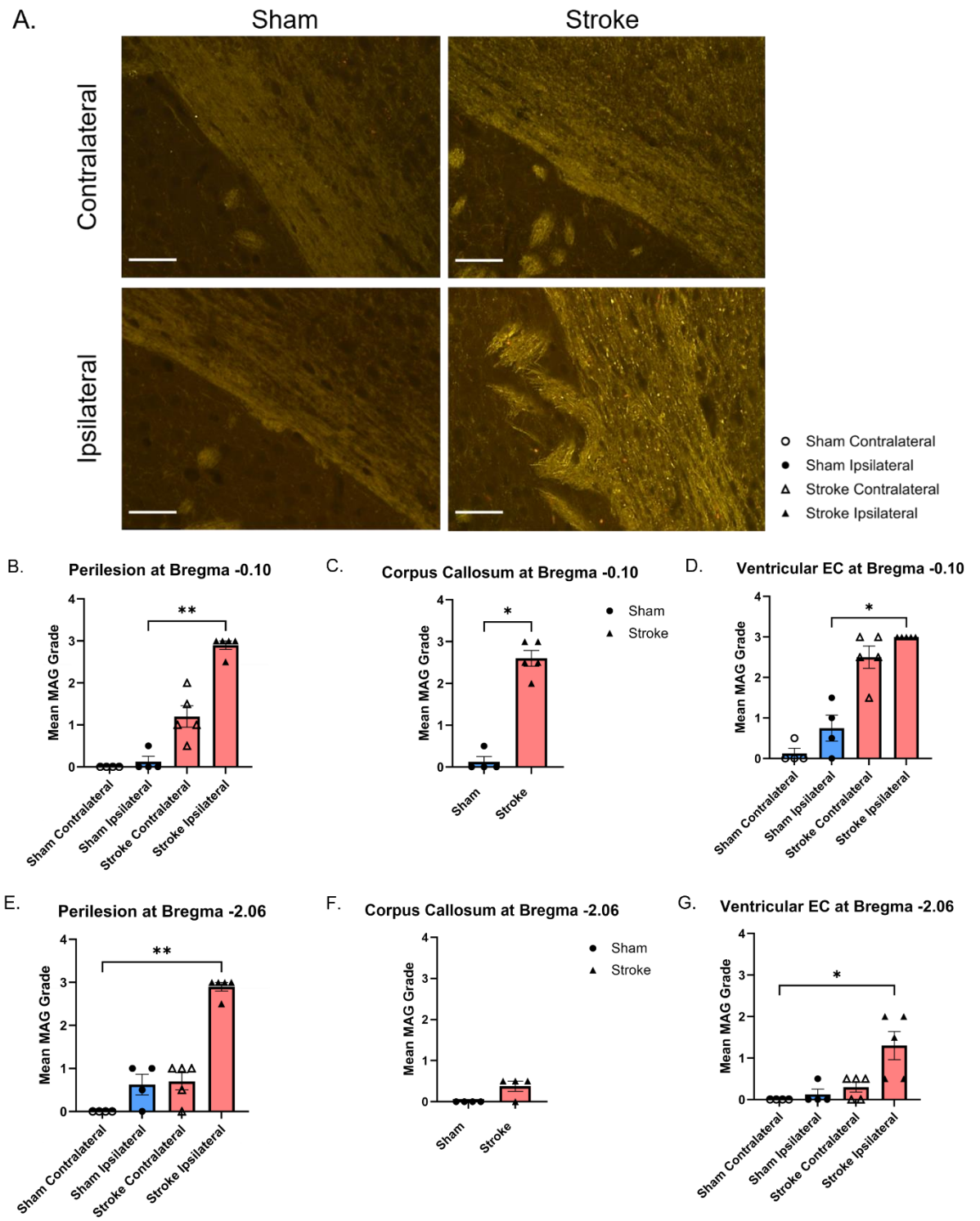

Figure 4.19. Axon-myelin integrity in rostro-caudal sections of the white matter tracts is disrupted post-stroke. (A) Representative images of MAG grading between sham and stroke in the perilesion white matter (bregma -0.10). (B-D) Quantification at the rostral level revealed significantly greater myelin damage at the perilesion (B) (**P=0.0098), corpus callosum (C)(*P=0.016) and ventricular EC (D) (*P=0.049) in ipsilateral stroke animals. (E-G) Quantification at the caudal level showed a significant stroke effect on MAG damage scores in both the perilesion white matter (E) (H(3, N=18)=13.70, p<0.0001) and the external capsule (G) (H(3, N=18)=10.21, p=0.0078). However, Dunn's post-hoc tests did not identify differences between the comparisons of primary interest. No changes were observed in the corpus callosum at this level (F)(p>0.05). Data represent mean ± SEM; individual animals overlaid (n=4 sham, n=5 stroke. Kruskal-Wallis with Dunn's post hoc test for perilesion and EC. Mann-Whitney test for CC. Scale bar = 50 µm

4.6.1.1 Axon-myelin integrity is disrupted in the internal capsule

To further investigate whether myelin pathology extends into distant white matter pathways, we examined the internal capsule. MAG immunostaining revealed clear evidence of myelin disruption in stroke animals in the ipsilateral internal capsule compared to the contralateral group (Figure 4.20A).

Quantification confirmed these observations, with the Kruskal–Wallis test demonstrating a significant effect of stroke on MAG damage scores ($H(3, N=18)=12.89$, $P=0.0004$). Dunn's post hoc analyses indicated significantly higher MAG damage scores in the ipsilateral internal capsule of stroke animals compared to the contralateral stroke ($P=0.044$). No other group comparisons reached significance ($P>0.05$) (Fig. 4.20B).

Together, these findings show that stroke induced widespread myelin pathology, evident across white matter tracts, including the internal capsule. This widespread disruption of axon-myelin integrity highlights the vulnerability of white matter pathways to secondary degeneration following post-stroke.

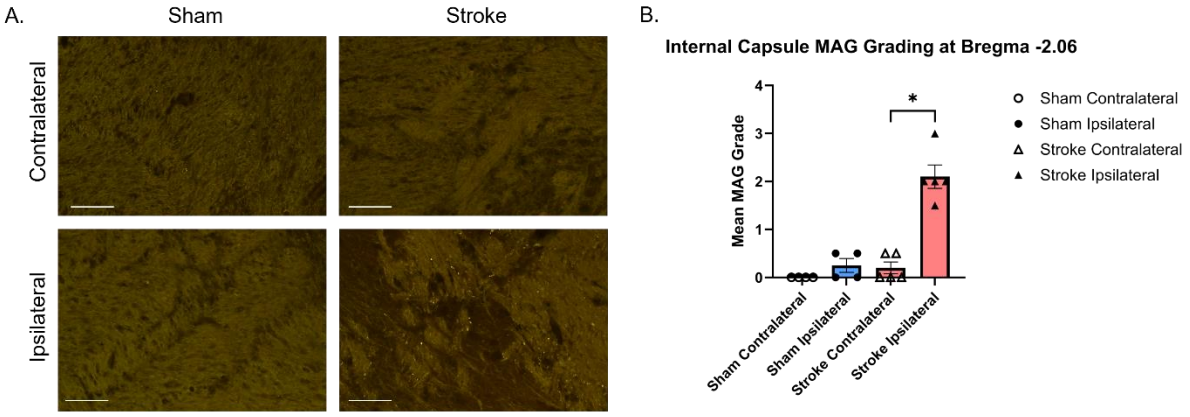

Figure 4.20. Axon-myelin integrity is disrupted in the internal capsule at the caudal level. (A) Representative MAG debris immunostaining shows minimal to no myelin debris in contralateral regions of sham and stroke animals, but disorganization of the fibres and loss of myelin integrity is seen in ipsilateral stroke animals. (B) Quantification of the mean MAG grading confirmed axon-myelin disruption in the ipsilateral stroke compared to the contralateral stroke (*P=0.044). Data represent mean ± SEM; individual animals overlaid (n=4 sham, 5 stroke. Kruskal-Wallis with Dunn's post hoc test. Scale bar = 50 µm.

4.6.2 Axon-myelin integrity is disrupted in grey matter regions

To further investigate myelin pathology, we examined peri-infarct cortex at both rostral and caudal levels. To further examine the myelin pathology to see whether it extends into distant but anatomically connected grey matter regions, we examined the ventral posterior medial (VPM) and ventral posterior lateral (VPL) thalamic nuclei, as well as the striatum at both rostral and caudal levels. These areas, while primarily composed of grey matter, contain myelinated fibres that form key connections between the cortex and thalamus. Building on this anatomical context, MAG immunostaining revealed clear evidence of myelin disruption in the ipsilateral thalamic nuclei, cortex, and striatum of stroke animals. In contrast, contralateral regions showed significantly lower levels of pathology (Fig. 4.21A,B,C).

In the cortex, at the rostral level, the Kruskal-Wallis test demonstrated a significant group effect on MAG damage scores ($H(3, N=18)=14.43$, $P<0.0001$). Dunn's post hoc analyses confirmed significantly higher MAG damage scores in the ipsilateral cortex of stroke animals compared to sham ipsilateral groups ($P=0.0083$). No other comparisons reached significance ($P>0.05$) (Fig. 4.21D). At the caudal level, the Kruskal–Wallis test revealed a significant group effect on MAG damage scores ($H(3, N=18)=13.29$, $P=0.0004$). Dunn's post hoc analyses indicated significantly higher MAG damage scores in the ipsilateral cortex of stroke animals compared to sham ipsilateral ($P=0.0443$) and stroke contralateral groups ($P=0.046$) (Fig. 4.21E).

In the striatum at the rostral level, the Kruskal-Wallis test revealed a significant group effect on MAG damage scores ($H(3, N=18)=15.04$, $P=0.0002$). Dunn's post hoc analyses indicated significantly higher MAG damage scores in the ipsilateral striatum of stroke animals compared to sham ipsilateral groups ($P=0.0087$), as well as compared to stroke contralateral ($P=0.021$) (Fig. 4.21F). At the caudal level, the Kruskal-Wallis test in the striatum revealed a significant group effect on MAG damage scores ($H(3, N=18)=12.88$, $P=0.0009$). Dunn's post hoc analyses indicated significantly higher MAG damage scores in the ipsilateral striatum of stroke animals compared to stroke contralateral groups ($P=0.027$). No other group comparisons reached significance ($P>0.05$) (Fig. 4.21G).

In the VPM thalamic nucleus, the Kruskal–Wallis test revealed a significant group effect on MAG damage scores ($H(3, N=18)=13.50$, $P=0.0003$). Dunn's post hoc analyses indicated significantly higher MAG damage scores in the ipsilateral VPM of stroke animals compared to sham ipsilateral ($P=0.038$) and stroke contralateral groups ($P=0.0036$). No other comparisons reached significance ($P>0.05$) (Fig. 4.21H).

Similarly, in the VPL thalamic nucleus, the Kruskal–Wallis test demonstrated a significant group effect on MAG damage scores ($H(3, N=18) = 14.09$, $P=0.0001$). Dunn's post hoc analyses revealed significantly higher MAG damage scores in the ipsilateral VPL of stroke animals

compared to stroke contralateral groups (P=0.0027). No other comparisons reached significance (P>0.05) (Fig. 4.21I).

Together, these findings demonstrate that stroke disrupts axon-myelin integrity and causes loss of myelin organisation that extends into distant grey matter regions, with increased damage observed at both rostral and caudal levels of the striatum and cortex. The widespread pattern of myelin disruption was present in both nuclei of the thalamus as well. This highlights the vulnerability of white matter pathways and connected grey matter structures to secondary degeneration following stroke, providing further evidence that white matter pathology is a major contributor to post-stroke brain injury.

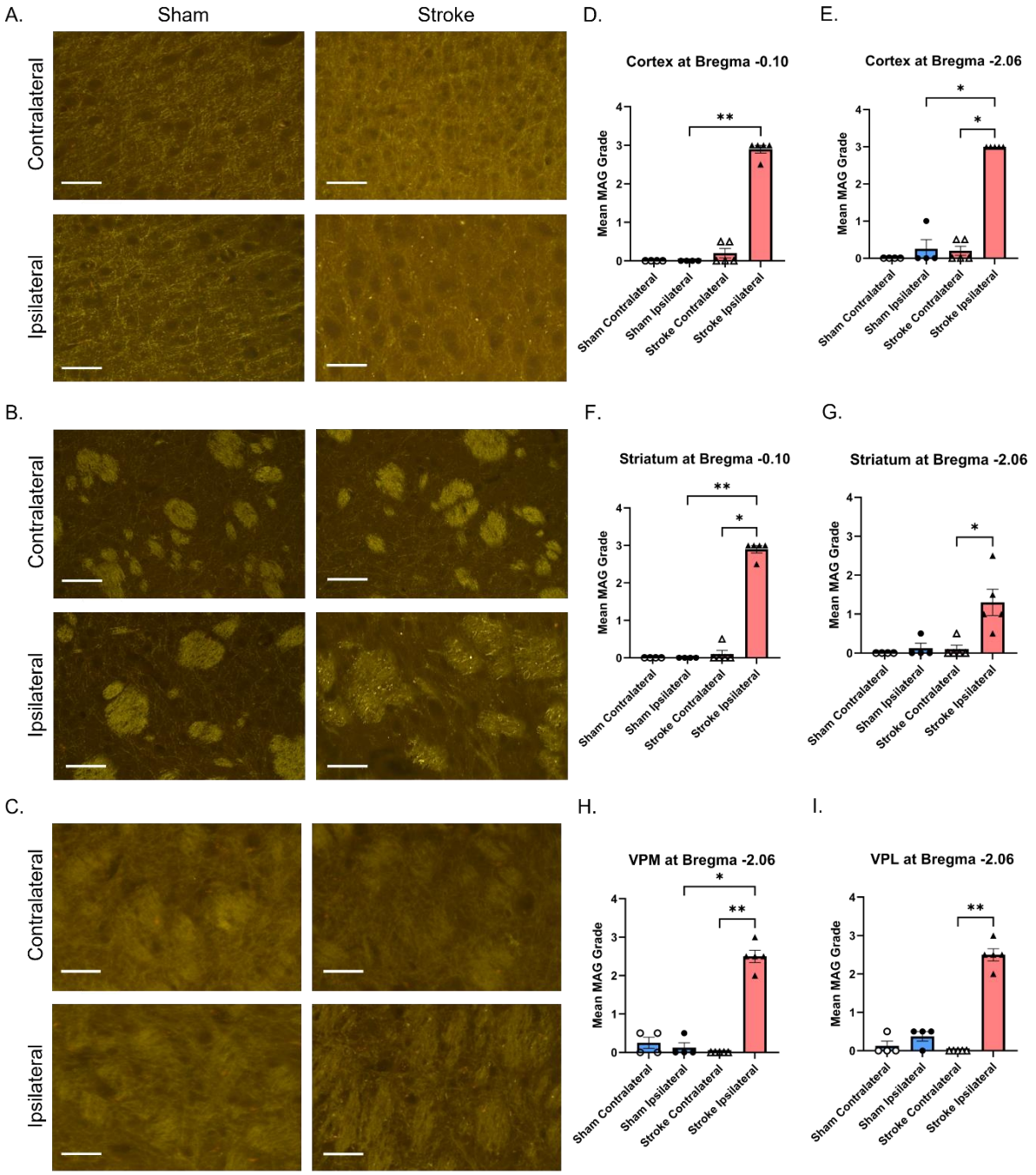

Figure 4.21. Axon-myelin integrity in grey matter regions following chronic ischaemic stroke. (A-C) Representative MAG immunostaining in sham and stroke animals, showing myelin debris in the thalamic nuclei, striatum and cortex, respectively. (D) Quantification at the rostral level cortex revealed greater myelin debris in ipsilateral side in stroke animals compared to sham (**P=0.0083). (I) Quantification of caudal level cortex revealed greater MAG debris in the ipsilateral side in stroke animals compared to the sham (*P=0.0443) and stroke contralateral groups (*P=0.0457). (F) Quantification of MAG debris at the rostral level of striatum revealed greater myelin disruption in ipsilateral stroke compared to contralateral stroke animals (*P=0.0214) and ipsilateral sham animals (**P=0.0087). (G) Quantification of MAG debris in the caudal level striatum revealed greater myelin disruption between the hemispheres in stroke animals (*P=0.0271). (H) Quantification of MAG debris revealed significantly greater myelin disruption in the ipsilateral side in stroke VPM compared to sham (*P=0.0375) and contralateral stroke (**P=0.0036). (E) Quantification of MAG debris revealed significantly greater myelin disruption in the ipsilateral side in stroke VPL compared to contralateral stroke (**P=0.0027) and contralateral sham (P=0.0288). Data represent mean ± SEM; individual animals overlaid (n=4 sham, 5 stroke. Kruskal-Wallis with Dunn's post hoc test. Scale bar = 50 µm.

4.7 Secondary neurodegeneration in distant but anatomically connected brain regions in chronic ischaemic stroke

Having evaluated the glial cell responses and myelin integrity, we next assessed secondary neurodegeneration in areas clinically known to be affected after cortical stroke, such as the thalamus (Kuchcinski et al. 2017). This was examined by analysing neuronal loss using NeuN immunostaining. NeuN is a pre-mRNA alternative splicing regulator and binds to the neuronal nuclei (NeuN) protein, so its expression is restricted to mature neurons. If there is a loss of nuclear localisation of NeuN, it confirms neurodegeneration (Arenas-Mosquera et al. 2022).

4.7.1 Secondary neurodegeneration in the thalamus four weeks post-stroke

Given the thalamus's vulnerability to secondary neurodegeneration after cortical stroke, we quantified neuronal density using NeuN immunostaining to evaluate neuronal loss four weeks post-stroke. For this, we observed both nuclei of the thalamus, VPM and VPL, as well as the reticular nucleus of the thalamus. The reticular nucleus (RTN) plays a crucial role in sensory processing, as it receives input from both thalamocortical and corticothalamic pathways. Neurons in the ipsilateral nuclei of the thalamus in stroke mice looked shrunken, and there was a complete loss of neurons in some regions; however, the density and morphology of neurons in the contralateral hemisphere appeared normal (Fig. 4.22A,C,E). The neuronal loss in these regions was quantified as neuronal density (neurons per mm^2). This way, we were able to compare the loss of neurons between different thalamic nuclei.

To quantify these changes, we used two-way mixed-effects ANOVA to determine the effects of stroke and hemisphere in the RTN. The analysis revealed significant effects of hemisphere ($F_{(1,4)}$=39.60; P=0.0033) and an interaction between hemisphere and surgery type ($F_{(1,2)}$=178.9; P=0055), but no significant effects of surgery ($F_{(1,4)}$=1.600; P=0.27). Bonferroni-corrected post hoc analysis revealed that the ipsilateral hemisphere of the stroke animals showed lower neuronal density in the RTN compared to the ipsilateral sham animals (P=0.0052), with no difference observed at the contralateral sites (P> 0.05) (Fig. 4.22B).

Two-way mixed-effects ANOVA in VPL showed significant effects of surgery ($F_{(1,4)}$=17.73; P=0.014) and hemisphere ($F_{(1,4)}$=34.08; P=0.0043). Additionally, there was a significant interaction between surgery and hemisphere (F(1,2) = 26.73; P = 0.035). Stroke resulted in lower neuronal density in the VPL ipsilateral to the stroke lesion (P=0.0012), but the contralateral hemisphere was unaffected (P>0.05) (Fig. 4.22D).

We next investigated VPM, and a two-way mixed-effects ANOVA revealed significant effects of surgery ($F_{(1,4)}$=18.72; P=0.012) and hemisphere ($F_{(1,4)}$=72.20; P=0.0011), as well as an interaction between surgery and hemisphere ($F_{(1,2)}$=116.8; P=0.0011). Stroke resulted in lower neuronal density in the VPL ipsilateral to the stroke lesion (P=0.0001), but the contralateral hemisphere was unaffected (P>0.05) (Fig. 4.22F).

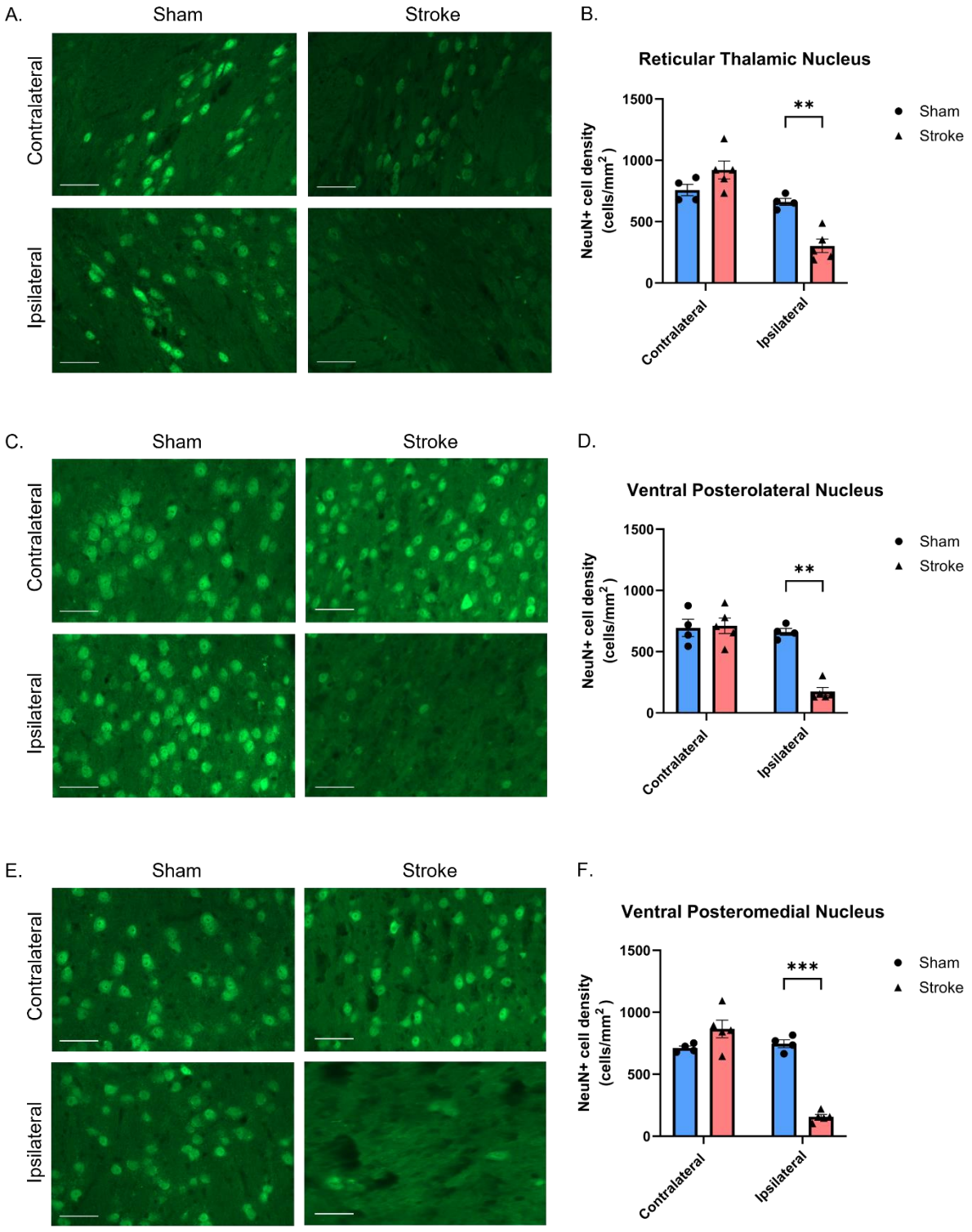

Figure 4.22. NeuN immunostaining reveals secondary neurodegeneration in thalamic nuclei four weeks post-stroke. (A-C-E) Representative NeuN-stained coronal sections showing neuronal density in the RTN, VPL and VPM, respectively, in sham and stroke mice four weeks post-surgery. Neurons in the ipsilateral side of the nuclei in stroke animals appear shrunken, with some regions showing complete loss, but neuronal density and morphology on the contralateral side were preserved. (B-D-F) Quantitative analysis of NeuN density showed a significant reduction in the ipsilateral RTN **P=0.0052) (B), VPL **P=0.0012 (D), and VPM ***P=0.0001 (F). Data represent mean ± SEM; individual animals overlaid (n=4 sham, 5 stroke). Two-way mixed-effects ANOVA with Bonferroni post hoc tests. Scale bar = 50 µm.

4.7.2 Secondary neurodegeneration in the striatum four weeks post-stroke

We next examined the striatum to determine if there was any neuronal loss following stroke. The striatum receives dense cortico-striatal projections from the sensorimotor cortex, making this region potentially vulnerable to secondary neurodegeneration following cortical injury. However, both the ipsilateral and contralateral hemispheres of stroke and sham animals showed normal density and size of the neurons (Fig. 4.23A)

Two-way mixed-effects ANOVA analysis confirmed there was no significant effect of surgery ($F_{(1,4)}$=0.11; P=0.76), or hemisphere ($F_{(1,4)}$=3.10; P=0.15), or of an interaction between surgery and hemisphere ($F_{(1,2)}$=2.31; P=0.27). Bonferroni corrected post hoc analysis confirmed this by showing that there was no neuronal loss on the ipsilateral side of the stroke animals compared to sham (P>0.05) (Fig. 4.23B).

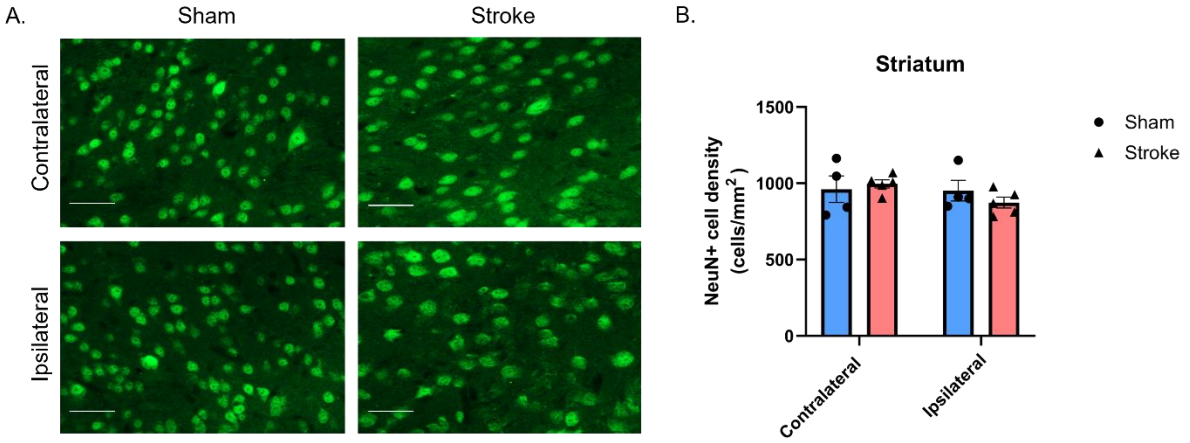

Figure 4.23. NeuN immunostaining reveals preserved neuronal density in the striatum four weeks post-stroke. **(A)** Representative NeuN-stained coronal section showing neuronal density in the striatum in sham and stroke mice four weeks post-surgery. No neuronal loss or morphological abnormalities were observed in stroke animals. (B) Quantitative analysis showed that neuron density was preserved on the ipsilateral side in stroke animals (P>0.05). Data represent mean ± SEM; individual animals overlaid (n=4 sham, 5 stroke). Two-way mixed-effects ANOVA with Bonferroni post hoc tests. Scale bar = 50 µm.

5. Discussion

In this study, we hypothesised that chronic ischaemic stroke would result in remote cellular changes in brain areas that are distant but anatomically connected to the primary lesion site, which, in turn, would trigger a global brain inflammatory glial cell response. Using MRI, we identified distinct perfusion and diffusion changes four weeks post-stroke, which included hypoperfusion in the peri-infarct cortex and the corpus callosum, and hyperperfusion in the ipsilateral thalamus. DTI showed increased FA in peri-infarct white matter and thalamic regions, suggesting microstructural reorganisation and compensatory white matter reorganisation. Our histological analysis further confirmed this by showing widespread astrocytic and microglial reactivity across both rostral and caudal white matter levels, as well as APP accumulation and MAG debris along major white matter tracts, including spread to the contralesional hemisphere. We observed neuronal loss in thalamic nuclei, accompanied by increased glial cell reactivity and axon-myelin disruption, suggesting secondary neurodegeneration and gliovascular remodelling in distant, but anatomically connected regions. In contrast, the striatum did not exhibit neuronal loss but showed persistent glial cell activation and disrupted axon-myelin integrity. In conclusion, these findings demonstrate that cortical ischaemic stroke triggers network-wide structural and cellular alterations within the white and grey matter tracts, resulting in global inflammation and secondary neurodegeneration. Meanwhile, diffusion MRI revealed early microstructural signatures of chronic remodelling. A summary table of the key MRI and histological findings is shown in Table 5 below.

ROIs	Level	MRI			IHC			
		CBF	FA	MD	Glial Cell	Axon Damage	Myelin Integrity	Neuron Loss
Cortex	Rostral	↓	↑	↔	↑	↑	↑	n/a
	Caudal	↓	↑	↔	↔	↑	↑	n/a
Peri-lesion WM	Rostral	↓	↑	↔	↑	↑	↑	n/a
	Caudal	↓	↑	↔	↑	↑	↔	n/a
Ventricular EC WM	Rostral	↔	↔	↔	↑	↑	↑	n/a
	Caudal	↓	↑	↔	↔	↑	↔	n/a
Midline CC	Rostral	↔	↔	↔	↑	↑	↑	n/a
	Caudal	↔	↔	↔	↔	↑	↔	n/a
Internal capsule		↔	↔	↔	↑	↑	↑	n/a
Striatum	Rostral	↔	↑	↔	↑	↑	↑	↔
	Caudal	↔	↔	↔	↑	↑	↑	n/a
Thalamus		↑	↑	↓	↑	↑	↑	↑

Table 5. Summary of MRI and IHC findings across rostral and caudal levels in the ipsilateral hemisphere. This is a summary of the ipsilateral hemisphere regions and how they were impacted after 4 4-weeks of dMCAO surgery. ↑ represents an increase in the value compared to sham or pre-surgery. For IHC, it means reactive glial and inflammatory cells, increased axonal damage and increased myelin disruptions. ↓ represent a decrease in the value compared to the sham or pre-surgery. ↔ represent no change. n/a means that the region for that parameter was not tested.

MRI reveals structural and functional changes in dMCAO mice

Our multimodal MRI analysis revealed distinct perfusion and diffusion signatures across cortical, subcortical and white matter regions at four weeks post-stroke. At four weeks post-cortical ischaemic stroke, we observed a decrease in cerebral blood flow within both white matter and cortical regions in the ischaemic hemisphere. This hypoperfusion in the white and grey matter regions is also observed in humans (Brumm et al. 2010), making the dMCAO model useful for pre-clinical studies. While reduced CBF does not necessarily equate to tissue hypoxia, since the brain is initially able to compensate for hypoperfusion by increasing the oxygen extraction fraction (OEF), this response reflects an increased metabolic strain on the tissue and may not be sufficient in the long term (Fan et al. 2022). Thus, persistent hypoperfusion likely represents ongoing tissue stress and microvascular dysfunction. This chronic hypoperfusion and tissue loss in the infarct and peri-infarct areas are consistent with previous reports of persistent vascular compromise following MCAO, as evidenced by longitudinal MRI in rodents, which shows prolonged cortical hypoperfusion in the subacute to chronic window (Hayward et al. 2011; Li et al. 2009). Moreover, white matter may be particularly vulnerable under these conditions since it possesses lower baseline CBF, fewer capillaries, and reduced capacity for compensation in oxygen extraction compared to grey matter. The reduction in perfusion is not only mechanistically important but also carries clinical relevance, as lower cortical CBF in vascular cognitive impairment predicts subsequent cognitive decline (Dinther et al. 2023). Additionally in post-stroke, lower cortical perfusion has been associated with cognitive impairment, as demonstrated by ASL-MRI studies showing reduced CBF in stroke survivors with dementia (Firbank et al. 2011).

In contrast to local hypoperfusion, at 1-month post-stroke, we observed an increase in CBF in the thalamus of the ipsilesional hemisphere. T2 scans in this region revealed a hypointense area (Fig. 4.2), suggesting possible thalamic tissue alterations associated with chronic ischaemic stroke. In the acute and subacute periods following cortical infarction, studies described thalamic alterations called ‘diaschisis’ in which structurally intact but functionally connected region exhibit reduced metabolic activity, impaired synaptic signalling, neuronal disconnections and functional alterations such as electrophysiological changes and hypoperfusion (Li et al. 2009; Cao et al. 2020). However, our findings differ from this early hypoperfusion profile. In chronic stages, one preclinical study reported increased thalamic perfusion (Hayward et al. 2011). In addition, other chronic stroke models demonstrate vascular and gliovascular remodelling, inflammation and secondary neuronal loss within the ipsilesional thalamus (C. Xia et al. 2021), even though these studies do not directly measure perfusion. The hyperperfusion in this distant, connected region suggests adaptive hemodynamic compensation or gliovascular remodelling in thalamocortical circuits that remain structurally intact but functionally reorganised following injury. The thalamus is highly interconnected with cortical and subcortical structures, so an infarction in the cortex can result in the disruption of these functional connections, leading to anterograde/retrograde degeneration and dysfunction (Cao et al. 2020). These results suggest that post-stroke

thalamic perfusion changes are not static but may evolve from early hypoperfusion to compensatory hyperperfusion in chronic stroke recovery. However, it would be useful to conduct a time course study to determine temporal changes in this mouse dMCAO model, including acute time points such as 24-48 hours post-stroke to very chronic points such as 3-6 months. In addition, to understand more about the mechanism of hyperperfusion, it would be helpful to examine vascular remodelling in the thalamus. Hayward et al (2011) demonstrated that chronic thalamic hyperperfusion is accompanied by increased RECA-1 positive vessel branching, elevated VEGF expression and evidence of BBB disruption. Aligning with this, in future studies we could stain for CD31, an endothelial and vascular marker; collagen IV, a basement membrane marker; and α-SMA or PDGFRβ to evaluate mural cell and pericyte changes. These could help us determine whether altered vessel density, branching or angiogenic remodelling contributes to increased CBF.

The increase in FA in peri-infarct white matter further supports the idea of microstructural reorganisation. Although some preclinical stroke studies show decreased FA due to axonal degeneration and demyelination (Wang et al. 2006; Yang et al. 2022; Z. Li et al. 2021), others demonstrate that in chronic stroke, glial cell proliferation, extracellular matrix reorganisation, or compensatory axonal sprouting can lead to increased FA (Budde et al. 2011; Y. Xia et al. 2021). Several studies have also reported increased FA in ipsilesional white matter in chronic stages, where post-mortem histology revealed high-density axons and myelin consistent with tissue reorganisation (van der Zijden et al. 2008; Jiang et al. 2006; Ding et al. 2008). Additionally, MD remained unchanged in these regions. Typically, in the literature, an increase in MD is reflective of white matter disruption (Gupta et al. 2006; Holland et al. 2011), but this is more severe than the model used in this study. Since MD is a measure of average water diffusion, its stability indicates preserved overall water mobility, implying that FA elevations likely result from directional remodelling (Christidi et al. 2022). Since white matter FA relates to microstructural integrity, which is associated with processing speed and executive function, it is likely to predict cognitive outcome after stroke (Fruhwirth et al. 2024). In humans, FA alterations evolve temporally. Early work shows that as injury evolves, FA values can remain stable at first in the hyperacute stage, then progressively decline (Sotak 2002; Puig et al. 2011). However, studies have reported that in the chronic phase, there can be local increases in FA value or partial recovery in peri-lesional white matter, consistent with structural reorganisation (Schaechter et al. 2009).

Most studies show decreased values of FA in the grey matter regions in acute stroke (Feng et al. 2022). In contrast, we observed increased values in the peri-infarct cortex and thalamus, without any change in MD. Since FA captures the directionality of water diffusion, this increase may suggest microstructural remodelling rather than necrosis. Budde and colleagues demonstrated that reactive/anisomorphic gliosis can increase anisotropy, even in the grey matter, by imposing more coherent cellular processes (Budde et al. 2011). Literature supports this in the context of brain injury (Feng et al. 2022). The thalamus also aligns with this chronic remodelling after stroke. Literature shows there is a persistent inflammatory response and

progressive remodelling in the thalamus (Cao et al. 2020; Necula et al. 2022), consistent with chronic remodelling and astrogliosis observed in chronic stroke.

Very few studies have used ASL as a way of assessing white matter integrity following dMCAO in the context of chronic stroke, showing regionally diverse peri-infarct and cortex hypoperfusion along with thalamic hyperperfusion. This study extends the field's focus from subacute diaschisis to a compensatory, chronic gliovascular phase; therefore, the results of this study are novel. We also observed an integrated perfusion and diffusion signature that supports a coordinated, network-level remodelling rather than local damage. Furthermore, reports of FA and MD findings in MCAO studies tend to use a 60-minute intraluminal thread MCAO model which induces large infarcts, whereas this one is representative of a more modest stroke.

The main limitation of this study is the single chronic time point used for post-stroke imaging, which limits our ability to look at the temporal trajectory of diffusion and perfusion changes. To overcome this in the future, longitudinal MRI imaging at multiple post-stroke windows can be done to understand the temporal sequence of events. This limitations profile is not unique to our study; many chronic MCAO reports rely on a single post-stroke timepoint and standard DTI/ASL protocols. Therefore, our findings are directly comparable to prior literature using similar designs; however, future studies should incorporate MRI at multiple post-stroke timepoints spanning from acute (24 hours), subacute and chronic phases (6 months) to determine when these perfusion and diffusion changes first emerge and how they evolve over time.

Glial cell changes in chronic stroke

To better understand the pathological correlates of the MRI findings, we examined astrocytic and microglial responses across white and grey matter regions. Glial cells play a crucial role in the response to stroke. Rapidly activated after ischaemia (Xu et al. 2020), both microglia and astrocytes proliferate at the lesion site and microglia migrate to the lesion site to exert both neuroprotective and inflammatory processes (Zhang et al. 2021; Zhang 2019). As the stroke progressed into its chronic stages, glial expression remained elevated throughout remote anatomically connected brain regions. Astrocytes are involved in the homeostasis and protection of the central nervous system. In stroke, they are rapidly activated to aid in remodelling and repair; however, they may also exert further damage through the release of toxic mediators and the aggravation of inflammation (Li et al. 2022).

Glial cell changes in the white matter

We used GFAP to identify astrocytes; although GFAP is highly upregulated in reactive astrocytes (Escartin et al. 2021), we also observed basal GFAP expression in shams in white matter and the hippocampus. We observed increased GFAP expression in the stroke animals at the rostral level in the midline of the corpus callosum, along the external capsule, right

above the ventricles, as well as the perilesion area, indicating widespread astroglial reactivity extending beyond the infarct core. At the caudal level, these cells were more restricted to the perilesion area and the internal capsule, suggesting regional differences in the persistence and intensity of astrogliosis. In line with our results, Wan et al. (2022) also observed increased GFAP+ cells in the corpus callosum post-stroke (Wan et al. 2022). However, astrocytic reorganisation and gliosis within the internal capsule remain relatively understudied (Zhuang et al. 2025), and our results therefore provide novel insight into region-specific white matter responses and the potential for persistent glial activation along descending projection pathways. Additionally, post-stroke white matter alteration can vary by rostro-caudal level (Zalewska et al. 2021); our findings provide new anatomical specificity on the spatial heterogeneity of chronic astroglial responses.

Observing this persistent astroglial reactivity in remote white matter regions may have a broader implication for long-term cognitive outcomes. Chronic astrogliosis can contribute to white matter disconnection, axonal degeneration, and Wallerian degeneration (Huang et al. 2025; Wan et al. 2022), which can ultimately lead to impaired network communication, all of which are strongly associated with post-stroke cognitive decline (Poirier et al. 2025; Schaapsmeerders et al. 2016). However, while astrocytes play a crucial role in preventing the spread of the lesion, their prolonged activity can have an adverse effect, such as inhibiting axonal regrowth and remyelination through the re-release of pro-inflammatory cytokines (Wan et al. 2022). Additionally, it is essential to note that, as we used GFAP as our astrocyte marker, we cannot strictly report an increase in astrocyte numbers; the increased density of reactive astrocytes could be due to existing astrocytes that upregulate GFAP expression, rather than cell proliferation. Therefore, our results may represent astrocytic hypertrophy and enhanced GFAP expression rather than proliferation. Previous work in the Fowler lab found no evidence of increased astrocyte nuclei in the thalamus when Sox9 was used as a nuclear astrocyte marker, suggesting that proliferation could be restricted to perilesional areas. In the future, we can incorporate proliferation markers such as BrdU and EdU to label dividing cells directly and also use additional astrocyte markers such as Sox9 and Aldh1l1 to quantify astrocyte populations and phenotypes more accurately (Escartin et al. 2021; Verkhratsky and Nedergaard 2018). Additionally, recent research suggests that astrocytes may actively contribute to secondary white matter pathology (Huang et al. 2025). Huang Z et al. (2025) and colleagues show that lipocalin-2-dependent astrocyte-oligodendrocyte interactions can drive post-stroke demyelination and promote transcallosal spread of myelin damage. Integrating these mechanistic analyses with longitudinal MRI would help us understand astrocyte reactivity in remote regions.

Importantly, astrocytes and microglia act in close coordination to regulate post-stroke inflammation and repair. Astrocyte phagocytosis has been suggested to be a compensatory mechanism when the phagocytic capacity of microglia is overwhelmed (Ponath et al. 2017), and astrocytes can allow for the recruitment of microglia to clear myelin debris (Skripuletz et al. 2013). Microglia, the resident immune cells of the CNS, regulate brain development and

play a pivotal role in sustaining neural homeostasis. Following a stroke, microglia have been said to promote recovery through the production of anti-inflammatory cytokines and growth factors (J. Li et al. 2021). Controversially, there is also evidence of neurodegeneration through the release of microglial-derived cytotoxic factors (Pawluk et al. 2020).

We used Iba1 to identify microglia post-stroke. We observed an increased Iba1 expression within the white matter, indicating persistent microglial activation in the chronic phase of ischaemic stroke. Similar to astrocytes, at the rostral level, microglia/macrophage were markedly elevated at the midline of the corpus callosum and at the perilesion site. At the caudal level, Iba1 cells were increased only in the perilesional site and at the internal capsule, showing a sustained microglial response along the white matter tracts that are anatomically connected to the primary cortical lesion. The spatial distribution of Iba1 cells aligns closely with that of reactive astrocytes, supporting a coordinated response of glial cells across both caudal and rostral levels. This coordinated response of spatial pattern is consistent with studies that show astrocyte-microglia interaction plays a key role in regulating white-matter inflammation, demyelination, and glial cell remodelling after an injury (Huang et al. 2025; Liang et al. 2023; Guo et al. 2025).

Previous research has shown that chronic microglial activation occurs in remote and peri-infarct white matter regions following stroke (Shi et al. 2019). However, most of these studies have focused on the rostral areas, but the caudal regions have received comparatively little attention in chronic stroke models. Our study provides a novel insight into the descending projection pathways, which are vulnerable to Wallerian degeneration. This prolonged microglial activation, observed at both levels, may represent a shift toward a chronic pro-inflammatory phenotype. Although microglia are essential for debris clearance and tissue remodelling after an injury, prolonged activation can drive axon and myelin damage through the release of cytotoxic mediators, such as TNF-α, IL-1β, and reactive oxygen species (Shui et al. 2024). Moreover, chronic microgliosis has been linked to reduced white matter integrity and cognitive decline in both clinical and preclinical studies (Zeng et al. 2024).

Future work could use FIRE mice to investigate the causal relationship between microglia and white matter changes. FIRE mice are genetically altered so they lack microglia due to the deletion of a regulatory enhancer in Csfr1 (Munro et al. 2024; Rojo et al. 2019). This would allow us to determine whether the absence of microglia affects Wallerian degeneration or preserves axonal and myelin integrity in remote tracts. Since subtle changes to white matter have already been reported with ageing in these mice, remote white matter alterations would be exacerbated in these mice, showing the importance of healthy white matter integrity. In addition, high-resolution transcriptomic approaches, such as single-cell RNA sequencing, could be employed to map microglial gene expression in white matter tracts. Recent studied have showed distinct microglia subclusters following ischaemic stroke (Del Águila et al. 2024; F. Zeng et al. 2023), as well as white-matter associated microglia with unique transcriptional signatures (Safaiyan et al. 2021). Using these approaches in pathways identified in our study

would provide an insight into how microglia states can affect long-term degeneration or recovery.

Glial cell changes in the grey matter following stroke

Increased expression of glial cells in distant regions has been linked to cognitive impairment due to a dysregulation in neurogenesis, homeostatic imbalance, and neurodegeneration (Stuckey et al. 2021). We next examined anatomically connected grey matter regions, such as the striatum and the thalamus, to determine whether they exhibit a similar heterogeneous, level-dependent glial cell response in chronic ischaemic stroke. GFAP expression was elevated in the striatum at both rostral and caudal levels, indicating persistent astrogliosis in subcortical regions. In contrast, in the cortex, we observed increased GFAP only at the rostral level but not at the caudal level, reflecting that the infarct did not extend into this region. Recent work has demonstrated that peri-infarct cortical GFAP remains elevated into the chronic phase, and a higher GFAP burden is associated with poorer functional recovery (Stokowska et al. 2023). However, most studies focus on characterising the peri-infarct cortex at a single coronal level; rostro-caudal mapping of GFAP and inclusion of striatal grey matter are rare (Chen et al. 2025). Our findings imply that striatal astrocytes remain chronically engaged, likely reflecting secondary neurodegeneration and differentiation of cortico-striatal projections.

Iba1 showed a similar pattern, with high microglial activation in the striatum at both rostral and caudal levels. In contrast, cortical microgliosis was only present at the rostral level, closer to the lesion site. This is consistent with previous findings that microglia, while essential for debris clearance and tissue remodelling, can remain chronically activated and contribute to neuroinflammation (Planas 2024). In this context, persistent microgliosis in the corticostriatal pathways may reflect an incomplete resolution state, never reverting to a homeostatic state and remaining partially active, thereby producing and/or maintaining pro-inflammatory signals, which potentially contribute to secondary neurodegeneration. This is supported by reduced white matter integrity and worsening of cognitive outcome in clinical studies (Poirier et al. 2025). In the future, this could be investigated more directly by using fate-mapping to track microglia lineage changes over time, or through depleting microglia by using models such as FIRE mice to determine whether removing microglia has an effect downstream with axonal and synaptic loss.

The parallel distribution of GFAP and Iba1 in the grey matter suggests crosstalk between reactive astrocytes and microglia, which serves as a driver of regional heterogeneity, aligning with recent research showing the bidirectionality of the signal between the regions (Yang et al. 2025). In the future, we can use single-cell or single-nucleus RNA sequencing to define ligand-receptor interactions that mediate this bidirectional signalling, similar to recent astrocyte-oligodendrocyte crosstalk study (Huang et al. 2025). We can selectively knock down or overexpress key astrocyte- or microglia-derived signalling molecules and examine their effects on white matter integrity and cognitive outcomes. These persistent glial cell responses

along cortico-striatal pathways may contribute to deficits in executive function and learning observed in chronic stroke.

One key limitation of this study is the use of % area to assess astrocyte and microglial responses. Although this captures the overall signal changes, it does not distinguish between different cellular phenotypes. Glial cells can have similar morphological changes, but markedly different phenotypes. In the future, more informative approaches, such as quantifying individual cells and performing morphological analysis of microglia, assessing soma size, process length, and branching complexity, could be done. Observing the general activation of astrocytes and microglia is a beneficial first step; however, assessing cell function is pivotal to understanding the underlying mechanisms.

Myelin and axonal damage in chronic stroke

Myelin and axonal damage in the white matter following stroke

To further investigate pathological correlates of the MRI findings, we next examined markers of axonal and myelin integrity, including APP and MAG, within the same ipsilateral and contralateral white and grey matter regions. At the rostral level, we observed increased APP accumulation at both contralateral and ipsilateral external capsule, above the ventricles, midline of the corpus callosum and peri-lesion white matter tracts, suggesting a widespread axonal transport disruption beyond the infarct core. At the caudal level, we observed a similar pattern in which APP accumulated in the ipsilateral EC, midline of the corpus callosum and peri-lesion site, suggesting axonal damage descends through these remote but connected white matter tracts in chronic stroke. These findings are consistent with previous work that demonstrates cortical ischaemia induces APP accumulation in remote white matter tracts and causes Wallerian degeneration (Zuo et al. 2019). However, most recent research focuses on acute or subacute MCAO; our data revealed chronic APP accumulation at four weeks, indicating axonal vulnerability following stroke.

Furthermore, the bilateral and rostro-caudal distribution observed here suggests that neuronal damage resulting from primary cortical injury can extend distally along the axon, leading to axonal degeneration and myelin damage in remote regions in which it has projections, such as the corpus callosum (Zuo et al. 2019). This axonal degeneration may prevent the transport of essential neurotrophic factors to remote areas, thus exacerbating injury. We also observed APP accumulation in the internal capsule, which highlights the ongoing degeneration in key projection fibres linking cortical and subcortical regions. Although APP accumulation in the internal capsule has been reported in other injury models (Uehara et al. 1999), to our knowledge, its chronic accumulation following cortical ischaemia has not been described previously. Research shows that damage in these regions can impair network connectivity and contribute to deficits in executive function, ultimately leading to post-stroke cognitive decline (X. Cao et al. 2021).

In line with previous studies, we observed bilateral myelin damage using MAG immunostaining in the white matter tracts following stroke (Wan et al. 2022; Zuo et al. 2019). At the caudal level, the overall pattern of disruption was less pronounced than in rostral regions, although still showing an effect of stroke. This could potentially be due to a regional difference in the severity of ischaemic injury or the timing of the white matter degeneration, where caudal tracts may show a delayed vulnerability compared to rostral regions. Another explanation could be that axon-myelin disruption seen in the caudal region may be more subtle, as the axonal damage observed there is not as severe as in the rostral region, falling below the detection threshold of semi-quantitative scoring. Since myelin integrity is essential for interhemispheric communication and cognitive processing, chronic myelin alterations can contribute to long-term deficits that are observed in post-stroke cognitive impairment.

Even though DTI revealed peri-lesional white matter changes, our histological analyses revealed a more extensive pattern of APP accumulation and MAG disruption across both hemispheres. This highlights a key limitation of MRI in small-animal stroke models. The white matter is very small, and DTI lacks the spatial resolution and sensitivity that is required to detect these subtle changes. Since axonal damage and myelin disruption are detectable microscopically and DTI does not show the corresponding abnormalities, they fall below the sensitivity threshold of diffusion MRI. This could also be due to the fact that DTI captures average diffusion environment within each voxel rather than specific axon and myelin pathology. As a result, if there is subtle degeneration, that might not alter diffusion metrics thus MRI can underestimate secondary neurodegeneration.

Additionally, we employed a semi-quantitative grading analysis of the white matter damage, which is helpful for the initial assessment of myelin changes; however, it may not be sensitive enough and risks subjectivity. We can employ more sensitive methods, such as combining myelin fibre markers, including myelin basic protein (MBP), MAG, and NF200 (Wan et al. 2022) and importantly a degraded MBP, which has recently been shown to serve as a sensitive marker of active myelin breakdown (Huang et al. 2025). Wan and colleagues also used Luxol fast blue and black gold staining to assess the integrity of myelin and the area of myelination. Finally, electron microscopy would allow us to analyse changes in myelin structure, which would give us a detailed evaluation of myelin integrity post-stroke. Although recent studies that used EM focused on remote white matter regions at earlier timepoints following cortical ischaemia (Zuo et al. 2019; Huang et al. 2025), to our knowledge, no study has examined axon-myelin disruption in more distant caudal white matter regions such as the internal capsule.

Myelin and axonal damage in the grey matter following stroke

Given the widespread axon-myelin degeneration observed in the white matter tracts, we next examined the cortex itself, where there was a marked increase in APP accumulation, consistent with disrupted axonal transport within the peri-infarct cortical tissue. We then assessed anatomically connected grey matter regions, which showed similar alterations in glial and inflammatory cell responses. Across both rostro-caudal regions, APP immunostaining

was increased in the striatum and cortex after ischaemic stroke, supporting our previous findings of disrupted axonal transport and chronic axonal injury beyond the infarct core. This was also seen in both nuclei of the thalamus, where APP was markedly accumulated in the ipsilateral hemisphere. We therefore see a chronic and widespread APP expression that is not only confined to white matter tracts but also affects grey matter that shares reciprocal cortical projections. While prior research has shown APP accumulation in striatal fibre tracts in permanent/transient MCAO in rat models in which the striatum is directly within the infarct region, to our knowledge, APP increase in the striatum as a consequence of cortical infarct, particularly at chronic timepoints, has not been reported before (Mäkinen et al. 2008; Yam et al. 1997).

Axonal degeneration seems to be bilateral and projects into distant regions, which supports a model of progressive, network-mediated degeneration. A key limitation of this analysis is that APP is an indirect measure of axonal injury since it accumulates at the damaged membrane and does not distinguish between reversible dysfunction and irreversible degeneration. Future work needs to be done to look at tract-specific expression to see if APP accumulation reflects ongoing degeneration.

In parallel with our APP findings, we found increased MAG debris in the striatum and cortex after stroke. We discovered that alteration to axon-glial integrity was greater in the ipsilateral striatum compared to the contralateral striatum of stroke animals at both rostral and caudal regions, suggesting sustained myelin vulnerability in subcortical grey matter regions. Previous research has shown myelin injury and remyelination in the striatum after MCAO; however, they used dMBP, and the striatum was likely to be adjacent to or within the infarct core (Xu et al. 2023). Our findings extend this by showing the striatum as a remote anatomically connected region that has disrupted axon-myelin integrity after cortical ischaemia.

We included bilateral and rostro-caudal mapping of myelin integrity within the grey matter, extending beyond prior studies that focused on white matter tracts or single coronal levels. Together, APP accumulation and MAG loss reflect disruption of axon-myelin integrity, secondary to axonal deficits observed with APP. These findings highlight that axon-myelin degeneration is coupled in the chronic stage of ischaemic stroke.

Thalamic changes in chronic stroke

Neurodegeneration in the ipsilateral thalamic nuclei

Neuronal loss was observed in the ipsilateral thalamus, specifically in the reticular thalamic nucleus (RTN), ventral posterior medial nucleus (VPM), and the ventral posterior lateral nucleus (VPL) four weeks post-stroke. Both clinical (Nakane et al. 2002) and preclinical (Cao et al. 2017) studies show secondary thalamic degeneration; however, neurodegeneration can develop in different subtypes of the thalamus, depending on the site of initial injury and the connected cortico-thalamic projections (Cao et al. 2017; Nakane et al. 2002). In our model, we included VPM and VPL, which aligns with previous reports showing that lesions in the

somatosensory cortex produced by dMCAO can lead to neuronal loss in these ventral posterior nuclei that serve as a primary relay hub for somatosensory information between the thalamus and the cortex (Iizuka et al. 1990; Cao et al. 2017). This means that damage in these nuclei results in anterograde and retrograde degeneration along the pathways that send projections from the primary somatosensory cortex and thalamus (Viaene et al. 2011).

Furthermore, we detected significant neuronal loss in the RTN, a region that is not directly innervated by the cortex but involved in inhibitory regulation of thalamic relay nuclei (Pinault 2004). Loss of neurons in this region may therefore exacerbate the excitatory-inhibitory imbalance within thalamocortical circuits, potentially contributing to the network hyperexcitability observed in chronic stroke models (Bokor et al. 2005; Wimmer et al. 2015). Although some studies showed RTN degeneration following stroke, they examine mice with a more extensive cortical infarct (Dihné et al. 2002), or proposed mechanistic pathways involving basal ganglia and RTN inhibitory input (Yamauchi et al. 2022). Therefore, to our knowledge, our findings are the first to demonstrate RTN neuronal loss in the dMCAO model of cortical stroke. This combined degeneration across RTN, VPM and VPL highlights that secondary thalamic injury extends beyond the isolated relay nuclei and may even disrupt both the sensory transmission and inhibitory gating mechanism within the thalamocortical system.

Even though we showed the significance of this thalamic neuronal loss, such widespread involvement suggests potential consequences for somatosensory processing, arousal regulation, and cognitive function. This is supported clinically, where individuals with MCA or cortical territory stroke also develop secondary thalamic alterations remote from the infarct, which is characterised by focal iron accumulation which authors hypothesised to be marker of neurodegeneration (Kuchcinski et al. 2017). Future studies need to be done to combine thalamic structural analysis with behavioural outcome to show how chronic thalamic injury contributes to post-stroke sensory and cognitive deficits. In particular, we can use adhesive removal tasks and whisker-dependent tasks, such as the gap-crossing test, to assess VPM/VPL dysfunction, whereas EEG-based sleep-wake cycle could test RTN-related alterations. In addition, cognitive assays such as novel object recognition and spontaneous alterations in a Y-maze could help assess how secondary thalamic degeneration impacts attention and memory in the chronic phase.

Glial cell changes in the ipsilateral thalamus

Alongside thalamic neuronal loss, in parallel with our MRI-detected hyperperfusion, we observed increased density of GFAP+ astrocytes and Iba1+ microglia/macrophages in the ipsilateral thalamus at four weeks post stroke. This glial cell activation suggests that thalamic hyperperfusion and secondary neurodegeneration are accompanied by ongoing neuroinflammatory and glial-remodelling processes. Several previous studies have also shown similar glial cell activation in the thalamus following cortical stroke (Langen et al. 2007; Kim et al. 2021; Cao et al. 2017). Cao and colleagues (2021) demonstrated that thalamic neurodegeneration was present 7 to 84 days post-stroke, and this was associated with

upregulation of GFAP expression and microglial activation. These microglia transitioned into a less homeostatic phenotype, characterised by ApoE, Axl, and LpL expression, which are markers of the disease-associated microglia phenotype, indicative of active phagocytosis and metabolic reprogramming (Z. Cao et al. 2021; Deczkowska et al. 2018).

This glial cell reactivity likely reflects a response to secondary neurodegeneration arising from the disrupted cortico-thalamic projections. This reparative role has been shown by Kluge and his colleagues that microglia internalise NeuN material in the degenerative thalamus (Kluge et al. 2019). It has also been shown that modulation of microglia function, such as using Spp1 knockout mice, can directly alter the extent of secondary neurodegeneration, causing exacerbated degeneration after cortical stroke (Schroeter et al. 2006). In addition to this, astrocytes have been found in the thalamus long after stroke, leading to glial scar-like characterisation and ultimately a sustained metabolic stress (Kim et al. 2021), which may contribute to chronic thalamic dysfunction. This co-localisation of perfusion changes with reactive glial response suggests an active attempt to restore homeostasis in surviving thalamic tissue. Future studies should utilise transcriptomic profiling to clarify gliovascular interactions and blood flow regulation in the thalamus after cortical stroke.

Myelin and axonal damage in the ipsilateral thalamus

In addition to glial cell response, we also observed increased APP accumulation and reduced MAG expression in the ipsilateral VPM and VPL, consistent with axonal damage and myelin degeneration secondary to cortical infarction. This extends the MRI findings of thalamic hyperperfusion by identifying structural correlates of chronic thalamic remodelling. APP accumulation in the VPM and VPL reflect retrograde degeneration along damaged cortico-thalamic pathways (van Groen et al. 2005). Similar to this, accumulation of the MAG debris suggests myelin sheath disruption in the thalamus, suggesting early myelin instability associated with axonal degeneration.

This combination of APP and MAG supports the idea that the hyperperfusion seen in the thalamus can be due to a compensatory mechanism of tissue remodelling rather than simple recovery. Increased blood flow to the thalamus may be required for the metabolic demands associated with glial activation that is present long after the injury, axonal sprouting, or gliovascular reorganisation; although persistent axon-myelin disruption could reduce conduction and drive compensatory gliovascular remodelling to sustain metabolic support in disconnected thalamic tissue. Research shows that in the long-term response to rodent cerebral ischaemia, hyperperfusion is detected with MRI in the ipsilateral thalamus accompanied by increased vessel branching (angiogenesis), consistent with our findings that there is sustained remodelling that also exhibits neuronal loss (Hayward et al. 2011). This can be interpreted as a remote plasticity response to secondary neurodegeneration. Together, these findings make the thalamus a critical hub of secondary pathology and these changes potentially contribute to chronic network dysfunction and cognitive decline (Kuchcinski et al. 2017).

Neuronal preservation in the striatum

In contrast to the thalamus, no significant neuronal loss was observed in the striatum at the rostral level four weeks post-stroke. Striatum receives dense cortico-striatal projections from the sensorimotor cortex, which could suggest this region may be vulnerable to secondary neurodegeneration following cortical injury (Butler et al. 2002). However, we did not detect alterations to NeuN immunostained cells in our dMCAO model, which suggests that the severity of the ischaemic injury and subsequent disconnection was not sufficient to trigger neuronal death in this region. This finding is consistent with previous research that shows dMCAO primarily produces superficial cortical infarcts that spare subcortical structures such as the striatum (Liu et al. 2020).

Our additional analyses revealed increased APP accumulation, MAG disruption and elevated GFAP and Iba1 expression in the striatum as reported previously (Figure 4.12,4.15,4.18,4.21). These results indicated disruption of axonal-myelin pathology as well as persistent glial cell activation that *occurs in the absence of neuronal death*. These results suggest that the striatum undergoes secondary, connectivity-driven remodelling, which likely reflects a chronic response due to disrupted cortico-striatal projections rather than direct ischaemic injury or secondary neurodegeneration.

These results suggest that there is regional specificity of secondary injury after cortical stroke, where the thalamus appears more vulnerable to neuronal degeneration, whereas the striatum shows more subtle, chronic remodelling. There are differences between metabolic demand, vascular supply and projection pathways between the striatum and the thalamus, and this can underlie this selective vulnerability. Further work is needed to combine NeuN with markers of synaptic integrity (synaptophysin, PSD-95, Homer1) and neuronal stress (MAP2, Fluoro-Jade C) to clarify neuronal dysfunction in the chronic phase.

Limitations and future directions

Some general limitations in our methods of analysis and potential future directions have been outlined above. However, there are some other general limitations to our study.

The use of relatively young, otherwise healthy mice allowed us to examine the direct effects of cortical ischaemia without the confounding variables such as age, diabetes, hypertension or neurodegenerative changes. This work provides a clean framework for identifying fundamental mechanisms of post-stroke injury and recovery. However, this experimental design creates a limitation as stroke predominantly occurs in older individuals with comorbidities. Another limitation is that we exclusively used male mice in this study. Male mice were used to minimise the hormonal variability and maintain consistency with existing stroke models. It is well known that sex differences play an important role in stroke; therefore, a large limitation of our study is the use of male mice. In the future, sex differences in stroke recovery and secondary pathology should be investigated. The lifetime risk of stroke is higher in women, and they tend to have poorer functional recovery compared to men (Rexrode et

al. 2022). Several factors, such as pregnancy, the use of oral contraceptives, and menopause related loss of oestrogen, which is neuroprotective, have been linked to this poor recovery (Girijala et al. 2017).

Additionally, electrophysiology such as compound action potential recordings could be used to assess white matter conduction deficits to help characterise functional disruption within transcallosal projections (Fowler et al. 2018). Advanced diffusion MRI techniques and graph-theory based structural and connectivity analyses (Boehm-Sturm et al. 2017; Hall et al. 2022) could be used to map large-scale thalamocortical network alterations better characterise anterograde and retrograde degeneration. Since the white matter in mice is so small, sometimes, subtle pathological changes are not reflected with traditional DTI. However, neurite orientation dispersion and density imaging (NODDI) could allow for a mechanistic insight into microstructural pathology while giving more information about the axonal and glial changes (Gazdzinski et al. 2020). Furthermore, spatial transcriptomic techniques could determine the molecular correlates of imaging changes. This is already being incorporated into our experimental plan, as we have undertaken CosMx spatial transcriptomic profiling in a subset of the mice used in this study.

We used Iba1 staining; however, Iba1 is not a specific marker for microglia as it also labels macrophages. Additional microglia-specific markers, such as TMEM119 and P2RY12, can be used as well as markers of disease associated microglia, such as SPP1. We only used GFAP as the astrocyte marker, but this only labels reactive astrocytes. Additional astrocyte markers, such as Sox9 and Aldh1I1, would allow us to gain further insight into glial cell changes. Sex differences in properties of microglia and astrocytes in response to ischaemic stroke have also been reported (Kerr et al. 2019). So, it is essential to investigate sex differences in glial cell responses in the future.

We used APP staining, but it only reflects the impairment of the axonal transport and does not distinguish between reversible dysfunction and irreversible degeneration. Synaptophysin could be used to assess axonal integrity and synaptic integrity. We used MAG, but it does not tell us the total myelin content. Further markers, such as MBP and PLP, can be used for more comprehensive myelin integrity.

It is known that the older population is more susceptible to injury and disease. These glial cells can be highly heterogeneous depending on age and disease context. Age is a risk factor for stroke and cognitive decline post-stroke. Thus, it is important to investigate the molecular and functional properties of ageing glial cells in aged mice and the impact of stroke to further understand their roles in disease pathology (Grabert et al. 2016).

We only looked at glial cell changes and axon-myelin integrity within the VPM and VPL nuclei of the thalamus. Future work should include RTN to complement the NeuN data and provide a more comprehensive understanding of secondary thalamic neurodegeneration and glial remodelling following cortical ischaemic stroke.

Another limitation to our study were the challenges encountered during statistical analysis. Because measurements were taken repeatedly across anatomical levels within the same animal, analysing each anatomical area separately with 2 or 3 way ANOVAs risks pseudoreplication (treating non-independent within-animal observations as independent); a more appropriate approach would be hierarchical/mixed-effects modelling (animal as a random effect, with anatomical level as a within-subject factor). We attempted to do this using both R and SPSS to analyse the dataset using linear mixed effects models. However, due to the complex experimental design, including multiple levels of repeated measures and nested factors, these software packages were unable to handle the structure of data without extensive restructuring. Future studied with more streamlined experimental design or more specialised statistical support may allow for more advanced modelling approaches.

6. Conclusion

Chronic ischaemic stroke triggers a cascade of events that results in secondary structural and cellular alterations that extend beyond the primary lesion site. Mechanisms underlying these remote changes in the distant but anatomically connected brain regions remain poorly understood. In this study, we showed that chronic dMCAO induces widespread network-level alterations, such as decreased cerebral blood flow in the cortex and white matter with a compensatory thalamic hyperperfusion, and an increased FA due to microstructural organisation. Pathological analyses revealed persistent glial cell activation, axon-myelin disruption across major white matter tracts, and a secondary loss in the thalamus. This establishes that chronic stroke drives progressive, network-wide remodelling beyond the initial infarct core, contributing to long-term structural disconnection. This work highlights the relevance of the dMCAO model in chronic ischaemic stroke and provides a foundation for identifying therapeutic strategies to preserve white matter integrity and cognitive function following stroke.

7. Acknowledgement

I would like to sincerely thank my supervisor, Dr. Jill Fowler, for her constant support, encouragement and guidance throughout this project. I have learnt an incredible amount during my time in the Fowler lab, which would not have been possible without her generosity, patience and dedication to mentorship. I am truly thankful for every opportunity she has given me.

I would also like to thank Dr. Kirsty Haddow for her guidance in the lab, as well as all other members of the Fowler and Horsburgh labs. I am thankful to every lab member for creating such a friendly and supportive environment. It's genuinely been a joy to work alongside such kind and welcoming colleagues.

I also want to acknowledge Dr. Axel Montagne and Dr. Audrey Chagnot for helping me with MRI registration as well as Dr. Tracy Farr for sharing her expertise in MRI analysis and for always offering support whenever I needed it, and Mr Ross Lennen for his assistance throughout the MRI components of the project. I appreciate the time and effort each researcher has invested in helping me succeed.

I am especially grateful to my family for their endless support and belief in me. Finally, to Eric, thank you for always listening, supporting and believing in me. Your presence and encouragement have meant more than I can express.

8. References

Alber, Jessica, Suvarna Alladi, Hee-Joon Bae, et al. 2019. 'White Matter Hyperintensities in Vascular Contributions to Cognitive Impairment and Dementia (VCID): Knowledge Gaps and Opportunities'. *Alzheimer's & Dementia (New York, N. Y.)* 5: 107–17. https://doi.org/10.1016/j.trci.2019.02.001.

Arenas-Mosquera, David, Alipio Pinto, Natacha Cerny, et al. 2022. 'Cytokines Expression from Altered Motor Thalamus and Behavior Deficits Following Sublethal Administration of Shiga Toxin 2a Involve the Induction of the Globotriaosylceramide Receptor'. *Toxicon: Official Journal of the International Society on Toxinology* 216 (September): 115–24. https://doi.org/10.1016/j.toxicon.2022.07.003.

Beard, Elidie, Sylvain Lengacher, Sara Dias, Pierre J. Magistretti, and Charles Finsterwald. 2022. 'Astrocytes as Key Regulators of Brain Energy Metabolism: New Therapeutic Perspectives'. *Frontiers in Physiology* 12 (January). https://doi.org/10.3389/fphys.2021.825816.

Boehm-Sturm, Philipp, Martina Füchtemeier, Marco Foddis, et al. 2017. 'Neuroimaging Biomarkers Predict Brain Structural Connectivity Change in a Mouse Model of Vascular Cognitive Impairment'. *Stroke* 48 (2): 468–75. https://doi.org/10.1161/STROKEAHA.116.014394.

Bokor, Hajnalka, Samuel G. A. Frère, Mark D. Eyre, et al. 2005. 'Selective GABAergic Control of Higher-Order Thalamic Relays'. *Neuron* 45 (6): 929–40. https://doi.org/10.1016/j.neuron.2005.01.048.

Brumm, Kathleen P., Joanna E. Perthen, Thomas T. Liu, Frank Haist, Liat Ayalon, and Tracy Love. 2010. 'An Arterial Spin Labeling Investigation of Cerebral Blood Flow Deficits in Chronic Stroke Survivors'. *NeuroImage* 51 (3): 995–1005. https://doi.org/10.1016/j.neuroimage.2010.03.008.

Brunelli, Stefano, Emilia Giannella, Mirko Bizzaglia, Domenico De Angelis, and Giulia Maria Sancesario. 2023. 'Secondary Neurodegeneration Following Stroke: What Can Blood Biomarkers Tell Us?' *Frontiers in Neurology* 14: 1198216. https://doi.org/10.3389/fneur.2023.1198216.

Budde, Matthew D., Lindsay Janes, Eric Gold, Lisa Christine Turtzo, and Joseph A. Frank. 2011. 'The Contribution of Gliosis to Diffusion Tensor Anisotropy and Tractography Following Traumatic Brain Injury: Validation in the Rat Using Fourier Analysis of Stained Tissue Sections'. *Brain: A Journal of Neurology* 134 (Pt 8): 2248–60. https://doi.org/10.1093/brain/awr161.

Butler, Tanya L., Cheryl A. Kassed, Paul R. Sanberg, Alison E. Willing, and Keith R. Pennypacker. 2002. 'Neurodegeneration in the Rat Hippocampus and Striatum after Middle Cerebral Artery Occlusion'. *Brain Research* 929 (2): 252–60. https://doi.org/10.1016/s0006-8993(01)03371-6.

Cao, Xuejin, Zan Wang, Xiaohui Chen, et al. 2021. 'White Matter Degeneration in Remote Brain Areas of Stroke Patients with Motor Impairment Due to Basal Ganglia Lesions'. *Human Brain Mapping* 42 (14): 4750–61. https://doi.org/10.1002/hbm.25583.

Cao, Yingying, Zhenzhen Lai, Jingwen Wang, Bijun Ye, Weiqiang Fan, and Jiajia Ruan. 2025. 'Research Progress on the Application of Functional Magnetic Resonance Imaging in Cognitive Dysfunction in Patients with Cerebral Small Vessel Disease'. *Frontiers in Neurology* 16: 1622274. https://doi.org/10.3389/fneur.2025.1622274.

Cao, Zhijuan, Adithya Balasubramanian, Steen E. Pedersen, Jonathan Romero, Robia G. Pautler, and Sean P. Marrelli. 2017. 'TRPV1-Mediated Pharmacological Hypothermia Promotes Improved Functional Recovery Following Ischemic Stroke'. *Scientific Reports* 7 (1): 17685. https://doi.org/10.1038/s41598-017-17548-y.

Cao, Zhijuan, Sean S. Harvey, Tonya M. Bliss, Michelle Y. Cheng, and Gary K. Steinberg. 2020. 'Inflammatory Responses in the Secondary Thalamic Injury After Cortical Ischemic Stroke'. *Frontiers in Neurology* 11: 236. https://doi.org/10.3389/fneur.2020.00236.

Cao, Zhijuan, Sean S. Harvey, Terrance Chiang, et al. 2021. 'Unique Subtype of Microglia in Degenerative Thalamus After Cortical Stroke'. *Stroke* 52 (2): 687–98. https://doi.org/10.1161/STROKEAHA.120.032402.

Chen, Shiyu, Liuwang Zeng, and Zhiping Hu. 2014. 'Progressing Haemorrhagic Stroke: Categories, Causes, Mechanisms and Managements'. *Journal of Neurology* 261 (11): 2061–78. https://doi.org/10.1007/s00415-014-7291-1.

Chen, Wei, Gang Su, Miao Chai, Yang An, Jinyang Song, and Zhenchang Zhang. 2025. 'Astrogliosis and Glial Scar in Ischemic Stroke - Focused on Mechanism and Treatment'. *Experimental Neurology* 385 (March): 115131. https://doi.org/10.1016/j.expneurol.2024.115131.

Christidi, Foteini, Dimitrios Tsiptsios, Aggeliki Fotiadou, et al. 2022. 'Diffusion Tensor Imaging as a Prognostic Tool for Recovery in Acute and Hyperacute Stroke'. *Neurology International* 14 (4): 841–74. https://doi.org/10.3390/neurolint14040069.

Dacosta-Aguayo, Rosalia, Manuel Graña, Marina Fernández-Andújar, et al. 2014. 'Structural Integrity of the Contralesional Hemisphere Predicts Cognitive Impairment in Ischemic Stroke at Three Months'. *PloS One* 9 (1): e86119. https://doi.org/10.1371/journal.pone.0086119.

Deczkowska, Aleksandra, Hadas Keren-Shaul, Assaf Weiner, Marco Colonna, Michal Schwartz, and Ido Amit. 2018. 'Disease-Associated Microglia: A Universal Immune Sensor of Neurodegeneration'. *Cell* 173 (5): 1073–81. https://doi.org/10.1016/j.cell.2018.05.003.

Del Águila, Ángela, Ran Zhang, Xinyuan Yu, et al. 2024. 'Microglial Heterogeneity in the Ischemic Stroke Mouse Brain of Both Sexes'. *Genome Medicine* 16 (1): 95. https://doi.org/10.1186/s13073-024-01368-7.

Dichgans, Martin, and Didier Leys. 2017. 'Vascular Cognitive Impairment'. *Circulation Research* 120 (3): 573–91. https://doi.org/10.1161/CIRCRESAHA.116.308426.

Dihné, Marcel, Christian Grommes, Michael Lutzenburg, Otto W. Witte, and Frank Block. 2002. 'Different Mechanisms of Secondary Neuronal Damage in Thalamic Nuclei after Focal Cerebral Ischemia in Rats'. *Stroke* 33 (12): 3006–11. https://doi.org/10.1161/01.str.0000039406.64644.cb.

Ding, Guangliang, Quan Jiang, Lian Li, et al. 2008. 'Magnetic Resonance Imaging Investigation of Axonal Remodeling and Angiogenesis after Embolic Stroke in Sildenafil-Treated Rats'. *Journal of Cerebral Blood Flow and Metabolism: Official Journal of the International Society of Cerebral Blood Flow and Metabolism* 28 (8): 1440–48. https://doi.org/10.1038/jcbfm.2008.33.

Dinther, M. van, A. M. Hooghiemstra, E. E. Bron, et al. 2023. 'Lower Cerebral Blood Flow Predicts Cognitive Decline in Patients with Vascular Cognitive Impairment'. *Alzheimer's &*

Dementia: The Journal of the Alzheimer's Association 20 (1): 136–44. https://doi.org/10.1002/alz.13408.

Egorova, Natalia, Thijs Dhollander, Mohamed Salah Khlif, Wasim Khan, Emilio Werden, and Amy Brodtmann. 2020. 'Pervasive White Matter Fiber Degeneration in Ischemic Stroke'. *Stroke* 51 (5): 1507–13. https://doi.org/10.1161/STROKEAHA.119.028143.

Egorova-Brumley, Natalia, Thijs Dhollander, Wasim Khan, Mohamed Salah Khlif, Deena Ebaid, and Amy Brodtmann. 2023. 'Changes in White Matter Microstructure Over 3 Years in People With and Without Stroke'. *Neurology* 100 (16): e1664–72. https://doi.org/10.1212/WNL.0000000000207065.

Escartin, Carole, Elena Galea, András Lakatos, et al. 2021. 'Reactive Astrocyte Nomenclature, Definitions, and Future Directions'. *Nature Neuroscience* 24 (3): 312–25. https://doi.org/10.1038/s41593-020-00783-4.

Fama, Rosemary, and Edith V. Sullivan. 2015. 'Thalamic Structures and Associated Cognitive Functions: Relations with Age and Aging'. *Neuroscience and Biobehavioral Reviews* 54 (July): 29–37. https://doi.org/10.1016/j.neubiorev.2015.03.008.

Fan, Jui-Lin, Patrice Brassard, Caroline A Rickards, et al. 2022. 'Integrative Cerebral Blood Flow Regulation in Ischemic Stroke'. *Journal of Cerebral Blood Flow & Metabolism* 42 (3): 387–403. https://doi.org/10.1177/0271678X211032029.

Feigin, Valery L., Benjamin A. Stark, Catherine Owens Johnson, et al. 2021. 'Global, Regional, and National Burden of Stroke and Its Risk Factors, 1990–2019: A Systematic Analysis for the Global Burden of Disease Study 2019'. *The Lancet Neurology* 20 (10): 795–820. https://doi.org/10.1016/S1474-4422(21)00252-0.

Feng, Xue-Feng, Jian-Feng Lei, Man-Zhong Li, et al. 2022. 'Magnetic Resonance Imaging Investigation of Neuroplasticity After Ischemic Stroke in Tetramethylpyrazine-Treated Rats'. *Frontiers in Pharmacology* 13 (April). https://doi.org/10.3389/fphar.2022.851746.

Fernández-Andújar, Marina, Fleur Doornink, Rosalía Dacosta-Aguayo, et al. 2014. 'Remote Thalamic Microstructural Abnormalities Related to Cognitive Function in Ischemic Stroke Patients'. *Neuropsychology* (US) 28 (6): 984–96. https://doi.org/10.1037/neu0000087.

Filley, Christopher M., and R. Douglas Fields. 2016. 'White Matter and Cognition: Making the Connection'. *Journal of Neurophysiology* 116 (5): 2093–104. https://doi.org/10.1152/jn.00221.2016.

Firbank, M.J., J. He, A.M. Blamire, et al. 2011. 'Cerebral Blood Flow by Arterial Spin Labeling in Poststroke Dementia'. *Neurology* 76 (17): 1478–84. https://doi.org/10.1212/WNL.0b013e318217e76a.

Fowler, Jill H, Jamie McQueen, Philip R Holland, et al. 2018. 'Dimethyl Fumarate Improves White Matter Function Following Severe Hypoperfusion: Involvement of Microglia/Macrophages and Inflammatory Mediators'. *Journal of Cerebral Blood Flow & Metabolism* 38 (8): 1354–70. https://doi.org/10.1177/0271678X17713105.

Fruhwirth, Viktoria, Lisa Berger, Thomas Gattringer, et al. 2024. 'White Matter Integrity and Functional Connectivity of the Default Mode Network in Acute Stroke Are Associated with

Cognitive Outcome Three Months Post-Stroke'. *Journal of the Neurological Sciences* 462 (July): 123071. https://doi.org/10.1016/j.jns.2024.123071.

Gazdzinski, Lisa M., Miranda Mellerup, Tong Wang, et al. 2020. 'White Matter Changes Caused by Mild Traumatic Brain Injury in Mice Evaluated Using Neurite Orientation Dispersion and Density Imaging'. *Journal of Neurotrauma* 37 (16): 1818–28. https://doi.org/10.1089/neu.2020.6992.

Girijala, Raghavendra L., Farida Sohrabji, and Ruth L. Bush. 2017. 'Sex Differences in Stroke: Review of Current Knowledge and Evidence'. *Vascular Medicine (London, England)* 22 (2): 135–45. https://doi.org/10.1177/1358863X16668263.

Grabert, Kathleen, Tom Michoel, Michail H. Karavolos, et al. 2016. 'Microglial Brain Region−dependent Diversity and Selective Regional Sensitivities to Aging'. *Nature Neuroscience* 19 (3): 504–16. https://doi.org/10.1038/nn.4222.

Groen, Thomas van, Kirsi Puurunen, Hanna-Mari Mäki, Juhani Sivenius, and Jukka Jolkkonen. 2005. 'Transformation of Diffuse Beta-Amyloid Precursor Protein and Beta-Amyloid Deposits to Plaques in the Thalamus after Transient Occlusion of the Middle Cerebral Artery in Rats'. *Stroke* 36 (7): 1551–56. https://doi.org/10.1161/01.STR.0000169933.88903.cf.

Guo, Yi-Sha, Yunlin Shang, Jiajia Yao, and Xia Bi. 2025. 'Role and Mechanism of Microglia in White Matter Injury Recovery in Ischemic Stroke'. *Immunity, Inflammation and Disease* 13 (8): e70226. https://doi.org/10.1002/iid3.70226.

Gupta, Rakesh K., Sona Saksena, Khader M. Hasan, et al. 2006. 'Focal Wallerian Degeneration of the Corpus Callosum in Large Middle Cerebral Artery Stroke: Serial Diffusion Tensor Imaging'. *Journal of Magnetic Resonance Imaging: JMRI* 24 (3): 549–55. https://doi.org/10.1002/jmri.20677.

Hall, Gerard R., Philipp Boehm-Sturm, Ulrich Dirnagl, et al. 2022. 'Long-Term Connectome Analysis Reveals Reshaping of Visual, Spatial Networks in a Model With Vascular Dementia Features'. *Stroke* 53 (5): 1735–45. https://doi.org/10.1161/STROKEAHA.121.036997.

Han, Lijuan, Wei Cai, Leilei Mao, et al. 2015. 'Rosiglitazone Promotes White Matter Integrity and Long-Term Functional Recovery After Focal Cerebral Ischemia'. *Stroke* 46 (9): 2628–36. https://doi.org/10.1161/STROKEAHA.115.010091.

Hayward, Nick M. E. A., Pavel Yanev, Annakaisa Haapasalo, et al. 2011. 'Chronic Hyperperfusion and Angiogenesis Follow Subacute Hypoperfusion in the Thalamus of Rats with Focal Cerebral Ischemia'. *Journal of Cerebral Blood Flow and Metabolism: Official Journal of the International Society of Cerebral Blood Flow and Metabolism* 31 (4): 1119–32. https://doi.org/10.1038/jcbfm.2010.202.

Hilkens, Nina A, Barbara Casolla, Thomas W Leung, and Frank-Erik de Leeuw. 2024. 'Stroke'. *The Lancet* 403 (10446): 2820–36. https://doi.org/10.1016/S0140-6736(24)00642-1.

Holland, Philip R., Mark E. Bastin, Maurits A. Jansen, et al. 2011. 'MRI Is a Sensitive Marker of Subtle White Matter Pathology in Hypoperfused Mice'. *Neurobiology of Aging* 32 (12): 2325.e1-6. https://doi.org/10.1016/j.neurobiolaging.2010.11.009.

Horsburgh, Karen, Joanna M. Wardlaw, Tom van Agtmael, et al. 2018. 'Small Vessels, Dementia and Chronic Diseases – Molecular Mechanisms and Pathophysiology'. *Clinical Science* 132 (8): 851–68. https://doi.org/10.1042/CS20171620.

Huang, Wen-Qing, Qing Lin, and Chi-Meng Tzeng. 2024. 'Leukoaraiosis: Epidemiology, Imaging, Risk Factors, and Management of Age-Related Cerebral White Matter Hyperintensities'. *Journal of Stroke* 26 (2): 131–63. https://doi.org/10.5853/jos.2023.02719.

Huang, Zhenqian, Xiaohao Zhang, Ying Zhao, et al. 2025. 'Lipocalin-2 Regulates Astrocyte-Oligodendrocyte Interaction to Drive Post-Stroke Secondary Demyelination'. *Cell Reports* 44 (7): 115899. https://doi.org/10.1016/j.celrep.2025.115899.

Iadecola, Costantino. 2004. 'Neurovascular Regulation in the Normal Brain and in Alzheimer's Disease'. *Nature Reviews. Neuroscience* 5 (5): 347–60. https://doi.org/10.1038/nrn1387.

Iadecola, Costantino, Marco Duering, Vladimir Hachinski, et al. 2019. 'Vascular Cognitive Impairment and Dementia: JACC Scientific Expert Panel'. *Journal of the American College of Cardiology* 73 (25): 3326–44. https://doi.org/10.1016/j.jacc.2019.04.034.

Iizuka, H., K. Sakatani, and W. Young. 1990. 'Neural Damage in the Rat Thalamus after Cortical Infarcts'. *Stroke* 21 (5): 790–94. https://doi.org/10.1161/01.str.21.5.790.

Jiang, Quan, Zheng Gang Zhang, Guang Liang Ding, et al. 2006. 'MRI Detects White Matter Reorganization after Neural Progenitor Cell Treatment of Stroke'. *NeuroImage* 32 (3): 1080–89. https://doi.org/10.1016/j.neuroimage.2006.05.025.

Jung, Won-Beom, Yong Hee Han, Julius Juhyun Chung, et al. 2017. 'Spatiotemporal Microstructural White Matter Changes in Diffusion Tensor Imaging after Transient Focal Ischemic Stroke in Rats'. *NMR in Biomedicine* 30 (6). https://doi.org/10.1002/nbm.3704.

Kenigsbuch, Mor, Pierre Bost, Shahar Halevi, et al. 2022. 'A Shared Disease-Associated Oligodendrocyte Signature among Multiple CNS Pathologies'. *Nature Neuroscience* 25 (7): 876–86. https://doi.org/10.1038/s41593-022-01104-7.

Keren-Shaul, Hadas, Amit Spinrad, Assaf Weiner, et al. 2017. 'A Unique Microglia Type Associated with Restricting Development of Alzheimer's Disease'. *Cell* 169 (7): 1276-1290.e17. https://doi.org/10.1016/j.cell.2017.05.018.

Kern, Kyle C., Clinton B. Wright, and Richard Leigh. 2022. 'Global Changes in Diffusion Tensor Imaging during Acute Ischemic Stroke and Post-Stroke Cognitive Performance'. *Journal of Cerebral Blood Flow and Metabolism: Official Journal of the International Society of Cerebral Blood Flow and Metabolism* 42 (10): 1854–66. https://doi.org/10.1177/0271678X221101644.

Kerr, Nadine, Dalton W. Dietrich, Helen M. Bramlett, and Ami P. Raval. 2019. 'Sexually Dimorphic Microglia and Ischemic Stroke'. *CNS Neuroscience & Therapeutics* 25 (12): 1308–17. https://doi.org/10.1111/cns.13267.

Kim, Gab Seok, Jessica M. Stephenson, Abdullah Al Mamun, et al. 2021. 'Determining the Effect of Aging, Recovery Time, and Post-Stroke Memantine Treatment on Delayed Thalamic Gliosis after Cortical Infarct'. *Scientific Reports* 11 (1): 12613. https://doi.org/10.1038/s41598-021-91998-3.

King, Derek, Raphael Wittenberg, Anita Patel, Zahid Quayyum, Vladislav Berdunov, and Martin Knapp. 2020. 'The Future Incidence, Prevalence and Costs of Stroke in the UK'. *Age and Ageing* 49 (2): 277–82. https://doi.org/10.1093/ageing/afz163.

Kluge, Murielle G, Mahmoud Abdolhoseini, Katarzyna Zalewska, et al. 2019. 'Spatiotemporal Analysis of Impaired Microglia Process Movement at Sites of Secondary Neurodegeneration Post-Stroke'. *Journal of Cerebral Blood Flow & Metabolism* 39 (12): 2456–70. https://doi.org/10.1177/0271678X18797346.

Kuchcinski, Grégory, Fanny Munsch, Renaud Lopes, et al. 2017. 'Thalamic Alterations Remote to Infarct Appear as Focal Iron Accumulation and Impact Clinical Outcome'. *Brain: A Journal of Neurology* 140 (7): 1932–46. https://doi.org/10.1093/brain/awx114.

Lalancette-Hébert, Mélanie, Geneviève Gowing, Alain Simard, Yuan Cheng Weng, and Jasna Kriz. 2007. 'Selective Ablation of Proliferating Microglial Cells Exacerbates Ischemic Injury in the Brain'. *The Journal of Neuroscience* 27 (10): 2596–605. https://doi.org/10.1523/JNEUROSCI.5360-06.2007.

Langen, Karl-Josef, Dagmar Salber, Kurt Hamacher, et al. 2007. 'Detection of Secondary Thalamic Degeneration after Cortical Infarction Using Cis-4-18F-Fluoro-D-Proline'. *Journal of Nuclear Medicine: Official Publication, Society of Nuclear Medicine* 48 (9): 1482–91. https://doi.org/10.2967/jnumed.107.041699.

Le Bihan, D., J. F. Mangin, C. Poupon, et al. 2001. 'Diffusion Tensor Imaging: Concepts and Applications'. *Journal of Magnetic Resonance Imaging: JMRI* 13 (4): 534–46. https://doi.org/10.1002/jmri.1076.

Li, Huiya, Pinyi Liu, Bing Zhang, et al. 2023. 'Acute Ischemia Induces Spatially and Transcriptionally Distinct Microglial Subclusters'. *Genome Medicine* 15 (1): 109. https://doi.org/10.1186/s13073-023-01257-5.

Li, Jiaxin, Xinyu Shui, Ruizheng Sun, et al. 2021. 'Microglial Phenotypic Transition: Signaling Pathways and Influencing Modulators Involved in Regulation in Central Nervous System Diseases'. *Frontiers in Cellular Neuroscience* 15 (September). https://doi.org/10.3389/fncel.2021.736310.

Li, Leiyang, Jinpeng Zhou, Liying Han, et al. 2022. 'The Specific Role of Reactive Astrocytes in Stroke'. *Frontiers in Cellular Neuroscience* 16: 850866. https://doi.org/10.3389/fncel.2022.850866.

Li, Lian, Quan Jiang, Guangliang Ding, et al. 2009. 'MRI Identification of White Matter Reorganization Enhanced by Erythropoietin Treatment in a Rat Model of Focal Ischemia'. *Stroke; a Journal of Cerebral Circulation* 40 (3): 936–41. https://doi.org/10.1161/STROKEAHA.108.527713.

Li, Zhaoqing, Huan Gao, Pingmei Zeng, et al. 2021. 'Secondary Degeneration of White Matter After Focal Sensorimotor Cortical Ischemic Stroke in Rats'. *Frontiers in Neuroscience* 14 (January). https://doi.org/10.3389/fnins.2020.611696.

Liang, Shengxiang, Jiayong Zhang, Qingqing Zhang, et al. 2020. 'Longitudinal Tracing of White Matter Integrity on Diffusion Tensor Imaging in the Chronic Cerebral Ischemia and Acute Cerebral Ischemia'. *Brain Research Bulletin* 154 (January): 135–41. https://doi.org/10.1016/j.brainresbull.2019.10.015.

Liang, Zhen, Yingyue Lou, Yulei Hao, Hui Li, Jiachun Feng, and Songyan Liu. 2023. 'The Relationship of Astrocytes and Microglia with Different Stages of Ischemic Stroke'. *Current Neuropharmacology* 21 (12): 2465–80. https://doi.org/10.2174/1570159X21666230718104634.

Liu, Che-Wei, Kate Hsiurong Liao, Hsin Tseng, Ching Mei Wu, Hsiao-Yun Chen, and Ted Weita Lai. 2020. 'Hypothermia but Not NMDA Receptor Antagonism Protects against Stroke Induced by Distal Middle Cerebral Arterial Occlusion in Mice'. *PloS One* 15 (3): e0229499. https://doi.org/10.1371/journal.pone.0229499.

Mäkinen, Susanna, Thomas van Groen, Jared Clarke, et al. 2008. 'Coaccumulation of Calcium and β-Amyloid in the Thalamus after Transient Middle Cerebral Artery Occlusion in Rats'. *Journal of Cerebral Blood Flow & Metabolism* 28 (2): 263–68. https://doi.org/10.1038/sj.jcbfm.9600529.

Martin, Seth S., Aaron W. Aday, Zaid I. Almarzooq, et al. 2024. '2024 Heart Disease and Stroke Statistics: A Report of US and Global Data From the American Heart Association'. *Circulation* 149 (8): e347–913. https://doi.org/10.1161/CIR.0000000000001209.

McCabe, Christopher, Mariana M. Arroja, Emma Reid, and I. Mhairi Macrae. 2018. 'Animal Models of Ischaemic Stroke and Characterisation of the Ischaemic Penumbra'. *Neuropharmacology* 134 (Pt B): 169–77. https://doi.org/10.1016/j.neuropharm.2017.09.022.

Munro, David A. D., Nadine Bestard-Cuche, Conor McQuaid, et al. 2024. 'Microglia Protect against Age-Associated Brain Pathologies'. *Neuron* 112 (16): 2732-2748.e8. https://doi.org/10.1016/j.neuron.2024.05.018.

Nakane, M., A. Tamura, Y. Sasaki, and A. Teraoka. 2002. 'MRI of Secondary Changes in the Thalamus Following a Cerebral Infarct'. *Neuroradiology* 44 (11): 915–20. https://doi.org/10.1007/s00234-002-0846-3.

Necula, Deanna, Frances S. Cho, Andrea He, and Jeanne T. Paz. 2022. 'Secondary Thalamic Neuroinflammation after Focal Cortical Stroke and Traumatic Injury Mirrors Corticothalamic Functional Connectivity'. *The Journal of Comparative Neurology* 530 (7): 998–1019. https://doi.org/10.1002/cne.25259.

Pandey, Shristi, Kimberle Shen, Seung-Hye Lee, et al. 2022. 'Disease-Associated Oligodendrocyte Responses across Neurodegenerative Diseases'. *Cell Reports* 40 (8): 111189. https://doi.org/10.1016/j.celrep.2022.111189.

Pawluk, Hanna, Alina Woźniak, Grzegorz Grześk, et al. 2020. 'The Role of Selected Pro-Inflammatory Cytokines in Pathogenesis of Ischemic Stroke'. *Clinical Interventions in Aging* 15: 469–84. https://doi.org/10.2147/CIA.S233909.

Percie du Sert, Nathalie, Viki Hurst, Amrita Ahluwalia, et al. 2020. 'The ARRIVE Guidelines 2.0: Updated Guidelines for Reporting Animal Research'. *BMC Veterinary Research* 16 (1): 242. https://doi.org/10.1186/s12917-020-02451-y.

Pinault, Didier. 2004. 'The Thalamic Reticular Nucleus: Structure, Function and Concept'. *Brain Research. Brain Research Reviews* 46 (1): 1–31. https://doi.org/10.1016/j.brainresrev.2004.04.008.

Pinter, Daniela, Thomas Gattringer, Simon Fandler-Höfler, et al. 2020. 'Early Progressive Changes in White Matter Integrity Are Associated with Stroke Recovery'. *Translational Stroke Research* 11 (6): 1264–72. https://doi.org/10.1007/s12975-020-00797-x.

Pitkonen, Miia, Usama Abo-Ramadan, Ivan Marinkovic, et al. 2012. 'Long-Term Evolution of Diffusion Tensor Indices after Temporary Experimental Ischemic Stroke in Rats'. *Brain Research* 1445 (March): 103–10. https://doi.org/10.1016/j.brainres.2012.01.043.

Planas, Anna M. 2024. 'Role of Microglia in Stroke'. *Glia* 72 (6): 1016–53. https://doi.org/10.1002/glia.24501.

Poirier, Stefan E., Rachel Wagner, Linshan Liu, et al. 2025. 'Association of White Matter Injury and Neuroinflammation in the Post-Acute Phase after Ischemic Stroke Using [18F]FEPPA-PET/MRI'. *EJNMMI Research* 15 (1): 91. https://doi.org/10.1186/s13550-025-01288-6.

Pollock, Alex, Bridget St George, Mark Fenton, and Lester Firkins. 2014. 'Top 10 Research Priorities Relating to Life after Stroke--Consensus from Stroke Survivors, Caregivers, and Health Professionals'. *International Journal of Stroke: Official Journal of the International Stroke Society* 9 (3): 313–20. https://doi.org/10.1111/j.1747-4949.2012.00942.x.

Ponath, Gerald, Sriram Ramanan, Mayyan Mubarak, et al. 2017. 'Myelin Phagocytosis by Astrocytes after Myelin Damage Promotes Lesion Pathology'. *Brain: A Journal of Neurology* 140 (2): 399–413. https://doi.org/10.1093/brain/aww298.

Puig, J., S. Pedraza, G. Blasco, et al. 2011. 'Acute Damage to the Posterior Limb of the Internal Capsule on Diffusion Tensor Tractography as an Early Imaging Predictor of Motor Outcome after Stroke'. *AJNR. American Journal of Neuroradiology* 32 (5): 857–63. https://doi.org/10.3174/ajnr.A2400.

Rawji, Khalil S., Björn Neumann, and Robin J. M. Franklin. 2023. 'Glial Aging and Its Impact on Central Nervous System Myelin Regeneration'. *Annals of the New York Academy of Sciences* 1519 (1): 34–45. https://doi.org/10.1111/nyas.14933.

Rexrode, Kathryn M., Tracy E. Madsen, Amy Y. X. Yu, Cheryl Carcel, Judith H. Lichtman, and Eliza C. Miller. 2022. 'The Impact of Sex and Gender on Stroke'. *Circulation Research* 130 (4): 512–28. https://doi.org/10.1161/CIRCRESAHA.121.319915.

Rojo, Rocío, Anna Raper, Derya D. Ozdemir, et al. 2019. 'Deletion of a Csf1r Enhancer Selectively Impacts CSF1R Expression and Development of Tissue Macrophage Populations'. *Nature Communications* 10 (1): 3215. https://doi.org/10.1038/s41467-019-11053-8.

Rost, Natalia S., Amy Brodtmann, Matthew P. Pase, et al. 2022. 'Post-Stroke Cognitive Impairment and Dementia'. *Circulation Research* 130 (8): 1252–71. https://doi.org/10.1161/CIRCRESAHA.122.319951.

Safaiyan, Shima, Simon Besson-Girard, Tuğberk Kaya, et al. 2021. 'White Matter Aging Drives Microglial Diversity'. *Neuron* 109 (7): 1100-1117.e10. https://doi.org/10.1016/j.neuron.2021.01.027.

Sagnier, Sharmila, Gwenaëlle Catheline, Bixente Dilharreguy, et al. 2020. 'Normal-Appearing White Matter Integrity Is a Predictor of Outcome After Ischemic Stroke'. *Stroke* 51 (2): 449–56. https://doi.org/10.1161/STROKEAHA.119.026886.

Schaapsmeerders, Pauline, Anil M. Tuladhar, Renate M. Arntz, et al. 2016. 'Remote Lower White Matter Integrity Increases the Risk of Long-Term Cognitive Impairment After Ischemic Stroke in Young Adults'. *Stroke* 47 (10): 2517–25. https://doi.org/10.1161/STROKEAHA.116.014356.

Schaechter, Judith D., Zachary P. Fricker, Katherine L. Perdue, et al. 2009. 'Microstructural Status of Ipsilesional and Contralesional Corticospinal Tract Correlates with Motor Skill in Chronic Stroke Patients'. *Human Brain Mapping* 30 (11): 3461–74. https://doi.org/10.1002/hbm.20770.

Schroeter, Michael, Philipp Zickler, David T. Denhardt, Hans-Peter Hartung, and Sebastian Jander. 2006. 'Increased Thalamic Neurodegeneration Following Ischaemic Cortical Stroke in Osteopontin-Deficient Mice'. *Brain: A Journal of Neurology* 129 (Pt 6): 1426–37. https://doi.org/10.1093/brain/awl094.

Seitz, R. J., N. P. Azari, U. Knorr, F. Binkofski, H. Herzog, and H. J. Freund. 1999. 'The Role of Diaschisis in Stroke Recovery'. *Stroke* 30 (9): 1844–50. https://doi.org/10.1161/01.str.30.9.1844.

Shan, Min, Kaili Liu, Kuankuan Huang, Yi Ma, Wenwei Yun, and Min Zhang. 2025. 'Contralateral Hemispheric Cerebral Blood Flow Can Predict Short-Term Clinical Outcomes in Patients with Recent Small Subcortical Infarcts'. *Neurological Sciences* 46 (8): 3719–26. https://doi.org/10.1007/s10072-025-08172-0.

Shen, Qiang, Hongxia Ren, Haiying Cheng, Marc Fisher, and Timothy Q. Duong. 2005. 'Functional, Perfusion and Diffusion MRI of Acute Focal Ischemic Brain Injury'. *Journal of Cerebral Blood Flow and Metabolism: Official Journal of the International Society of Cerebral Blood Flow and Metabolism* 25 (10): 1265–79. https://doi.org/10.1038/sj.jcbfm.9600132.

Shen, Xin-Ya, Zhen-Kun Gao, Yu Han, Mei Yuan, Yi-Sha Guo, and Xia Bi. 2021. 'Activation and Role of Astrocytes in Ischemic Stroke'. *Frontiers in Cellular Neuroscience* 15 (November). https://doi.org/10.3389/fncel.2021.755955.

Shi, Kaibin, De-Cai Tian, Zhi-Guo Li, Andrew F Ducruet, Michael T Lawton, and Fu-Dong Shi. 2019. 'Global Brain Inflammation in Stroke'. *The Lancet Neurology* 18 (11): 1058–66. https://doi.org/10.1016/S1474-4422(19)30078-X.

Shi, Ligen, Zeyu Sun, Wei Su, et al. 2021. 'Treg Cell-Derived Osteopontin Promotes Microglia-Mediated White Matter Repair after Ischemic Stroke'. *Immunity* 54 (7): 1527-1542.e8. https://doi.org/10.1016/j.immuni.2021.04.022.

Shira, Rosenzweig, and Carmichael S. Thomas. 2015. 'The Axon-Glia Unit in White Matter Stroke: Mechanisms of Damage and Recovery'. *Brain Research* 1623 (October): 123–34. https://doi.org/10.1016/j.brainres.2015.02.019.

Shui, Xinyao, Jingsong Chen, Ziyue Fu, Haoyue Zhu, Hualin Tao, and Zhaoyinqian Li. 2024. 'Microglia in Ischemic Stroke: Pathogenesis Insights and Therapeutic Challenges'. *Journal of Inflammation Research* 17 (May): 3335–52. https://doi.org/10.2147/JIR.S461795.

Singh, Aditya A., Akash Kharwar, and Manoj P. Dandekar. 2022. 'A Review on Preclinical Models of Ischemic Stroke: Insights Into the Pathomechanisms and New Treatment Strategies'. *Current Neuropharmacology* 20 (9): 1667–86. https://doi.org/10.2174/1570159X19666210907092928.

Skripuletz, Thomas, Diane Hackstette, Katharina Bauer, et al. 2013. 'Astrocytes Regulate Myelin Clearance through Recruitment of Microglia during Cuprizone-Induced Demyelination'. *Brain: A Journal of Neurology* 136 (Pt 1): 147–67. https://doi.org/10.1093/brain/aws262.

Sotak, Christopher H. 2002. 'The Role of Diffusion Tensor Imaging in the Evaluation of Ischemic Brain Injury - a Review'. *NMR in Biomedicine* 15 (7–8): 561–69. https://doi.org/10.1002/nbm.786.

Sozmen, Elif G., David J. DiTullio, Shira Rosenzweig, et al. 2019. 'White Matter Stroke Induces a Unique Oligo-Astrocyte Niche That Inhibits Recovery'. *The Journal of Neuroscience* 39 (47): 9343–59. https://doi.org/10.1523/JNEUROSCI.0103-19.2019.

Stokowska, Anna, Markus Aswendt, Daniel Zucha, et al. 2023. 'Complement C3a Treatment Accelerates Recovery after Stroke via Modulation of Astrocyte Reactivity and Cortical Connectivity'. *The Journal of Clinical Investigation* 133 (10): e162253. https://doi.org/10.1172/JCI162253.

Stuckey, Shannon M., Lin Kooi Ong, Lyndsey E. Collins-Praino, and Renée J. Turner. 2021. 'Neuroinflammation as a Key Driver of Secondary Neurodegeneration Following Stroke?' *International Journal of Molecular Sciences* 22 (23): 13101. https://doi.org/10.3390/ijms222313101.

Suenaga, Jun, Xiaoming Hu, Hongjian Pu, et al. 2015. 'White Matter Injury and Microglia/Macrophage Polarization Are Strongly Linked with Age-Related Long-Term Deficits in Neurological Function after Stroke'. *Experimental Neurology* 272 (October): 109–19. https://doi.org/10.1016/j.expneurol.2015.03.021.

Tamura, A., D. I. Graham, J. McCulloch, and G. M. Teasdale. 1981. 'Focal Cerebral Ischaemia in the Rat: 2. Regional Cerebral Blood Flow Determined by [14C]Iodoantipyrine Autoradiography Following Middle Cerebral Artery Occlusion'. *Journal of Cerebral Blood Flow and Metabolism: Official Journal of the International Society of Cerebral Blood Flow and Metabolism* 1 (1): 61–69. https://doi.org/10.1038/jcbfm.1981.7.

Tuladhar, Anil M., Anouk G.W. van Norden, Karlijn F. de Laat, et al. 2015. 'White Matter Integrity in Small Vessel Disease Is Related to Cognition'. *NeuroImage : Clinical* 7 (February): 518–24. https://doi.org/10.1016/j.nicl.2015.02.003.

Uehara, H., H. Yoshioka, S. Kawase, et al. 1999. 'A New Model of White Matter Injury in Neonatal Rats with Bilateral Carotid Artery Occlusion'. *Brain Research* 837 (1–2): 213–20. https://doi.org/10.1016/s0006-8993(99)01675-3.

Verkhratsky, Alexei, and Maiken Nedergaard. 2018. 'Physiology of Astroglia'. *Physiological Reviews* 98 (1): 239–389. https://doi.org/10.1152/physrev.00042.2016.

Viaene, Angela N., Iraklis Petrof, and S. Murray Sherman. 2011. 'Properties of the Thalamic Projection from the Posterior Medial Nucleus to Primary and Secondary Somatosensory Cortices in the Mouse'. *Proceedings of the National Academy of Sciences of the United States of America* 108 (44): 18156–61. https://doi.org/10.1073/pnas.1114828108.

Villa, Pia, Johan van Beek, Anna Kirstine Larsen, et al. 2007. 'Reduced Functional Deficits, Neuroinflammation, and Secondary Tissue Damage after Treatment of Stroke by Nonerythropoietic Erythropoietin Derivatives'. *Journal of Cerebral Blood Flow and Metabolism: Official Journal of the International Society of Cerebral Blood Flow and Metabolism* 27 (3): 552–63. https://doi.org/10.1038/sj.jcbfm.9600370.

Wan, Ting, Wusheng Zhu, Ying Zhao, et al. 2022. 'Astrocytic Phagocytosis Contributes to Demyelination after Focal Cortical Ischemia in Mice'. *Nature Communications* 13 (1): 1134. https://doi.org/10.1038/s41467-022-28777-9.

Wang, Changsheng, Glenn T. Stebbins, David L. Nyenhuis, et al. 2006. 'Longitudinal Changes in White Matter Following Ischemic Stroke: A Three-Year Follow-up Study'. *Neurobiology of Aging* 27 (12): 1827–33. https://doi.org/10.1016/j.neurobiolaging.2005.10.008.

Wang, Fei, Shu-Yu Ren, Jing-Fei Chen, et al. 2020. 'Myelin Degeneration and Diminished Myelin Renewal Contribute to Age-Related Deficits in Memory'. *Nature Neuroscience* 23 (4): 481–86. https://doi.org/10.1038/s41593-020-0588-8.

Wang, Yuan, Gang Liu, Dandan Hong, Fenghua Chen, Xunming Ji, and Guodong Cao. 2016. 'White Matter Injury in Ischemic Stroke'. *Progress in Neurobiology* 141 (June): 45–60. https://doi.org/10.1016/j.pneurobio.2016.04.005.

Wardlaw, Joanna M., Maria C. Valdés Hernández, and Susana Muñoz-Maniega. 2015. 'What Are White Matter Hyperintensities Made Of?' *Journal of the American Heart Association* 4 (6): e001140. https://doi.org/10.1161/JAHA.114.001140.

Wimmer, Ralf D., L. Ian Schmitt, Thomas J. Davidson, Miho Nakajima, Karl Deisseroth, and Michael M. Halassa. 2015. 'Thalamic Control of Sensory Selection in Divided Attention'. *Nature* 526 (7575): 705–9. https://doi.org/10.1038/nature15398.

Xia, Cong, Jiaying Zhou, Chunqiang Lu, et al. 2021. 'Characterizing Diaschisis-Related Thalamic Perfusion and Diffusion After Middle Cerebral Artery Infarction'. *Stroke* 52 (7): 2319–27. https://doi.org/10.1161/STROKEAHA.120.032464.

Xia, Yumei, Gelun Huang, Xuemei Quan, et al. 2021. 'Dynamic Structural and Functional Reorganizations Following Motor Stroke'. *Medical Science Monitor : International Medical Journal of Experimental and Clinical Research* 27 (March): e929092-1-e929092-8. https://doi.org/10.12659/MSM.929092.

Xu, Jinghui, Liying Zhang, Mingyue Li, et al. 2023. 'TREM2 Mediates Physical Exercise-Promoted Neural Functional Recovery in Rats with Ischemic Stroke via Microglia-Promoted White Matter Repair'. *Journal of Neuroinflammation* 20 (1): 50. https://doi.org/10.1186/s12974-023-02741-w.

Xu, Shenbin, Jianan Lu, Anwen Shao, John H. Zhang, and Jianmin Zhang. 2020. 'Glial Cells: Role of the Immune Response in Ischemic Stroke'. *Frontiers in Immunology* 11 (February). https://doi.org/10.3389/fimmu.2020.00294.

Yam, P. S., T. Takasago, D. Dewar, D. I. Graham, and J. McCulloch. 1997. 'Amyloid Precursor Protein Accumulates in White Matter at the Margin of a Focal Ischaemic Lesion'. *Brain Research* 760 (1–2): 150–57. https://doi.org/10.1016/s0006-8993(97)00290-4.

Yamauchi, Hiroshi, Shinya Kagawa, Kuninori Kusano, Miki Ito, and Chio Okuyama. 2022. 'Neuronal Alterations in Secondary Thalamic Degeneration Due to Cerebral Infarction: A 11C-Flumazenil Positron Emission Tomography Study'. *Stroke* 53 (10): 3153–63. https://doi.org/10.1161/STROKEAHA.122.038846.

Yang, Le, Manzhong Li, Yu Zhan, et al. 2022. 'The Impact of Ischemic Stroke on Gray and White Matter Injury Correlated With Motor and Cognitive Impairments in Permanent MCAO Rats:

A Multimodal MRI-Based Study'. *Frontiers in Neurology* 13 (March). https://doi.org/10.3389/fneur.2022.834329.

Yang, Shangsong, Yuxiong Chen, Jialin Tang, et al. 2025. 'Microglia-Astrocyte Crosstalk Following Ischemic Stroke'. *Molecular Brain* 18 (October): 75. https://doi.org/10.1186/s13041-025-01244-4.

Zalewska, Katarzyna, Rebecca J. Hood, Giovanni Pietrogrande, et al. 2021. 'Corticosterone Administration Alters White Matter Tract Structure and Reduces Gliosis in the Sub-Acute Phase of Experimental Stroke'. *International Journal of Molecular Sciences* 22 (13): 6693. https://doi.org/10.3390/ijms22136693.

Zeng, Fanning, Jun Cao, Zexuan Hong, et al. 2023. 'Single-Cell Analyses Reveal the Dynamic Functions of Itgb2+ Microglia Subclusters at Different Stages of Cerebral Ischemia-Reperfusion Injury in Transient Middle Cerebral Occlusion Mice Model'. *Frontiers in Immunology* 14: 1114663. https://doi.org/10.3389/fimmu.2023.1114663.

Zeng, Lang, Shengqi Hu, Lingcheng Zeng, et al. 2023. 'Animal Models of Ischemic Stroke with Different Forms of Middle Cerebral Artery Occlusion'. *Brain Sciences* 13 (7): 1007. https://doi.org/10.3390/brainsci13071007.

Zeng, Tianxiang, Jun Liu, Wenjun Zhang, et al. 2024. 'Update on the Mechanism of Microglia Involvement in Post-Stroke Cognitive Impairment'. *Frontiers in Aging Neuroscience* 16 (June). https://doi.org/10.3389/fnagi.2024.1366710.

Zhang, Rongrong, Yanping Wu, Fei Xie, et al. 2018. 'RGMa Mediates Reactive Astrogliosis and Glial Scar Formation through TGFβ1/Smad2/3 Signaling after Stroke'. *Cell Death & Differentiation* 25 (8): 1503–16. https://doi.org/10.1038/s41418-018-0058-y.

Zhang, Shengxiang. 2019. 'Microglial Activation after Ischaemic Stroke'. *Stroke and Vascular Neurology* 4 (2): 71–74. https://doi.org/10.1136/svn-2018-000196.

Zhang, Shufen, Deshu Shang, Han Shi, Weiyu Teng, and Li Tian. 2021. 'Function of Astrocytes in Neuroprotection and Repair after Ischemic Stroke'. *European Neurology* 84 (6): 426–34. https://doi.org/10.1159/000517378.

Zhang, Yueman, Yunlu Guo, Ruqi Li, et al. 2023. 'Novel CH25H+ and OASL+ Microglia Subclusters Play Distinct Roles in Cerebral Ischemic Stroke'. *Journal of Neuroinflammation* 20 (1): 115. https://doi.org/10.1186/s12974-023-02799-6.

Zhuang, Yu-ming, Ming-cong Li, Zi-yue Lin, et al. 2025. 'Buyang Huanwu Decoction Improves Motor Function by Enhancing Internal Capsule Reorganization through Inhibiting Notch Signaling after Ischemic Stroke'. *Journal of Ethnopharmacology* 348 (May): 119812. https://doi.org/10.1016/j.jep.2025.119812.

Zijden, Jet P. van der, Annette van der Toorn, Kajo van der Marel, and Rick M. Dijkhuizen. 2008. 'Longitudinal in Vivo MRI of Alterations in Perilesional Tissue after Transient Ischemic Stroke in Rats'. *Experimental Neurology* 212 (1): 207–12. https://doi.org/10.1016/j.expneurol.2008.03.027.

Zuo, Meng, Hongquan Guo, Ting Wan, et al. 2019. 'Wallerian Degeneration in Experimental Focal Cortical Ischemia'. *Brain Research Bulletin* 149 (July): 194–202. https://doi.org/10.1016/j.brainresbull.2019.04.023.

Appendix

Appendix A

Buffer Recipes

10X Phosphate buffer (10X PB)

10X PB was made by dissolving 2.57 g of mono-sodium phosphate (NaH_2PO_4; Sigma) and 11.95 g di-sodium phosphate (Na_2HPO_4; Sigma) in distilled water to make up to 1L. This solution was then filtered and diluted 1:10 in distilled water to be used (1X PB).

10X Phosphate buffer saline (10X PBS) - pH 7.4

10X PBS was made by dissolving 2.57 g of mono-sodium phosphate (NaH_2PO_4; Sigma) and 11.95 g di-sodium phosphate (Na_2HPO_4; Sigma) in distilled water. The pH was adjusted to 7.4 and then 90 g of sodium chloride was added. The final solution was made up to 1L with distilled water and this solution was then filtered, to be diluted 1:10 in distilled water to be used (1X PBS).

10X Tris buffer (10X TB) - pH 7.6

10X TB was made by dissolving 60.6 g of Trizma HCl (Sigma) and 13.9 g of Trizma base (Sigma) in distilled water to make up to 1L. The solution pH was adjusted to 7.6 and then filtered. The solution was diluted 1:10 in distilled water to be used (1X TB).

Paraformaldehyde 4% (PFA 4%) - pH 7.4

800 ml of PBS was heated at 60°C in a fume hood. 40g of P6148 paraformaldehyde (Sigma) was added to the hot PB and stirred for 15 minutes. After cooling to room temperature, the final solution was made up to 1L with distilled water. The solution pH was adjusted to 7.4 and then filtered.

Appendix B

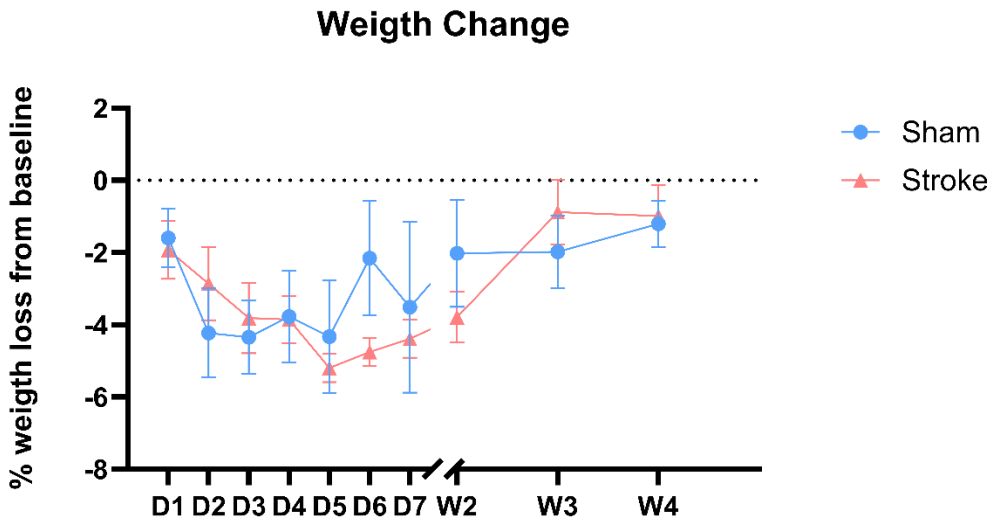

Ischaemic Stroke has no impact on body weight. Graph demonstrating weight change from baseline over time. Body weight decreased transiently in both sham and stroke groups after surgery (main effect of Time, $F_{(9,70)}$=2.809; P=0.0071). However, there was no effect of surgery or surgery and time interaction. Two-way mixed-effects ANOVA with Bonferroni correction. Results demonstrated as mean ± SEM. Sham n=4, stroke n=5.